From spectral statistics to decay in quantum chaotic systems: a semiclassical analysis beyond Random Matrix Theory

Dissertation

zur Erlangung des Doktorgrades
der Naturwissenschaften (Dr. rer. nat.)
der Naturwissenschaftlichen Fakultät II – Physik
der Universität Regensburg

vorgelegt von
Martha Lucía Gutiérrez Márquez
aus Bogota

Dezember 2008

Die Arbeit wurde von Prof. Dr. Klaus Richter und von Prof. Dr. Matthias Brack angeleitet.
Das Promotionsgesuch wurde am 07.11.2008 eingereicht.
Das Promotionskolloquium fand am 12.12.2008 statt.

Prüfungsausschuss:

Vorsitzender:	Prof. Dr. Christian Back
1. Gutachter:	Prof. Dr. Klaus Richter
2. Gutachter:	Prof. Dr. John Schliemann
Weiterer Prüfer:	Prof. Dr. Gunnar Bali

Contents

Chapter 1

Introduction

In classical mechanics the state of a particle at a time t is fully described by a point $\mathbf{x}(t) = (\mathbf{r}(t), \mathbf{p}(t))$ in phase space. The motion is given by the solution of the equations of motion (Newton, Lagrange or Hamilton). This solution is unique given the initial conditions, and therefore the motion is completely deterministic, though the dynamics can be extremely complicated. Let us consider an autonomous conservative system with f degrees of freedom, described by a Hamiltonian function $H(\mathbf{x})$. Due to conservation of energy the motion in phase-space is restricted to a $2f-1$-dimensional hyper-surface. Classically, the type of motion can be separated into integrable and non - integrable. The first situation appears if there are, apart from the energy, $f-1$ other independent constants of motion [1]. In this case, it is possible to perform a canonical transformation to a new set of phase-space coordinates, called the action-angle variables, such that the Hamiltonian depends only on the action variables, therefore the motion in phase space is restricted to an f-dimensional hyper-surface [2]. In the new coordinates, the dynamics is trivial, the angles vary linearly with time, while the actions remain constant, so, all the solutions are periodic or quasi-periodic, depending on the frequency ratio between the different angular degrees of freedom. Opposite to this situation, where there are apart from energy no other constants of motion, the system can display hard chaos: there is an extreme sensitivity to initial conditions, i.e. perturbing slightly the initial conditions leads to exponential separation in time of the solutions. This makes impossible to predict the long time behaviour of the solutions if the initial conditions are not known exactly.

On the other hand, a more general theory is the quantum theory, in which a physical state is depicted by a vector $|\psi(t)\rangle$ in Hilbert space, whose evolution is given through the Schrödinger equation:

$$i\hbar\frac{d}{dt}|\psi(t)\rangle = \hat{H}|\psi\rangle, \tag{1.1}$$

which has also a unique solution once the initial condition (state) is given. A first connection between the quantum and the classical dynamics, can be found by making the ansatz $\psi(\mathbf{r},t) = A(\mathbf{r},t)\exp(iS(\mathbf{r},t)/\hbar)$ in position representation for a Hamiltonian of the form $H(\mathbf{r},\mathbf{p}) = \mathbf{p}^2/2m + V(\mathbf{r})$, as first done in Ref. [3]. After substituting in Eq. (1.1), and neglecting all $\hbar$-dependent terms, one arrives to the Hamilton-Jacobi equation of motion

$$-\frac{\partial S(\mathbf{r},t)}{\partial t} = H(\mathbf{r}, \nabla S(\mathbf{r},t)). \tag{1.2}$$

This equation is satisfied by the action principal function

$$S(\mathbf{r},t) = S(\mathbf{r},\mathbf{r}',t-t') = \int_{t'}^{t} dt'' \mathcal{L}(\mathbf{r}(t''), \dot{\mathbf{r}}(t''), t''), \tag{1.3}$$

with the condition $\mathbf{r}(t') = \mathbf{r}'$, where $\mathcal{L}(\mathbf{r}(t), \dot{\mathbf{r}}(t), t)$ is the Lagrangian. Moreover, the next order in $\hbar$ corresponds to the classical continuity equation. So apparently, for small values of $\hbar$ the quantum solutions are closely related to the classical ones. This ansatz that we have just mentioned above, is the main ingredient to obtain a semiclassical quantization of integrable systems. For integrable systems one can relate the classical conserved quantities to "good" quantum numbers, in the sense that each invariant torus, characterized by its frequencies, can be linked to a quantum wave function through the quantization condition where each classical action coordinate is a multiple integer of Planck's constant $\hbar$ (plus phases). This is the well known EBK quantization introduced in Ref. [4] (based on WKB quantization for one-dimensional systems [5]) relating classical and quantum solutions in a direct way.

As pointed out by Einstein, the tori quantization is not applicable if the system is not longer integrable, and the way of quantizing this type of systems is still an issue in the semiclassical community. However, the complexity in the dynamics of chaotic systems is compensated by the simplicity in the statistical properties: all chaotic systems satisfy universal properties on the classical side, which are (i) ergodicity, i.e. almost any trajectory (apart from a set of zero measure), will homogeneously fill the energy shell after long times; (ii) mixing, i.e. correlations of functions in phase space decay exponentially fast; and (iii) hyperbolicity, i.e. a small initial separation between almost any two trajectories will grow exponentially fast [6]. On the quantum side it has been widely shown that chaotic systems display universal properties as well [7], e.g. the energy eigenvalues of a confined system display universal statistics, conductance and shot noise in chaotic open systems are also universal.

The quest of "quantum chaos" [8] is the study of quantum systems whose classical counterpart is chaotic. A phenomenological approach to these universal

features, is done in the frame of Random Matrix Theory (RMT), by considering ensembles over all Hamiltonians with the same symmetry properties instead of the original individual system itself. This was proposed first by Wigner and Dyson in Ref. [9, 10] in order to describe statistics of eigenvalues of highly excited atomic nuclei. Later on, it was conjectured in Ref. [11] that the energy levels of an individual classically chaotic system follows the RMT predictions (Bohigas-Giannoni-Schmit conjecture). A formal link between the classical and quantum theories has been done in the frame of the semiclassical approximation. Let us introduce this approximation and some of its basic tools.

1.1 The semiclassical approximation

The solution of the time dependent Schrödinger equation Eq.(1.1) for a time independent Hamiltonian can be written in position representation as

$$\psi(\mathbf{r},t) = \int d\mathbf{r}' K(\mathbf{r},\mathbf{r}',t-t')\psi(\mathbf{r}',t'), \tag{1.4}$$

where

$$K(\mathbf{r},\mathbf{r}',t-t') = \left\langle \mathbf{r} \left| \exp\left(-\frac{i}{\hbar}\hat{H}(t-t')\right) \right| \mathbf{r}' \right\rangle, \tag{1.5}$$

is the propagator and $\psi(\mathbf{r},t')$ is the wave function at t'. In Ref. [12] Feynman introduced a space-time formulation of quantum mechanics directly related to the propagator, from which one has that

$$K(\mathbf{r},\mathbf{r}',t-t') = \int \mathcal{D}[\mathbf{r}(t)] \mathrm{e}^{\frac{i}{\hbar}S[\mathbf{r}(t)]}, \tag{1.6}$$

where $S[\mathbf{r}(t)]$ is the action integral Eq. (1.3) along the path $\mathbf{r}(t)$ joining $\mathbf{r}'$ and $\mathbf{r}$ in a time $t-t'$.

Starting from the Feynman path integral approach to quantum mechanics and applying the method of stationary phase approximation a semiclassical propagator was derived [13]. The philosophy behind the semiclassical approximation is that all the typical actions, i.e. the typical values of $S[\mathbf{q}(t)]$, are much larger that $\hbar$, giving rise to a rapidly oscillating function in the integral. Therefore the main contributions will come from paths where the phase is stationary, which are actually the classical paths, i.e. the solutions of Eq. (1.2). The semiclassical propagator can be written as

$$K^{\mathrm{sc}}\left(\mathbf{r},\mathbf{r}',t-t'\right) = \frac{1}{(2\pi i\hbar)^{f/2}} \sum_{\gamma(\mathbf{r}'\to\mathbf{r},t-t')} D_\gamma \exp\left(\frac{i}{\hbar}S_\gamma(\mathbf{r},\mathbf{r}',t-t') - i\frac{\pi}{2}\mu_\gamma\right), \tag{1.7}$$

where f is the dimension of the system, γ are classical trajectories traveling from $\mathbf{r}'$ to $\mathbf{r}$ in a time $t-t'$ with an stability given by

$$D_\gamma = \left| \det \left(-\frac{\partial^2 S_\gamma(\mathbf{r}, \mathbf{r}', t-t')}{\partial \mathbf{r} \partial \mathbf{r}'} \right) \right|^{1/2}, \tag{1.8}$$

called the Van Vleck determinant. $S_\gamma(\mathbf{r}, \mathbf{r}', t-t')$ is the action along the path γ and μ_γ is the so-called Morse index, related to phases gained at the turning points. A very useful quantity in many physical contexts, from spectral statistics to scattering processes, is the Fourier transform of the propagator to the energy domain: the Green function. The exact (retarded) Green function for a bounded system can be written in terms of the eigenfunctions $\phi_n(\mathbf{r})$ and eigenvalues E_n of H as

$$G^+\left(\mathbf{r}, \mathbf{r}', E\right) = \lim_{\epsilon \to 0^+} \sum_n \frac{\phi_n(\mathbf{r}) \phi_n^*(\mathbf{r}')}{E - E_n + i\epsilon}. \tag{1.9}$$

The corresponding semiclassical Green function obtained from the evaluation of the Fourier transform of Eq. (1.7) by stationary phase approximation, is given by

$$G^{\mathrm{sc}}\left(\mathbf{r}, \mathbf{r}', E\right) = \frac{2\pi}{(2\pi i\hbar)^{(f+1)/2}} \sum_{\gamma(\mathbf{r}' \to \mathbf{r}, E)} \tilde{D}_\gamma \exp\left(\frac{i}{\hbar} \tilde{S}_\gamma(\mathbf{r}, \mathbf{r}', E) - i\frac{\pi}{2} \nu_\gamma \right), \tag{1.10}$$

where trajectories γ are now fixed in energy, the phase is $\tilde{S}_\gamma(\mathbf{r}, \mathbf{r}', E) = \int_{\mathbf{r}'}^{\mathbf{r}} \mathbf{p}(\mathbf{q}) \cdot d\mathbf{q}$, ν_γ is μ_γ plus additional phases gained in the time integration, and

$$\tilde{D}_\gamma = \left| \det \left(\frac{\partial^2 S_\gamma}{\partial \mathbf{r} \partial \mathbf{r}'} \frac{\partial^2 \tilde{S}_\gamma}{\partial E^2} \right) \right|^{1/2}. \tag{1.11}$$

Eqs. (1.7) and (1.10) are the bones of the semiclassical approximation. Most of the semiclassical approximations are based on evaluating expressions involving either the propagator or the Green function. The semiclassical theory has given a formal way of studying quantum properties in terms of classical information. The evaluation of the path integral by stationary phase approximation is valid in systems where the typical actions are much larger than Planck's constant. This corresponds, for example, to mesoscopic systems, which are systems of a micron in size showing classical and quantum signatures. It is important to stress out that the semiclassical approximation takes into account interference effects through the phase terms, and therefore goes beyond a simple quasi-classical description. As mentioned before, through the semiclassical methods a formal link between RMT predictions and classical dynamics can be built. Let us have a more detailed look into this issue.

1.2 Spectral statistics

A prominent approach to the quest of "quantum chaos" involves spectral statistics to characterize the energy-level fluctuations in quantum systems and their interpretation in terms of the dynamics of the corresponding classical system. Classically integrable systems possess uncorrelated energy levels, described by a Poisson distribution [14], while the levels of classically chaotic quantum systems exhibit strong local repulsion, conjectured to be the same as for RMT. Spectral statistics has been investigated, for both integrable [15, 16, 17] and chaotic [18, 19, 20] systems employing semiclassical approaches. For the purely chaotic case, starting with Ref. [21], considerable progress has been recently made in understanding semiclassically energy level correlations beyond the so-called diagonal approximation [19] by means of classical correlations between (off-diagonal) pairs of periodic orbits.

1.2.1 Semiclassical density of states

Let $\{E_1, E_2, \ldots, E_n\}$ be the spectrum of the quantum Hamiltonian $\hat{H}$ for a bounded system. The level density $g(E)$ is defined as

$$g(E) = \sum_{i=1} \delta(E - E_i), \tag{1.12}$$

which is related to the Green function through

$$\pi g(E) = -\mathcal{I}m \int d\mathbf{r}\, G^{+}(\mathbf{r}, \mathbf{r}, E)\,. \tag{1.13}$$

Averaging this quantity over an energy window of width $\Delta E \ll E$ leads to the average density of states $\bar{g}(E) = \langle g(E) \rangle_{\Delta E}$. This average density of states is a smooth and slowly varying function of the energy E if the averaging includes enough energy levels.

Evaluating the trace integral in Eq. (1.13) by stationary phase approximation Gutzwiller, in Ref. [22], derived his famous trace formula, which relates the oscillatory part of the spectral density with classical solutions which are periodic. The semiclassical density of states $g^{\rm sc}(E)$ can be written in the form

$$g^{\rm sc}(E) = \bar{g}^{\rm sc}(E) + \delta g(E), \tag{1.14}$$

where the smooth part $\bar{g}^{\rm sc}(E)$ is given by the (extended) Thomas-Fermi model (cf. Chap. 4 in Ref. [23]), and the oscillating contribution is given by a trace formula which, to leading order in $1/\hbar$, has the following form:

$$\delta g(E) = \frac{1}{\hbar^{\mu+1}} \sum_j A_j(E) \cos\left[\frac{S_j(E)}{\hbar} - \frac{\pi}{2}\sigma_j\right]. \tag{1.15}$$

The sum is over all periodic orbits j (which form families with degenerate actions in the presence of continuous symmetries). $S_j(E) = \oint_j \mathbf{p} \cdot d\mathbf{q}$ is the action integral along a periodic orbit and σ_j a geometrical phase factor (usually called Maslov index). The amplitudes $A_j(E)$ and the power of $\hbar$ in Eq. (1.15) depend on the presence of continuous symmetries. For fully integrable systems, $\mu = s/2$, where s is the degree of degeneracy of the orbit families; the amplitudes were derived by Strutinsky and Magner [24] for specific cases and by Berry and Tabor [25] for general integrable systems. For non-integrable systems with continuous symmetries, further results were obtained by Creagh and Littlejohn [26].

For systems without continuous symmetries, where all orbits are isolated in phase space, one has $\mu = 0$, and the amplitudes $A_j(E)$ were given by Gutzwiller [22] in terms of their stability matrices $\mathrm{M}_j(E)$ and periods $T_j(E) = \mathrm{d}S_j(E)/\mathrm{d}E$.

1.2.2 The spectral form factor

Statistics of energy levels can be characterized by the two-point correlation function of the density of states, defined as

$$R(\omega, E) = \frac{1}{\bar{g}^2(E)} \langle g(E + \omega/2) g(E - \omega/2) \rangle_{\Delta E} - 1. \tag{1.16}$$

An energy average $\langle ... \rangle_{\Delta E}$ is taken in order to ensure that $R(\omega, E)$ is a slowly varying function of E. The window of average ΔE is chosen in a way that it is considered classically small $\Delta E \ll E$, but quantum mechanically large $\bar{g}(E)\Delta E \gg 1$. It is expected that for large energies E this quantity will be independent of E, and will be only a function of the energy difference ω. Therefore we will drop the energy E as an argument of the two-point correlation function, though it is an argument of all energy-dependent classical quantities. Moreover we will always assume a dimensionless spectrum with mean level separation equal to unity, which is obtained from the original spectrum by the standard process of unfolding: replacing the energy level E_i by the mean number of states at this energy, $\bar{N}(E_i)$.

The spectral form factor is defined as the Fourier transform of eq.(1.16) with respect to the energy difference ω

$$K(\tau) = \left\langle \bar{g} \int_{-\infty}^{\infty} R(\omega) e^{-2\pi i \omega \tau \bar{g}} \mathrm{d}\omega \right\rangle_{\Delta\tau}, \tag{1.17}$$

where $\tau = t/t_H$, and $t_H = 2\pi\hbar\bar{g}$ is the Heisenberg time, which represents the time scale associated with the mean level spacing.

Again a local average over a time window around τ is performed in order to obtain a slowly varying function of the time. For an integrable system, the spectrum is uncorrelated, which means that the two-point correlation function is

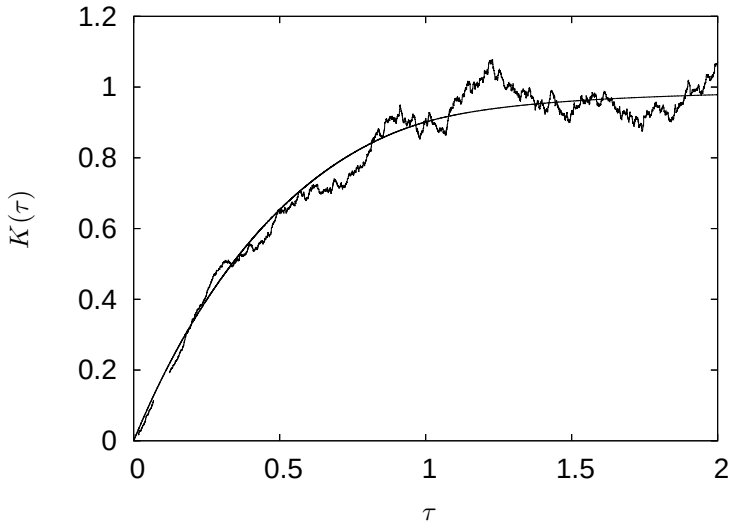

Figure 1.1: Spectral form factor for the quartic oscillator (cf. Chapter 2) showing hard chaos around an unfolded energy $\tilde{E} = 6000$ averaged over 2000 levels. In bold: RMT prediction.

a Dirac delta function and the form factor is equal to 1 for all τ [19]. A RMT prediction for $K(\tau)$ is obtained by taking averages over ensembles of random matrices preserving the general symmetries of the systems [10, 27]. For example, for systems without time-reversal symmetry (GUE), we know that the Hamiltonian has to be Hermitian, whereas for time-reversal invariant systems it must be real and symmetric (GOE). Averaging over all Hermitian or real symmetric matrices, and taking the limit of the matrix dimension $N \to \infty$, a prediction for the spectral form factor can be obtained, which is independent of system specific parameters and therefore is called universal:

$$K^{\mathrm{GOE}}(\tau) = \begin{cases} 2\tau - \tau\ln(1+2\tau) & \text{if } 0 < \tau < 1 \\ 2 - \tau\ln\left(\frac{2\tau+1}{2\tau-1}\right) & \text{if } \tau > 1 \end{cases} \tag{1.18}$$

As an example, we show in Fig. 1.1 the numerically calculated spectral form factor for a quartic oscillator potential (cf. Chapter 2) with chaotic dynamics in comparison with eq.(1.18) (bold line).

1.2.3 The diagonal approximation

By replacing the semiclassical density of states into Eq. (1.17) a semiclassical expression for the form factor can be derived as Ref. [19]:

$$K(\tau) = \frac{1}{\hbar^{2\mu}}\Big\langle \sum_{j,k} \frac{A_j A_k}{t_H^2} \exp\left[\frac{i}{\hbar}(S_j - S_k) - \frac{i\pi}{2}(\sigma_j - \sigma_k)\right] \delta_{\Delta\tau}\left(\tau - \frac{\bar{T}_{jk}}{t_H}\right)\Big\rangle, \tag{1.19}$$

where $\bar{T}_{jk} = \frac{1}{2}(T_j + T_k)$. The width of the delta-function is due to the local time average.

As expressed in Eq. (1.19) the spectral form factor is determined by a double sum over pairs of periodic orbits. The semiclassical limit $\hbar \to 0$ means that the typical classical actions of these paths are very large compared with $\hbar$, so that the energy average will strongly suppress the contributions of most pairs of orbits. The first approximation is to consider that only orbits paired with themselves ($j = k$) or, in case of time reversal symmetry, with their time-reserved partners ($j = \bar{k}$) give a contribution. This is known as the "diagonal approximation", introduced by Berry in Ref. [19]. In the diagonal approximation the double sum is reduced to a single one:

$$K^{\mathrm{diag}}(\tau) = \frac{1}{\hbar^{2\mu}} \Big\langle \sum_j \frac{|A_j|^2}{t_H^2} \delta_{\Delta\tau}\left(\tau - \frac{\bar{T}_{jk}}{t_H}\right) \Big\rangle. \tag{1.20}$$

For chaotic systems this sum can be evaluated using the sum rule of Hannay and Ozorio de Almeida [18], which is based on the properties of classical chaotic systems. For long enough times, the number of periodic orbits in a hyperbolic systems increases like $\mathrm{e}^{\lambda t}/t$, where λ is the Lyapunov exponent (characterizing the rate at which the distance between two close points will increase), while the amplitudes $|A_j|^2$ decrease exponential as $\mathrm{e}^{-\lambda t}$, yielding that

$$K^{\mathrm{diag}}(\tau) = 2\tau, \tag{1.21}$$

for the orthogonal case. For the unitary case GUE, $K^{\mathrm{diag}}(\tau) = \tau$.

1.2.4 Quantum corrections in the semiclassical approximation

It was only until 2001, with the work of Sieber and Richter in Ref. [21], that interference terms entered into the semiclassical approximation for fully chaotic systems. The orbits that give such a contribution are those with a self-crossing in configuration space as depicted in Fig. 1.2. It can be shown, for completely hyperbolic dynamics, that a trajectory avoiding the self-crossing exists and is exponentially close to the first one, in such a way that the difference in action can be smaller that $\hbar$. The original idea in Ref. [21] in configuration space, based on calculating the crossing angle distribution and considering a chaotic billiard on a surface of constant negative curvature to find the action difference, was then extended to graphs in Ref. [28], further extended in Ref. [29] to a phase space approach and thereby for any two dimensional chaotic system, in Ref. [30] for more than 2 dimensions and finally in Ref. [31] similar diagrams were included given rise to the next order contributions, recovering the full expansion in Eq. (1.18) for $\tau < 1$.

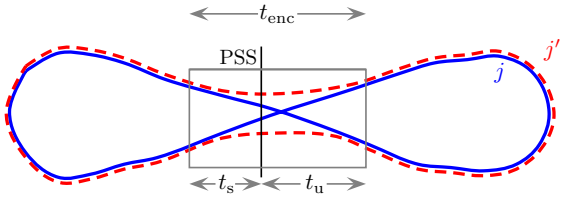

Figure 1.2: Sketch of a pair of orbits given a non-diagonal contribution to the form factor.

In each "loop" pair the trajectory j (full line in Fig. 1.2) contains an encounter region: two stretches of j are sufficiently close such that they are mutually linearizable. The time where this linearization is valid is defined as the encounter time $t_{\rm enc}$. Along j the two stretches are separated from each other by two links. The partner trajectory j' (dotted line) is distinguished from the original by differently connecting the links inside the encounter, due to time reversal symmetry.

To describe such diagrams a fundamental concept in classical chaos is needed: the concept of a Poincaré surface of section [32] (PSS) in the neighborhood of the orbit, describing the dynamics of the degrees of freedom transverse to the orbit (Fig. 1.3). For a periodic orbit the PSS is defined by fixing a surface of section in phase space perpendicular to the orbit. For a point $\mathbf{y}$ on the surface of section, the trajectory is followed until it intersects the surface again at $P\mathbf{y}$, the image of $\mathbf{y}$ under the Poincaré map P. The periodic orbit itself returns to its original point, so that it appears as a fixed point of the Poincaré map $\mathbf{x}_o$.

The way of calculating diagrams like the one in Fig. 1.2 in the phase space approach is defining a PSS perpendicular to the trajectory j. The most suitable coordinates, correspond to the stable and unstable coordinates in the PSS.

The local stable and unstable manifolds $W^{s,u}(\mathbf{x}_o)$ are defined such that [6]

$$W^s(\mathbf{x}_o) = \{\mathbf{x} \in \mathcal{M} : ||\mathbf{x}(t) - \mathbf{x}_o(t)|| \to 0 \qquad \text{for } t \to +\infty\}, \tag{1.22}$$

$$W^u(\mathbf{x}_o) = \{\mathbf{x} \in \mathcal{M} : ||\mathbf{x}(t) - \mathbf{x}_o(t)|| \to 0 \qquad \text{for } t \to -\infty\}, \tag{1.23}$$

where $\mathcal{M}$ is the phase space.

One defines a PSS perpendicular to j inside the encounter region. The sum is carried over trajectories that return to the PSS at a distance s and u along the stable and unstable directions, where the unstable and stable components are confined to a range $|u| < c$ and $|s| < c$, where c is a small phase space distance. The double sum can be replaced by a sum over orbits j and an integral over its density $w(u, s, T_j)$ of two-encounters. The action difference is $\Delta S(u, s) = su$, whose absolute value is smaller than a classical value c^2. The double sum is replaced by an integral over the stable and unstable coordinates, with a weight function counting the number of trajectories coming closer to themselves than a

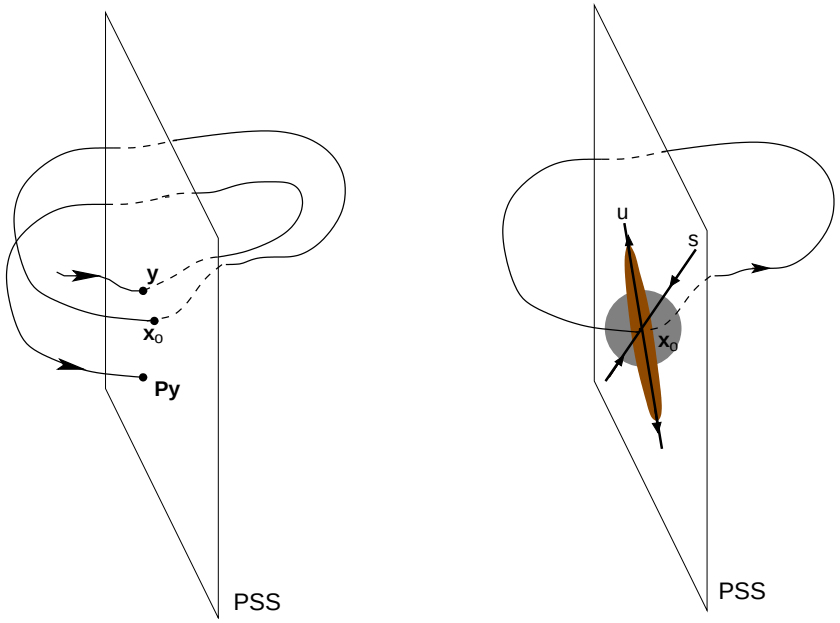

Figure 1.3: (a) Poincaré surface of section for a periodic orbit. (b) Stable and unstable manifolds of $\mathbf{x}_o$ (a fixed point of the Poincaré map). Components on the unstable manifold are stretched while the components in the stable direction become smaller.

distance c^2 in phase space:

$$K^{\mathrm{SR}}(\tau) = \Big\langle \sum_j \int_{-c}^{c} ds \int_{-c}^{c} du \frac{|A_j|^2}{t_H^2} w(u,s,T_j) \mathrm{e}^{\frac{i}{\hbar} su} \delta_{\Delta\tau}\left(\tau - \frac{T_j}{t_H}\right) \Big\rangle. \tag{1.24}$$

The Hannay-de Almeida sum rule can be applied to the sum over j, the number of trajectories having such an encounter $w(u,s,T_j)$ can be calculated assuming ergodicity. Moreover, since the trajectories have to close themselves, a minimum length for the trajectories is required. With the correct evaluation of the weight function this leads to the next order contribution in the expansion of Eq. (1.18), which is

$$K^{\mathrm{GOE}}(\tau) = 2\tau - 2\tau^2 + ... \tag{1.25}$$

In the unitary case, similar situations can happen, where no time reversal symmetry is required [31]. It turns out that for the form factor such diagrams cancel in a non-trivial way, yielding no corrections to the diagonal contribution for $\tau < 1$.

1.2.5 Deviations from universality

RMT is limited by the existence of finite time scales. In the context of spectral statistics, deviations appear at energies associated with the inverse of the period of the shortest orbit [19]. On the other hand, universality is expected to appear when

the wave functions can be split in to many partial waves that interfere randomly. The splitting of the wave packet is established when initial quantum uncertainties blow up to the classical level [33]. The related time scale is the Ehrenfest time [34]. The Ehrenfest correspondence principle stipulates that in the limit of large quantum numbers, the position and momentum average follow a classical path in phase space, i.e. the description of the quantum state can be done through a single classical particle. Those predictions differ faster if the system under consideration is chaotic. At the Ehrenfest time these deviations start to be noticeable, while for times shorter than the Ehrenfest time the quantum dynamics still bears signatures of classical determinism, not captured by RMT. It was first pointed out by Aleiner and Larkin in Ref.[35] that quantum effects require this minimal time to happen.

The semiclassical approach has been given a successful mechanism to correct RMT predictions for finite Ehrenfest-time in stationary problems (mainly in the study of transport through mesoscopic systems) [35, 36, 37, 38, 39, 40]. For the given example of the form factor, Ehrenfest time effects were studied in [41].

1.3 Semiclassical approximation near bifurcations

We have discussed up to now the quantum to classical correspondence in two extreme situations: full chaoticity and full integrability. They occur rather exceptionally. The most realistic physical situation is that of a system which is neither completely chaotic nor integrable, but whose phase space contains a mixture of stable and chaotic regions (Fig. 1.4). RMT does not provide a successful prediction for mixed systems. It is still an issue of the community whether there are universal properties in mixed systems or not. The semiclassical theory is applicable independent of the dynamics. For example, it has been successful in describing different kinds of phenomena typical of mixed dynamics, like dynamical tunneling [42].

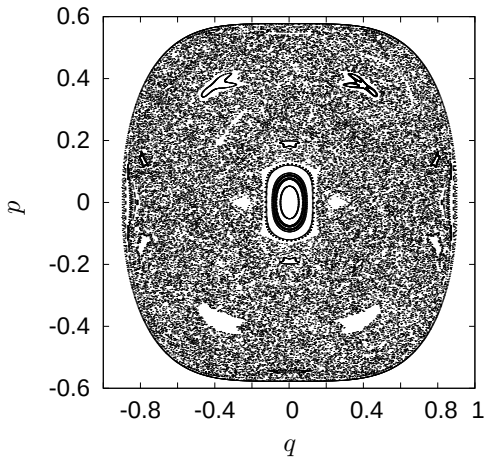

Figure 1.4: Typical phase space section of a mixed system.

In two dimensional systems with mixed dynamics, classical trajectories that are inside a regular island remain there forever, and trajectories that belong to the chaotic see will never enter the regular regions (though they can spend very long

times around them). Therefore it was argued in Ref. [43, 44] that on the quantum side, the statistics of mixed systems can be considered as a superposition of two independent statistics, that of regular systems and that of chaotic systems, where the weight of each one is given by the corresponding regular and irregular areas in phase space. This approximation is better the sharper the separation between regular and irregular region is, however, it fails in some situations. One main feature and structuring element of classical mixed phase space dynamics is the occurrence of bifurcations of periodic orbits upon variations of the energy or other parameters of the Hamiltonian.

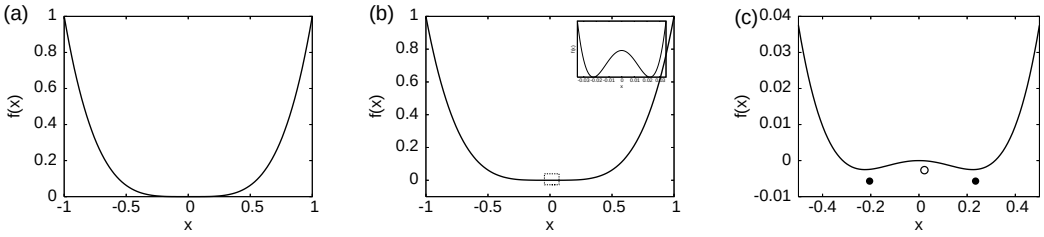

Figure 1.5: (a) $f(x) = x^4$ has a single fixed point at $x^* = 0$, the second derivative is null, therefore the fixed point is marginally stable. (b) After a small perturbation $\epsilon = -0.001$, two new fixed points are born, while the sign of the second derivative of $f(x)$ becomes negative, i.e. the fixed point at x^* becomes unstable. The upper inset is a zoom of the small region (dotted box) where the fixed points are born. The value of the perturbation is so small that they are almost indistinguishable. (c) For a large perturbation $\epsilon = -0.1$ the three points are clearly separated. The full dots indicate that the new fixed points are stable, while the empty dot indicates that the fixed point $x^* = 0$ is unstable.

The concept of bifurcations is strictly attached to the task of describing the creation of stationary points upon small perturbations, which is the subject of catastrophe theory [45, 46]. Let us consider a simple example, shown in Fig. 1.5. The function $f(x) = x^4$ has a single stationary point at $x^* = 0$. Now, let us add a small perturbation ϵx^2. The stationary points are now $x^* = 0, \pm\sqrt{-\epsilon/2}$. When $\epsilon < 0$ there are three real fixed points of $f(x)$, when $\epsilon \to 0$ these three fixed points collapse into a single one, this collapse is what is called a bifurcation. Periodic orbits are stationary points of the Poincaré map and their bifurcation theory can been described as in Ref. [46].

The method of stationary phase approximation is based on evaluating integrals like Eq. (1.13) near stationary points of the action. In this evaluation it is implied that the stationary solutions must be well separated from each other. If the dynamics of the system is chaotic this is always the case, but for general mixed systems, some periodic orbits neither appear in families (integrable system) nor can be treated as isolated orbits. This is the case, when periodic orbits are very near, and their action differences are smaller than $\hbar$, so that they lead to a

collective semiclassical contribution. This is the typical situation of a bifurcation.

Gutzwiller's trace formula is obtained by performing the stationary phase approximation in the evaluation of the trace of the semiclassical Green function. As mentioned before, those stationary points correspond to the periodic orbits of the system. When these periodic orbits bifurcate a special treatment has to be done in order to avoid divergent contributions. A first derivation of the contribution of such orbits to the density of states was done by Almeida and Hannay in Ref. [47], for a generic two dimensional system. Extensions of this approximation were later done in Ref. [48], where analytic formulae were derived, that interpolate over the regime from a bifurcation up to regions where the orbits can be considered isolated.

We can consider the trace in Eq. (1.13) in a mixed representation of coordinates and momentum. The contribution to the oscillatory part of the density of states of the trajectory ξ can be calculated for a two-dimensional system by an integral of the form

$$\delta g_\xi(E) = \frac{1}{\hbar^2} \int dq \int dp\, A_\xi(q,p) \exp\left(\frac{i}{\hbar}\Phi_\xi(q,p;E)\right), \tag{1.26}$$

where p and q are coordinates in the PSS perpendicular to the trajectory. If these stationary points are isolated the action in the integral can be expanded up to quadratic term in position and momentum around the periodic orbit recalling the result in Eq. (1.15). For bifurcating orbits, this procedure would diverge. In order to evaluate correctly the integral one has to write the action of the trajectories involved in the bifurcation as a mean action and a function describing the pattern of the stationary points that are created (usually after some canonical transformations [50]) called the normal form, which contains the characteristic local fixed-point scenario on the PSS in the neighborhood of a given type of bifurcation, i.e. the number of fixed points in the collapse, their configuration in phase space and the corresponding stabilities near the event. The creation of such points depends on the parameters $\{\alpha_n\}$ necessary to describe the "bifurcation scenario". The $\hbar$- scaling of the density of states is different for each scenario and usually larger than that of isolated orbits. Therefore bifurcating orbits can be dominant in the spectral statistics, as it was first shown in Ref. [49], where the semiclassical signature of a tangent bifurcation was studied on the context of spectral statistics at the level of the diagonal approximation.

More generally, in Ref. [51] a semiclassical approach was developed for the moments of the level counting function in the presence of several competing bifurcations. It was suggested that these moments diverge with a universal "twinkling exponent" in the semiclassical limit $\hbar \to 0$. The idea behind this new kind of

universality is the following: in a typical mixed systems many bifurcations take place, each one has a different $\hbar$-scaling. In the semiclassical limit $\hbar \to 0$ only the one that diverges faster will dominate, giving an universal contribution. This has actually never been observed numerically nor experimentally, since this required very small values of $\hbar$. Moreover, in this approach it is impossible to take into account "non-generic" bifurcations, where detailed knowledge of the individual bifurcations is required.

We have seen in this section, that semiclassical tools allow us to enter into the discussion of quantum to classical relation for mixed systems, where new interesting features like bifurcations show up, which cannot be studied in the frame of RMT. Another interesting field where semiclassical tools have been successfully applied is the field of decay and scattering processes.

1.4 Open systems

The first experimental evidence of universal properties of complex systems was coming from spectra of nuclear physics around 1980 which resulted in the development of RMT. After the Bohigas-Giannoni-Schmit conjecture it was until 1990 that the first experiments in quantum chaos were performed considering vibrating solids [52] and microwave cavities [53]. These experiments where focused on the spectral properties of closed systems, although strictly speaking they were always open, due to the measuring process. Therefore it became necessary to develop a scattering theory in order to analyse quantitatively those measurements (for a review see [54]). At the same time, a tremendous progress was achieved in the fabrication of semiconductor hetero-structures allowing the study of transport properties in systems of sub-micrometer size [55, 56]. Nowadays different aspects of open wave-chaotic systems have been intensely studied in semiconductor devices such as quantum dots and quantum wires [57, 58, 59], microwave cavities [60], acoustics [61], optically generated lattices [62, 63, 64, 65] or optical micro-cavities [66].

An open system can be described by non self-adjoint operator $H - i\Gamma/2$, where H corresponds to a bound system and Γ describes its coupling to the continuum. The energy eigenvalues (resonances) are not longer real and the eigenmodes, which are no longer orthogonal, are called quasi-bound states [67, 68]. The imaginary part of the energy of quasi-bound states is associated to its escape rate. For small values of Γ the problem can be approached considering the dynamics of H, whose classical counterpart is supposed to show chaotic dynamics. If the coupling with the exterior is small, the main properties of the classical chaotic dynamics are

preserved. It is expected that the distribution of resonances follow again some universal properties, which can be described by RMT, based in the assumption that H is a random Gaussian matrix. Though it is not obvious that the coupling to the continuum does not wash out the universal features. The key observation (coming from nuclear physics) is that there are typically two kind of well defined decay (or scattering) processes occurring at different time scales: an immediate response called *direct processes*, and a delayed one or equilibrated response. The latter is associated with the formation of long-living states, which can be related to the internal dynamics and therefore it is expected to show universal features. In this *indirect* processes the statistical properties of the closed system will be reflected in the statistical properties of the scattering or decay.

The semiclassical methods discussed before for closed systems hold for open systems with some modifications (due to the possibility of decaying) giving a link between universal properties and the classical dynamics, as we will see in more detail in this thesis.

Apart from the interest in open systems due to the possibility of measuring phenomena described by the theory, its study also provides very deep theoretical questions about the semiclassical approximation and the unitarity of the quantum evolution. Moreover, deviations from universality can become more important since another time scale enters into play, namely the typical decay rate. As we have mentioned before, quantum signatures need a time scale to show up, known as the Ehrenfest time. If the typical time that a particle expends in the scattering region τ_d is smaller than this time, the classical description of the system should contain all the important information, while only in the case that this typical decay time is larger than the Ehrenfest time, quantum effects should appear [33].

1.5 Overview of this thesis

We have introduced some of the main concepts that we will need in the development of this thesis. We have seen that the semiclassical approximation has been the main tool to connect classical and quantum mechanics, and some properties of classical chaotic systems with their quantum counterpart. Part of the community of quantum chaos has been concentrated in showing the dynamical mechanism behind the results of RMT through the semiclassical methods. As already pointed out, semiclassics goes beyond this, being able to estimate the limits of the RMT predictions, and describing phenomena that are beyond the scope of RMT. In this thesis, we are interested in studying two sources of deviations from RMT in closed and open systems: bifurcations and finite Ehrenfest time. In the first case, we will

consider the effect of bifurcations in the spectral statistics of closed systems with mixed dynamics. The existing numerical evidence of the magnitude of these effects in only available for maps [49, 69], which are easy to handle semiclassically, but do not represent the most realistic physical situations. We will consider the case of a Hamiltonian system and we will give a quantitative semiclassical analysis. In this study of bifurcations we will propose a definition of bifurcations in the context of scattering trajectories in open systems. On a second stage of the thesis, we will consider Ehrenfest time effects in the context of decay in open systems. Also in this case, the numerical evidence of Ehrenfest time features is mainly available for systems that are or can be reduced to maps (e.g. see Refs. [70, 71]). We will consider a system closer to experiments, namely a two-dimensional open cavity.
The outline of this thesis is the following:

- in Chapter 2 we present a detailed analysis of the trace formulae for different types of dynamics. We compare numerical results with the exact quantum calculation for a given system. The potential studied corresponds to the quartic oscillator, which can be tuned from integrability to hard chaos by a single regularity parameter. The system present discrete symmetries, which requires a special semiclassical treatment, which will be discussed in detail. We will discuss the bifurcations of one of the shortest periodic orbits, and its contribution to the density of states.

- In Chapter 3 we study the spectral statistics of the quartic oscillator. We numerically observe an enhanced effect of bifurcations, moreover this effect is stronger after the bifurcation. We give a quantitative explanation in terms of interference of trajectories born at the bifurcation.

- In Chapter 4 we define the concept of a bifurcation scenario in the context of transmission coefficients for an open system. The corresponding uniform approximations for two types of bifurcations is presented and their effect in the total conductance.

- In Chapter 5 we study the decay of a state in an open chaotic system and derive the RMT predictions for the leading quantum corrections. We present numerical calculations for a billiard system, showing deviations from the RMT prediction. The semiclassical approximation allows us to predict them by considering Ehrenfest time effects. We give an analytical expression that reproduces the numerical data.

- In Chapter 6 we consider the statistics of decay processes describing photo-ionization or dissociation. We observe in the semiclassical analysis, that the

statistics can be described by a joint contribution of periodic orbits and of open trajectories. We consider Ehrenfest time effects as well.

- In Chapter 7 we summarize and give some outlook of interesting open questions.

Part of the results presented here are available in Refs. [72], [73], [74], [76] and [75].

Chapter 2

Spectral density for the quartic oscillator: from integrability to hard chaos

In this chapter we will study in detail the semiclassical density of states for integrable, chaotic and mixed classical dynamics. Thereby, we will check the semiclassical approximation in a paradigmatic system for quantum chaos, namely the quartic oscillator (QO). First we will discuss the QO potential, together with its symmetries and the bifurcations of one of the shortest periodic orbits. Since this potential has discrete symmetries, we will analyze the semiclassical approximation for the density of states in this kind of systems, here we will study in detail the case of isolated orbits, where the Maslov indices of the *reduced orbits* are modified, and we show a numerical comparison for the QO. Finally, we discuss the global approximation for a particular type of bifurcation that takes place in the chosen potential, and we show how its semiclassical weight can be significant.

2.1 Model system: the quartic oscillator

As a representative system we investigate the coupled quartic oscillator (QO) in two dimensions. Its Hamiltonian reads:

$$H(x, y, p_x, p_y) = \frac{1}{2}\left(p_x^2 + p_y^2\right) + \frac{1}{4}\left(x^4 + y^4\right) + \frac{\alpha}{2}\, x^2 y^2 \,. \tag{2.1}$$

It has been extensively studied both classically, semiclassically and quantum-mechanically [77, 78, 79, 80, 81], as a smooth potential model exhibiting the transition from integrability to chaotic behaviour. Here we summarize the main classical features relevant for the subsequent semiclassical treatment. Since the Hamiltonian

(2.1) is homogeneous, its classical dynamics at different energies E can be related to each other by a simple scaling of coordinates, momenta and time. It is easy to show, that all actions scale with energy E as $E^{3/4}$ so that the semiclassical limit can be unambiguously taken as $E \to \infty$.

After scaling out the energy the parameter α in Eq. (2.1) solely determines the dynamics. The system is integrable for three different values of α: (i) $\alpha = 0$, since it is separable and can be solved independently in each dimension; (ii) $\alpha = 1$, where it can be written as the isotropic quartic oscillator $r^4/4$, with $r^2 = x^2 + y^2$; and (iii) $\alpha = 3$, where it is again separable after rotating the coordinates by $\pi/4$.

At $\alpha = 9$ the dynamics is almost completely chaotic: we could not locate any stable periodic orbit with a period less than about four times that of the shortest orbits. For values $\alpha > 9$ the regular fraction of the phase space keeps oscillating with a decreasing amplitude. In Fig. 2.1 we show a Poincaré surface of section for different values of α where the potential is integrable, mixed and almost fully chaotic.

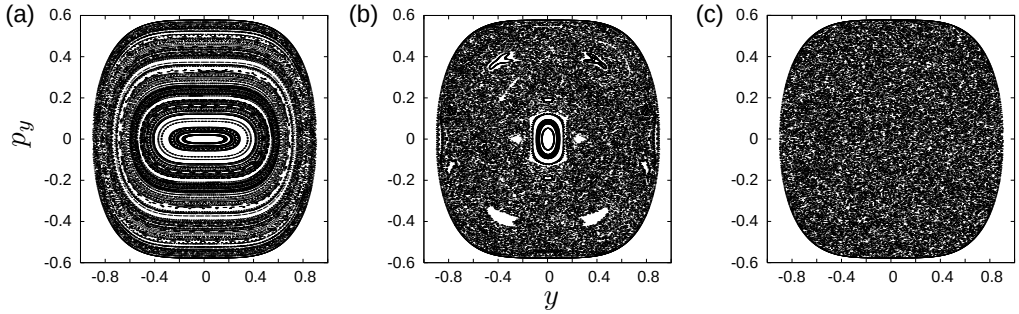

Figure 2.1: Poincaré surface of section for the QO at $x = 0$ for different values of the regularity parameter α. (a) Integrable QO, $\alpha = 0$. (b) $\alpha = 5$, the potential leads to mixed dynamics. (c) "hard" chaos is reached at $\alpha = 9$.

The QO in Eq. (2.1) possesses periodic straight-line librational orbits along both axes which we label by A. The motion of the A libration can be given analytically in terms of Lamé functions [79, 80]:

$$x_A(t) = 0 \qquad y_A = y_o \mathrm{cn}(y_o t, \kappa) \qquad y_o = (4E)^{1/4} \qquad \kappa^2 = \frac{1}{2}, \tag{2.2}$$

with the period $T_A = 4\mathbf{K}/y_o$, where $\mathbf{K} = K(\kappa) = F(\pi/2, \kappa)$ is the complete elliptic integral of the first kind modulus κ, and $\mathrm{cn}(z, \kappa)$ is one of the Jacobi elliptic functions [82]. The turning points are $\pm y_o$, and the solutions are independent of the value of α, however the stabilities of these solutions do depend on it. These librations undergo stability oscillations under the variation of α. Infinite cascades of new periodic orbits bifurcate from the A orbits and their repetitions. The trace of its stability matrix M (see [13, 23] for its definition) as a function of α is known

analytically [83]:

$$\mathrm{Tr\,M}(\alpha) = 4\cos\left(\frac{\pi}{2}\sqrt{1+8\alpha}\right) + 2\,. \tag{2.3}$$

Always when $\mathrm{Tr\,M} = 2$ a bifurcation takes place, i.e. the librational orbit A

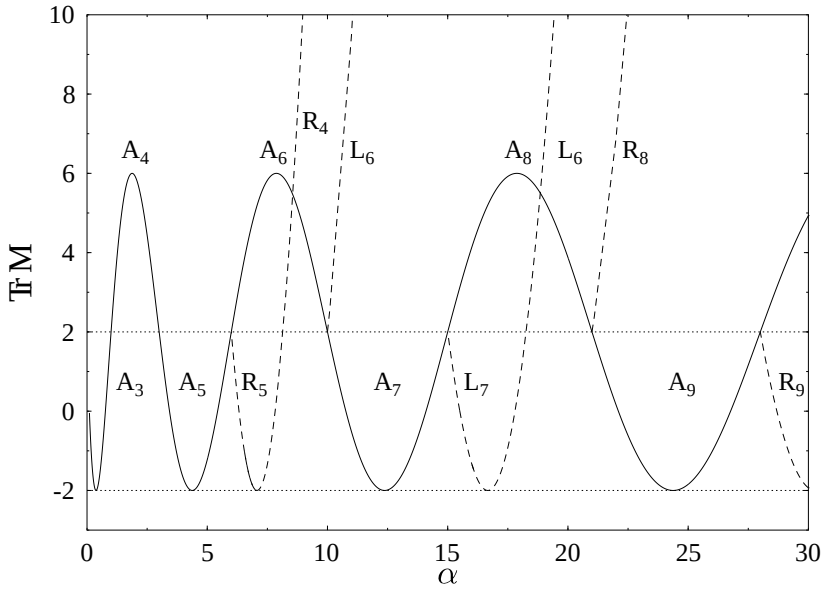

Figure 2.2: Trace of the stability matrix M as a function of α, Eq. (2.1), for the primitive A orbit (solid line) and the new orbits born at its bifurcations (dashed lines) at $\alpha = 6$, 10, 15, 21, and 28. Subscripts denote the Maslov indices σ_j.

changes its stability while new periodic orbits are born. Due to discrete symmetries, the kind of bifurcations that take place are isochronous pitchfork bifurcations. The pitchfork bifurcation scenario is like the one described in the introduction: two fixed points (in this case two periodic orbits) are born while the central one changes its stability. Typically this are period doubling bifurcations: they usually happen for the second repetition of a periodic orbit. Because of parity symmetry they can happen as isochronous bifurcations (for the first repetition) where the two solutions are related by symmetry. The values at which these bifurcations happens in the QO are

$$\alpha = \alpha_n = \frac{1}{2}\,n\,(n+1)\,, \qquad\qquad n = 0, 3, 4, 5, \ldots \quad . \tag{2.4}$$

(For $\alpha_1 = 1$ and $\alpha_2 = 3$, where the system is integrable, the A orbit is member of a degenerate family and does not bifurcate. See also [79, 80] for more details about the periodic orbits of this system.)

In Fig. 2.2 we show $\mathrm{Tr\,M}(\alpha)$ for the primitive A orbit and the new orbits born at its bifurcations at α_n with $n = 3$ to 7. These orbits are alternatingly stable or

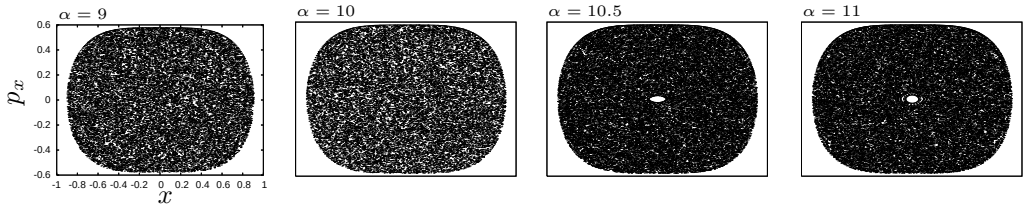

Figure 2.4: Poincaré surfaces of section for the QO near α_4. At $\alpha = 9$ and at the bifurcation point $\alpha = 10$ the phase space looks completely chaotic. A new stable island appears at $\alpha = 10.5$, which is slightly larger at $\alpha = 11$.

unstable rotational (R_σ) and librational orbits (L_σ) with a classical degeneracy of 2 due to the symmetries (cf. Ref. [79]).

In our numerical studies, we shall focus on the bifurcation at $\alpha = \alpha_4 = 10$ where the orbit L_6 is born (Fig. 2.3). Note that at each second bifurcation ($n = 3, 5, \dots$) a new stable orbit (R_5, $L_7, \dots$) is born, so that stable orbits exist on either side of these bifurcations.

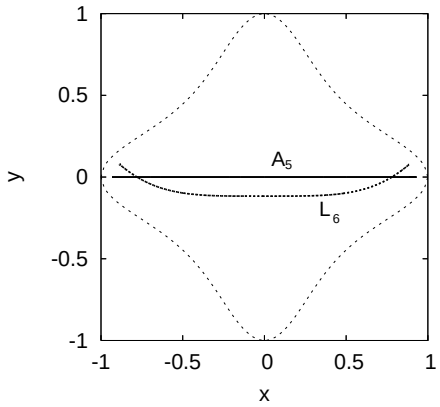

Figure 2.3: Orbits involved in the bifurcation at $\alpha_4 = 10$: A_5 (bold line) and L_6 (dotted line). A contour line of the potential is depicted by the dashed line.

At the other bifurcations ($n = 4, 6, \dots$), on the other hand, the new orbits (L_6, $R_8, \dots$) are unstable and just before these bifurcations, the A orbit is also unstable. This explains the oscillating regularity of the phase space and the fact that, even in the limit $\alpha \to \infty$, there always exist regions with stable orbits [81]).

In Fig. 2.4 we show Poincaré surfaces of section for the QO near α_4. As depicted, the phase space looks completely chaotic before and at the bifurcation, and later a tiny regular island is born. We choose this particular parameter, since we will see that universality in the level statistics is expected and observed before the bifurcation, and later affected by it.

The potential in Eq. (2.1) is invariant under the symmetry operations of the point group symmetry C_{4V}, which consists of the eight point operations that leave invariant a square, i.e. the identity operation (E), three rotation operations around the origin by multiples of $\pi/2$ (C_4, C_2 and C_4^3), and four reflection operations along the horizontal axes (σ_1), the vertical axes (σ_2) and the diagonals (σ_1' and σ_2'), as sketched in Fig. 2.5.

An important concept, which we will use in our semiclassical approach is the so-called fundamental domain, i.e., the smallest area that tessellates the whole space under application of the allowed symmetry operations.

This symmetry group has four one-dimensional irreducible representations and one (doubly-degenerate) two-dimensional representation.

Due to these symmetries, the Hamiltonian can be written in a block-diagonal form. Each submatrix can be diagonalised independently and corresponds to one of the irreducible representations, denoted in the following by EES, EEA, OOS, OOA and EO (doubly degenerate) [84]. The corresponding eigenfunctions satisfy certain symmetry properties. The eigenfunctions of the blocks EES (OOS) and EEA (OOA) are symmetric (anti-symmetric) under the operations σ_1 and σ_2, but EES (OOS) is symmetric under σ_1' while EEA (OOA) is antisymmetric. The eigenfunctions corresponding to EO are symmetric under σ_1 and anti-symmetric under σ_2. The character table of the group in shown in Table 2.1.

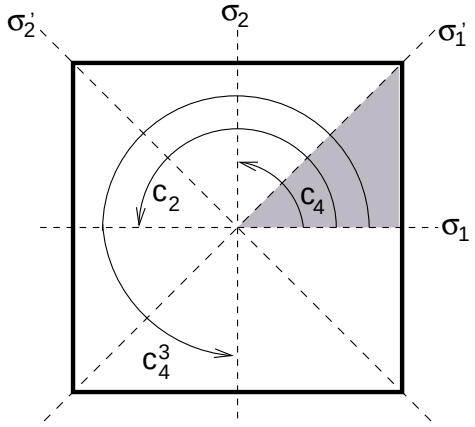

Figure 2.5: Point operations of the point group symmetry C_{4V}. The gray region corresponds to the fundamental domain.

In order to diagonalise the Hamiltonian we use a basis of symmetry-adapted

Classes Representation	E	$(C_4,\ C_4^3)$	(C_2)	(σ_1,σ_2)	(σ_1',σ_2')
EES	1	1	1	1	1
EEA	1	-1	1	-1	1
OOS	1	-1	1	1	-1
OOA	1	1	1	-1	-1
EO	2	0	-2	0	0

Table 2.1: The character table for C_{4v}.

linear combinations of harmonic oscillator states [85]:

$$|n_x, n_y\rangle_m = \frac{1}{\sqrt{2}}(|n_1, n_2\rangle \pm |n_2, n_1\rangle)\,, \tag{2.5}$$

where the sign and the parity of n_1 and n_2 depend on the representation. Since the independent symmetry-reduced blocks of the Hamiltonian matrix in this basis

are banded, we can obtain more than ten thousand well-converged eigenvalues, allowing for significant statistics. For an appropriate study of the spectral statistics, each symmetry class must therefore be treated separately. We shall study mainly the representation corresponding to eigenfunctions belonging to EES. This representation is easier to handle semiclassically, because all its characters are equal to unity.

2.2 Semiclassical density of states for discrete symmetries

In the presence of discrete symmetries it is necessary to define partial densities of states corresponding to the sub-spectra in each irreducible representation of the symmetry group.

In the Thomas-Fermi approximation the mean density of states $\bar{g}(E)$ is determined by the surface of the classical energy shell at energy E as

$$\bar{g}^{\rm sc}(E) = \frac{\Omega(E)}{(2\pi\hbar)^f}, \tag{2.6}$$

with

$$\Omega(E) = \int d\mathbf{q} \int d\mathbf{p}\, \delta(E - H(\mathbf{q},\mathbf{p})). \tag{2.7}$$

The corresponding reduced mean densities of states depend on the dimension of the irreducible representation d_m and on the order of the group $|\mathrm{G}|$, which corresponds to the number of operations of the group (in this case $|\mathrm{G}| = 8$). In first approximation [86] it is given by

$$\bar{g}_m(E) = \frac{d_m}{|\mathrm{G}|}\bar{g}(E). \tag{2.8}$$

In the following section, we will discuss the symmetry-reduced semiclassical oscillatory part of the density of states. For practical purposes, it is useful to coarse-grain the density of states by convolution with a normalized Gaussian $\exp[-(E/\gamma)^2]/(\sqrt{\pi}\gamma)$. Hence, we replace the quantum density of states $g(E) = \sum_n \delta(E - E_n)$ by the "coarse-grained" density of states

$$g_\gamma(E) = \frac{1}{\sqrt{\pi}\gamma}\sum_n \exp\left[-\frac{(E-E_n)^2}{\gamma^2}\right], \tag{2.9}$$

whereby the smoothing width γ defines the energy resolution at which one wishes to study the spectrum, i.e. making γ smaller corresponds to a better resolution.

The correspondingly semiclassical approximation for the coarse-grained oscillatory part of the level density becomes, to leading order in $\hbar$ (see, e.g., Ref. [23]),

$$\delta g_\gamma(E) = \frac{1}{\hbar^{\mu+1}} \sum_j A_j(E) \exp\left[-\left(\frac{\gamma T_j(E)}{2\hbar}\right)^2\right] \cos\left[\frac{S_j(E)}{\hbar} - \frac{\pi}{2}\sigma_j\right]. \qquad (2.10)$$

Hence, long orbits are suppressed which avoids convergence problems for any finite value of γ, since the number of orbits involved increases at most exponentially, while the suppression is faster. Details of the spectral density can be reveal while making γ smaller. For the integrable QO we have an analytical expression for the periods and actions of the tori that contribute to the spectral density, therefore it is numerically possible to include trajectories with very large periods, while for the chaotic and mixed case, we have to search numerically for periodic orbits and calculate their actions and periods, therefore we have taken larger values of γ in comparison with $1/\bar{g}$ (depending on the number of periodic orbits that we have found for the given parameter α).

2.2.1 Integrable Systems

For integrable systems with f degrees of freedom, it is useful to work with action-angle variables $(\mathbf{I}, \boldsymbol{\phi})$, with each set of actions $\mathbf{I} = \{I_1, \ldots, I_f\}$ defining a phase-space torus. The Hamiltonian can be transformed to $H(\mathbf{I}) = E$, and the frequencies $\mathrm{d}\boldsymbol{\phi}/\mathrm{d}t = \boldsymbol{\omega} = \{\omega_1, \ldots, \omega_f\}$ on the torus $\mathbf{I}$ are given by $\boldsymbol{\omega}(\mathbf{I}) = \boldsymbol{\nabla} H(\mathbf{I})$. Assuming smooth boundaries, the Einstein-Brillouin-Keller (EBK) quantization [4]

$$I_j(n_j) = \hbar(n_j + 1/2)\,, \qquad n_j = 0, 1, 2, , \ldots\,, \qquad j = 1, \ldots, f\,, \qquad (2.11)$$

defines a set of f quantum numbers $\mathbf{n} = (n_1, \ldots, n_f)$. Upon inserting Eq. (2.11) into $E = H(\mathbf{I})$, the EBK spectrum reads

$$E^{\mathrm{EBK}}_{\mathbf{n}} = E^{\mathrm{EBK}}_{n_1,\ldots,n_f} = H(I_1(n_1), \ldots, I_f(n_f))\,. \qquad (2.12)$$

Berry and Tabor in Ref. [25] started from the density of states in terms of the $E^{\mathrm{EBK}}_{\mathbf{n}}$ and converted it, by means of Poisson summation, into a semiclassical trace formula of the type of Eq. (1.15).

The EBK quantization of the integrable QO, Eq. (2.1), with $\alpha = 0$ has been performed in Ref. [80]. The action integral for the one dimensional quartic oscillator is simply

$$\begin{aligned} I_x &= \frac{2}{\pi}\int_0^{(4E)^{1/4}} \sqrt{2\left(E - \frac{x^4}{4}\right)}dx \qquad (2.13)\\ &= \frac{\sqrt{2}}{\pi}(4E)^{3/4}\int_0^1 \sqrt{1-u^4}du = \frac{2\mathbf{K}}{3\pi}(4E)^{3/4}, \end{aligned}$$

where $\mathbf{K} = K(\kappa)$ is the complete elliptic integral of first kind with modulus $\kappa = 1/\sqrt{2}$. By taking $I_x = \hbar(n_x + 1/2)$, one finds the one dimensional EBK - spectrum. Since the Hamiltonian (2.1) is separable for $\alpha = 0$, we can write $E^{\mathrm{EBK}}_{n_x,n_y} = E^{\mathrm{EBK}}_{n_x} + E^{\mathrm{EBK}}_{n_y}$, and the 2-dimensional spectrum is given by

$$E^{\mathrm{EBK}}_{n_x,n_y} = \frac{1}{4}\left(\frac{3\pi\hbar}{2\mathbf{K}}\right)^{\frac{4}{3}}\left[\left(n_x+\frac{1}{2}\right)^{\frac{4}{3}}+\left(n_y+\frac{1}{2}\right)^{\frac{4}{3}}\right], \quad (n_x, n_y = 0, 1, 2, \dots) \tag{2.14}$$

The separate one-dimensional densities of states are

$$g^{\mathrm{sc}}_j(E) = \sum_{n_j=0}^{\infty} \delta\left(E - E^{\mathrm{EBK}}_{n_j}\right), \qquad (j = x, y) \tag{2.15}$$

which are identical due to the symmetry, become after Poisson summation

$$g^{\mathrm{sc}}_j(E) = \frac{T_A(E)}{2\pi\hbar}\sum_{k_j=1}^{\infty}(-1)^{k_j}\cos[k_j S_A(E)/\hbar], \qquad (j = x, y) \tag{2.16}$$

corresponding to the Gutzwiller trace formula for a one-dimensional system. Here

$$S_A(E) = \frac{4}{3}\mathbf{K}(4E)^{3/4}, \tag{2.17}$$

is the action of the primitive A orbit and $T_A(E) = \mathrm{d}S_A(E)/\mathrm{d}E$ its period. The total density of states of the full two-dimensional system can then be written as a convolution integral of the one-dimensional densities:

$$g^{\mathrm{sc}}(E) = \int_0^E g^{\mathrm{sc}}_x(E - E')\, g^{\mathrm{sc}}_y(E')\,\mathrm{d}E'. \tag{2.18}$$

The asymptotic evaluation [87] of this integral in the limit $\hbar \to 0$ yields for the oscillating part [88]

$$\begin{aligned}\delta g(E) \;=\; & 2\left(\frac{2\mathbf{K}}{\pi\hbar}\right)^{\frac{3}{2}}(4E)^{\frac{1}{8}}\sum_{k_x=1}^{\infty}\sum_{k_y=1}^{\infty}(-1)^{k_x+k_y}\frac{k_x k_y}{(k_x^4+k_y^4)^{\frac{5}{8}}}\cos\left[\frac{1}{\hbar}S_{k_x k_y}(E) - \frac{\pi}{4}\right] \\ & + \frac{(4\mathbf{K})^{\frac{3}{4}}}{(\pi\hbar)^{\frac{5}{4}}}(4E)^{-\frac{1}{16}}\sum_{k=1}^{\infty}(-1)^k\frac{1}{k^{\frac{3}{4}}}\cos\left[\frac{k}{\hbar}S_A(E) - \frac{3\pi}{8}\right].\end{aligned} \tag{2.19}$$

The double sum in the first line above contains the contributions from the standard stationary-phase evaluation of the integral. It corresponds exactly to the Berry-Tabor trace formula [25], whereby the two numbers k_x, k_y label the rational tori corresponding to the simply degenerate families of periodic orbits with two-dimensional motion. The actions of these rational tori are given by

$$S_{k_x k_y}(E) = S_A(E)(k_x^4 + k_y^4)^{1/4}. \tag{2.20}$$

The term in the second line of Eq. (2.19) arises from the boundaries of the integral (2.18), corresponding to the A orbits which are one-dimensional librations with all energy in either x ($E' = 0$) or y direction ($E' = E$). Note that the amplitude of this term involves a prefactor $\hbar^{-5/4}$. This is due to the fact that the A orbit undergoes a pitchfork bifurcation at $\alpha = 0$ corresponding to $n = 0$ in Eq. (2.4). (The orbits L_3 born at this bifurcation exist only for $\alpha \leq 0$.) In Ref. [80], identically the same result (2.19) was obtained, whereby the local uniform approximation [47] for the contribution of the bifurcating A orbit was employed [89].

In the upper panel of Fig. 2.6 we compare the semiclassical density of states, Eq. (2.19) (dashed line), with the corresponding quantum-mechanical one (solid line), both coarse-grained with a Gaussian average with width $\gamma = 1$. We find perfect agreement up to very high energies.

We now calculate the symmetry-reduced densities of states by restricting ourselves to the sub-spectra, $E_{\mathbf{n}}^{\mathrm{EBK}}$, of a given irreducible representation. Hereby we can relate the parities of the quantum numbers to the symmetries of the irreducible representations. Thus, we restrict n_x and n_y to be even or odd, according to a given representation. For example, let us take the one-dimensional irreducible representation EES. This corresponds to taking $n_y \leq n_x$ with n_x, n_y even. Then the partial density of states can be calculated as a convolution

$$g_{\mathrm{EES}}^{\mathrm{sc}}(E) = \int_0^E g_{x,E}(E - E')\, g_{y,E}(E')\, \mathrm{d}E'$$

of the one-dimensional densities $g_{j,E}(E)$ defined as in Eq. (2.15), except that only the terms with even n_j are included in the sum. The asymptotic evaluation of the convolution integral leads to (see appendix A)

$$\begin{aligned}\delta g_{\mathrm{EES}}(E) \;=& \left(\frac{\mathbf{K}}{\pi\hbar}\right)^{\frac{3}{2}} (4E)^{\frac{1}{8}} \sum_{k_x,k_y=1}^{\infty} \frac{k_x k_y}{(k_x^4 + k_y^4)^{5/8}} \cos\left[\frac{1}{2\hbar} S_{k_x k_y}(E) - \frac{\pi}{2}(k_x + k_y) - \frac{\pi}{4}\right] \\ &+ \frac{1}{2^{\frac{3}{4}}} \frac{(\mathbf{K})^{\frac{3}{4}}}{(\pi\hbar)^{\frac{5}{4}}} (4E)^{-\frac{1}{16}} \sum_{k=1}^{\infty} \frac{1}{k^{\frac{3}{4}}} \cos\left[\frac{k}{2\hbar} S_A(E) - \frac{\pi}{2}k - \frac{3\pi}{8}\right]. \qquad (2.21)\end{aligned}$$

Again, the first term above corresponds to the Berry-Tabor result for the rational tori, and the second term comes from the bifurcating A orbit.

In the lower panel of Fig. 2.6 we compare the semiclassical and quantum-mechanical density of states, $\delta g_{\mathrm{EES}}(E)$, coarse-grained with a Gaussian average with width $\gamma = 1$. Again the agreement is nearly perfect. The same procedure can be followed for all symmetry classes. In Fig. 2.7 we show the numerical results for the symmetry representation OOS, coarse-grained with a Gaussian average with

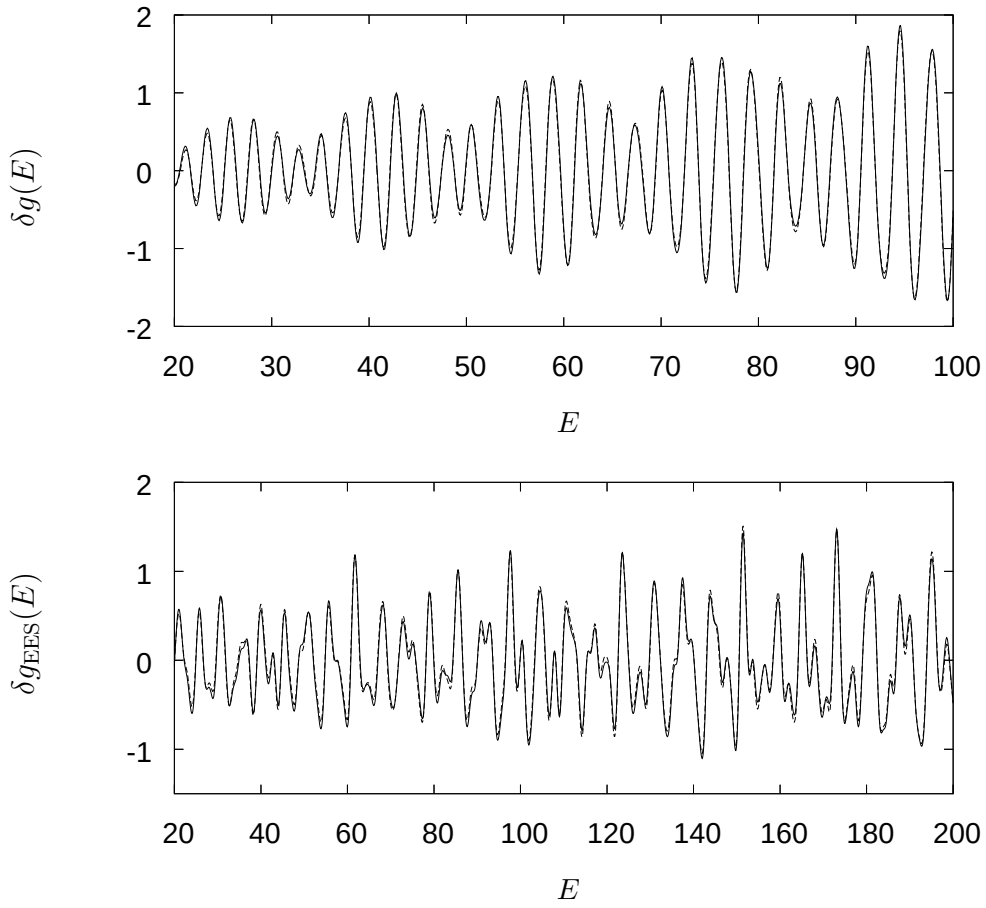

Figure 2.6: Upper panel: total density of states for $\alpha = 0$ coarse-grained by a Gaussian with width $\gamma = 1$ (in this energy range $\gamma = 1 \sim 0.08\bar{g}^{-1}$, and $\sim 0.7\bar{g}^{-1}$ for the total and reduced densities, respectively). Lower panel: symmetry-reduced density of states for the representation EES, see text. Solid line: quantum result, dashed line: semiclassical result, Eq. (2.19).

width $\gamma = 1$, and the semiclassical analogous to Eq. (2.21) for this symmetry class, the agreement is again very good.

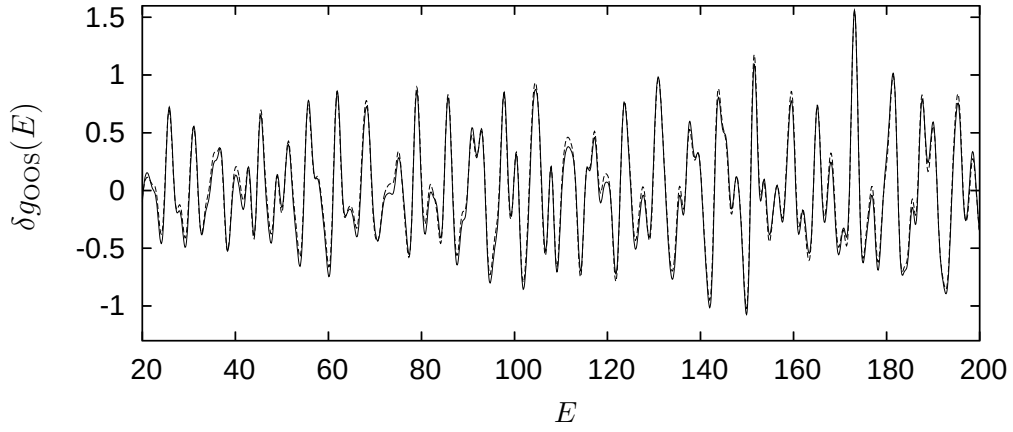

Figure 2.7: Symmetry-reduced density of states, coarse-grained by a Gaussian with width $\gamma = 1$, for the representation OOS. Solid line: quantum result, dashed line: semiclassical result.

2.2.2 Isolated orbits

For systems with isolated orbits, the corresponding symmetry-reduced semiclassical trace formulae have been derived in Refs. [90, 91, 92]. The symmetry-reduced densities of states for isolated orbits have been derived in Ref. [90, 91] by projecting the semiclassical Green function onto the irreducible representations and reducing the classical dynamics to the fundamental domain.

Let us recall the analysis in Ref. [90]: the projected Green function $G_m(\mathbf{r}, \mathbf{r}', E)$ can be written in term of the full Green function as

$$G_m^+(\mathbf{r}, \mathbf{r}', E) = \frac{d_m}{|\mathrm{G}|} \sum_{g \in \mathrm{G}} \chi_m(g) G^+(g \cdot \mathbf{r}, \mathbf{r}', E). \tag{2.22}$$

Here d_m is the dimension of the irreducible representation, $g \in \mathrm{G}$ are the symmetry operators under which the Hamiltonian is invariant, $\chi_m(g)$ is the character of g in the irreducible representation m, and $|\mathrm{G}|$ is the order of the symmetry group G.

The semiclassical reduced Green function involves sums of trajectories starting at $\mathbf{r}'$ and ending at a point related by symmetry at $\mathbf{r}$. The sum can be simplified by defining trajectories in the reduced phase space, which is constructed by finding the smallest volume that under symmetry operations tessellates the full space and identifying the points at the boundary related by symmetry. For the quartic oscillator the smallest volume that tessellates the full phase space corresponds to $\{(\mathbf{q}, \mathbf{p}) : 0 \leq q_x \leq q_y\}$, and the boundary identifications are

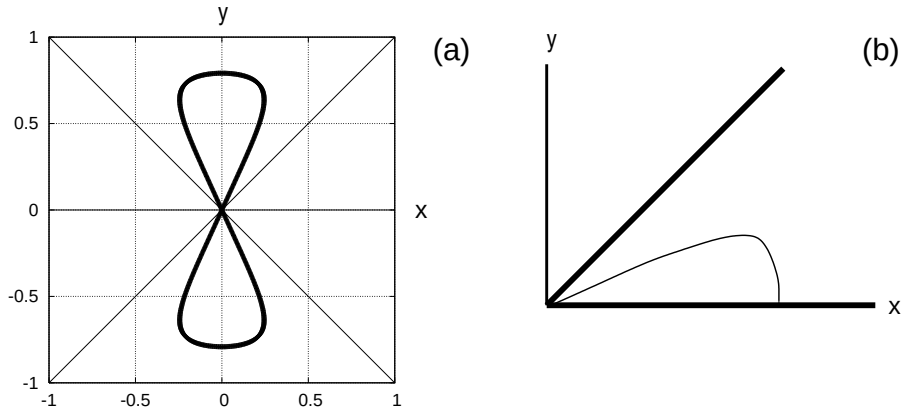

Figure 2.8: (a) The R_4 periodic orbit. (b) The symmetry reduced R_{4r} orbit.

$(q_x, 0, p_x, p_y) \to (q_x, 0, p_x, -p_y)$ and $(q_x, q_x, p_x, p_y) \to (q_x, q_x, p_y, p_x)$. The dynamics of the trajectory in the original phase space can be related to the dynamics in the reduced space.

The dynamics in the reduced phase space is constructed as follows: (i) the initial condition of the original orbit $\mathbf{x}'$ in the full phase space $\mathcal{M}$, is projected into the reduced phase space $\bar{\mathcal{M}}$ to $\mathbf{x}'_r$, (ii) inside the reduced phase space the dynamics is given according to the equations of motion of $\mathcal{M}$, (iii) when $\mathbf{x}_r(t)$ reaches a boundary at $\tilde{\mathbf{x}}$ it is continued to the point related by symmetry to $\tilde{\mathbf{x}}$. According to this all the trajectories related by symmetry in P are mapped into the same trajectory in $\bar{\mathcal{M}}$, but the symmetry operations that relate them are different for each trajectory, therefore the procedure can be inverted. The lifted trajectory $\mathbf{x}(t)$ can be constructed from the reduced one $\mathbf{x}_r(t)$ by keeping the information of the symmetry operations $g(t)$ relating them, which can be computed from the initial symmetry operation to map $\mathbf{x}'$ in $\mathcal{M}$ and multiplying the elements associated with the bounces at the boundaries.

Because we are considering point symmetries, the implementation in configuration space is straightforward. For example, consider the trajectory R_4 depicted in Fig. 2.8(a) , which is a periodic orbits for the QO at $\alpha = 9$. In the full phase space, there are 4 copies of this trajectory due to the symmetries: the one shown in Fig. 2.8(a), this one rotated by $\pi/2$ and two related to them by time reversal symmetry. The reduced trajectory of all of them is depicted in Fig. 2.8(b). The different four copies can be obtained from the original one by 'lifting' it with different operations.

This allows one to write the semiclassical reduced Green function only in terms

of trajectories in the reduced configuration space:

$$G_m^{\rm sc}(\mathbf{r},\mathbf{r}',E)=\frac{d_m}{|\mathrm{G}|}\frac{1}{i\hbar(2\pi i\hbar)^{(f-1)/2}}\sum_{j:\bar{\mathbf{r}}'\to\bar{\mathbf{r}}}\chi_m(g_jh'h^{-1})\bar{D}_j\mathrm{e}^{i\bar{S}_j/\hbar-i\bar{\mu}\pi/2}, \qquad (2.23)$$

where the bars indicate that the actions, the determinant and the phases are calculated in the fundamental domain, and $\mathbf{r}'=h'\bar{\mathbf{r}}'$, $\mathbf{r}=h\bar{\mathbf{r}}$, h^{-1} is the inverse of h and g_j correspond to the product of the operations applied in the bounces at the boundaries of the fundamental domain.

The reduced density of states in the irreducible representation m is obtained by taking the trace over Eq. (2.23) in stationary phase approximation:

$$\delta g_m^{\rm sc}(E)=\frac{d_m}{\hbar}\sum_l\frac{\overline{T}_l}{|K_l|}\sum_r\frac{\chi_m(g_l^r)}{|\overline{\mathrm{M}}_l^r-\mathrm{D_l}|^{\frac{1}{2}}}\cos\Big[\frac{r}{\hbar}\overline{S}_l(E)-\frac{\pi}{2}\overline{\sigma}_{rl}\Big]. \qquad (2.24)$$

Again the bars in Eq. (2.24) indicate that actions, periods, stability matrices and Maslov indices are calculated in the fundamental domain, while g_l^r is the operator that relates the r-th repetition of the reduced orbit l with its original lifted into the the whole phase space. $|K_l|$ is the order of the group K_l which leaves every point of the orbit l invariant. By the definition of the fundamental domain, this is the identity for orbits that stay in the interior of the fundamental domain, while there can exist more than one operation for orbits that lie on the boundaries (for example, the librational orbit labeled A is point invariant under two operations: the identity and the reflection σ_1). The matrix D_l is block-diagonal in coordinates with blocks given by $d(gq)/dq$ with $g\in K$. This matrix is again the identity for interior orbits, but can be different for boundary orbits. This correction for boundary orbits was first done in Ref. [91], where it was noticed that the evaluation the trace over orbits at the boundary requires a special treatment.

It is usually easier to solve the equations of motion in the whole space than in the fundamental domain, where one has hard-wall reflections. Given the classical quantities for the total space, the task is then to find their reduced counterparts (marked with bars in (2.24)). Take a Hamiltonian of the form $H(\mathbf{p},\mathbf{r})=\mathbf{p}^2/2m+V(\mathbf{r})$ which is invariant under the point-group symmetry G. Suppose that the subgroup H leaves the l orbit invariant (not pointwise), then the l orbit can be divided into $|H|$ copies related by symmetry [93]. There will be $|\mathrm{G}|/|H|$ copies of the orbit in the full phase space (if we consider time reversal, then there are $2|\mathrm{G}|/|H|$ copies of orbits without time-reversal symmetry). Therefore the lifted orbit should be equivalent to the $|H|=r$-th repetition of the reduced orbit (or to the $|H|/2$-th repetition for time-asymmetric orbits, which become librating orbits in the fundamental domain, and the $|H|/|K|$-th repetition for boundary orbits). Going back to our example of the R_4 orbits: in this case $H=\{E,\sigma_2\}$ and the

period and action of the lifted orbit are the same as for the second repetition of the reduced one. All the classical quantities are related as

$$S_l(E) = r\overline{S}_l(E)\,, \qquad T_l(E) = r\overline{T}_l(E)\,, \qquad \sigma_l = r\overline{\sigma}_l\,, \qquad \mathrm{M}_l = \overline{\mathrm{M}}_l^r\,, \tag{2.25}$$

since they are invariant under point transformations. The only difficulty remains to find out which of the roots of M_l must be taken. E.g., for $|H| = 2$ we have $\mathrm{M}_l = \overline{\mathrm{M}}_l^2$. Thus, if the eigenvalues of M_l are $\mathrm{e}^{\pm u_l}$, those of $\overline{\mathrm{M}}_l$ can be $\pm\mathrm{e}^{\pm u_l/2}$. We have found a rule in order to calculate the correct phases entering in the reduced density of states.

We know that for smooth two-dimensional Hamiltonian systems, hyperbolic orbits always have even Maslov indices, while elliptic and inverse-hyperbolic orbits always have odd Maslov indices [94]. We have observed that this rule can be reversed in the fundamental domain.

This is illustrated in Fig. 2.9 for the case of a single reflection symmetry with respect to the x axis. Then the fundamental domain is the upper plane ($y \geq 0$). We have calculated the Maslov index $\overline{\sigma}$ using the method of Creagh *et al.* [95] (as explained in Ref. [23], App. D) and verified that it is, indeed, either the same as for the lifted orbit for orbits without this symmetry, or half of it for orbits with reflection symmetry. However, the sign of the eigenvalues did not follow Sugita's rule [94]. This rule can, however, be applied to $\overline{\sigma} - \mathrm{mod}(R, 2)$, where R indicates the number of hard-wall reflections at the boundaries of the fundamental domain. Thus, if this number is odd, the rule is reversed.

We have calculated the reduced density of states (2.24) for the representation EES in the QO at $\alpha = 9$ [96]. The result is shown in Fig. 2.10 for Gaussian smoothing with width $\gamma = 4$. A considerable agreement between the semiclassical (dotted line) and the quantum-mechanical result (solid line) is achieved.

A closer way to compare the quantum and semiclassical spectral density in non-integrable systems is considering the Fourier transform of them. For systems with scaling properties, like the QO, it is possible to find the spectrum of actions of orbits that contribute to the density of states by taking the Fourier transform of the density of states using a suitable function $f(E)$:

$$\delta\tilde{g}_m(S) = \int_0^\infty \delta g_m(E) \cos\left(f(E)S/\hbar\right) dE. \tag{2.26}$$

In the QO potential the action of all trajectories scale like $S_j(E) = S_j(E_0)(E/E_0)^{3/4}$, where E_0 is some fixed energy, therefore the best choice for $f(E)$ is $f(E) = (E/E_0)^{3/4}$. We can replace Eq. (2.24) on Eq. (2.26) and make the change of variables $u = f(E)$. The remaining integral is easy to perform, taking into account the all the properties of the orbits like the stability, and the operators that relate

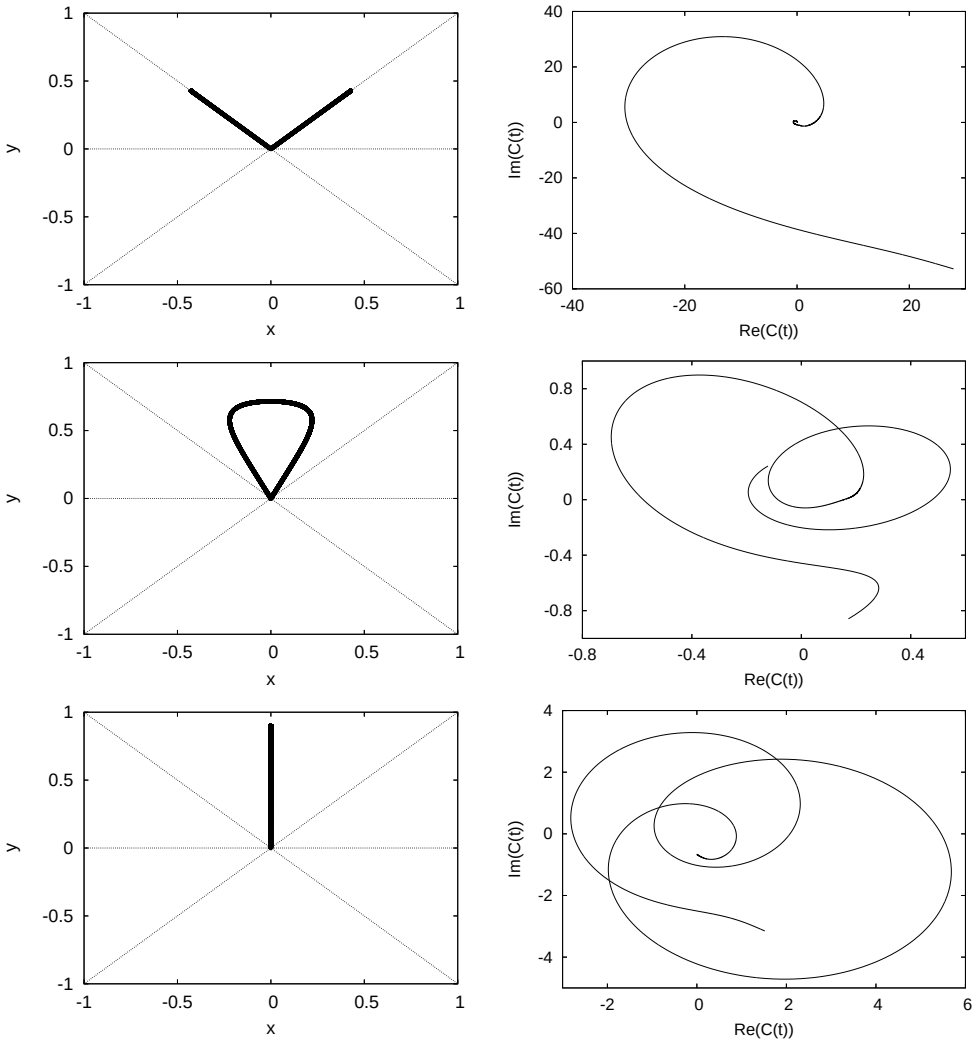

Figure 2.9: Calculation of Maslov indices for some reduced orbits of the QO at $\alpha = 9$, considering only the reflexion symmetry at the x axis. *Left panels:* reduced orbits in (x, y) plane. *Right panels:* evaluation of the Maslov index $\overline{\sigma}$ which corresponds to the winding number of the complex number $C(t)$ over one period (cf. [95]). *Top panels:* librational orbit B_2 along the diagonal. Here the length of the reduced orbit is the same as that of the lifted orbit, and their Maslov indices are equal. *Center panels:* orbit R_4. Here the reduced orbit is half of the lifted orbit and its Maslov index is $\overline{\sigma} = 2$ (i.e., half of the total σ) but $\mathrm{Tr}\,\mathrm{M}$ is negative in spite of the even Maslov index. *Bottom panels:* orbit A_6. The reduced orbit is again half of the total orbit, and so is the Maslov index. But $\mathrm{Tr}\,\mathrm{M}$ is positive in spite of the odd Maslov index.

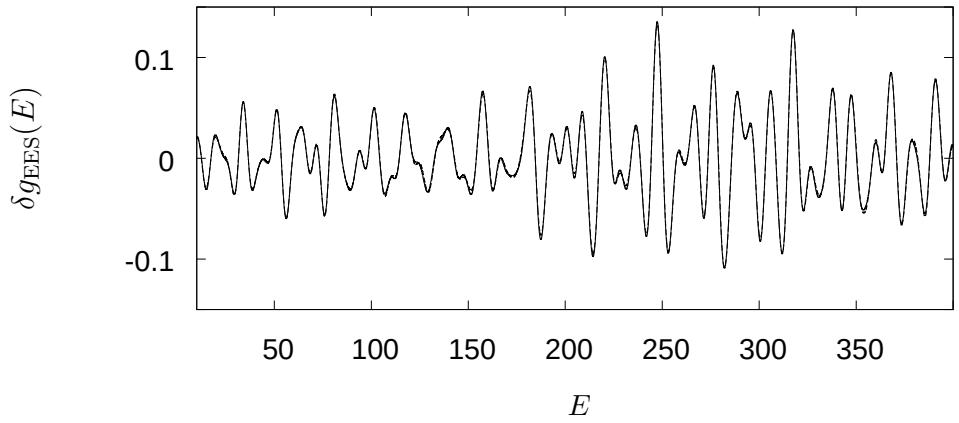

Figure 2.10: Reduced density of states for the representation EES in the QO at $\alpha = 9$ after Gaussian averaging with width $\gamma = 4$ ($\sim 5.6\bar{g}^{-1}$). The solid line shows the quantum result and the dotted line the semiclassical calculation using Eq. (2.24) with 90 periodic orbits.

the reduced orbit with the lifted one, are energy independent. The result is given by

$$\delta\tilde{g}_m^{\rm sc}(S) = \frac{\pi d_m}{2}\sum_l \frac{\overline{S}_l(E_0)}{|K_l|}\sum_r \frac{\chi_m(g_l^r)}{|\overline{\rm M}_l^r - {\rm D_l}|^{\frac{1}{2}}}\delta\left(r\overline{S}_l(E_0) - r\overline{S}\right)\cos\left(\frac{\pi}{2}\overline{\sigma}_{rl}\right). \quad (2.27)$$

This allows us to compare the quantum mechanical density with the semiclassical by looking at the positions and amplitudes of the Fourier spectrum, as shown in Fig. 2.11, where we can also observe the relevance of each periodic orbit individually. In Fig. 2.11 we compared the action spectrum of the reduced density of states, coarsed grained with $\gamma = 2$, showing good agreement in the action as well as in the amplitude with the semiclassical one.

2.3 Semiclassical approximation for bifurcating orbits

We have indicated in the introduction that near bifurcations of periodic orbits, Gutzwiller's trace formula fails and the semiclassical approximation has to be modified. The librational orbit A has isochronus pitchfork bifurcations as the parameter α is varied. The collective contribution of this type of bifurcation scenario has been considered in Ref. [48]. The normal form in Eq. (1.26) is a quartic function in the coordinates perpendicular to the trajectory given by $\Phi(q,p,E) = S_o(E) - \sigma p/2 - aq^4 - \epsilon q^2$, where ϵ is a parameter which is zero at the bifurcation, σ is a sign factor, and a is a parameter which depends on the potential. A more detail discussion on the evaluation of such integrals will be found in Chapter 4 in a slightly different context. For the moment we will restrict

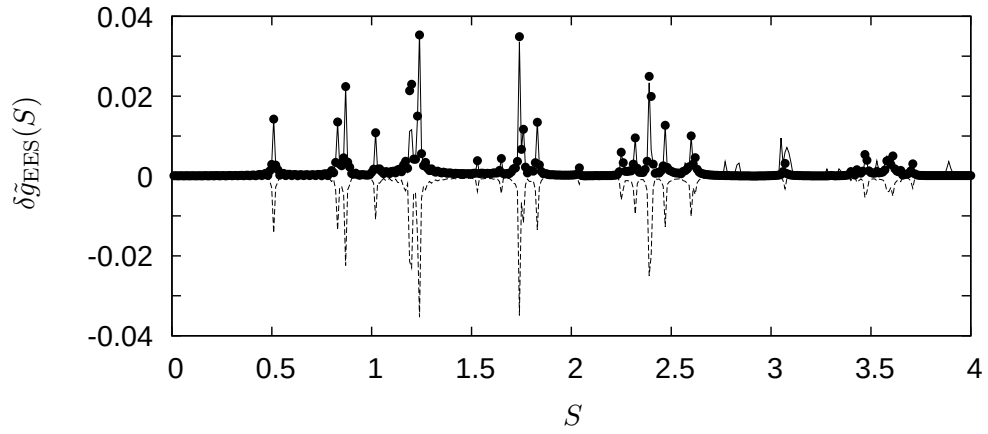

Figure 2.11: Action spectrum for the reduced density of states for $\alpha = 9$, coarsed grained with $\gamma = 2$ ($\sim 2.8\bar{g}^{-1}$). The solid curve corresponds to the quantum mechanical numerical calculation, the dots to the semiclassical calculation Eq. (2.27), also shown in dashed line multiply by -1.

to recall the result of Ref. [48] for the A orbit near α_4 and compare with the numerical calculations.

The contribution of the bifurcating (A_6) orbit to the total density of states, together with that of the L_6 orbits born at the bifurcation, is given in the *global uniform approximation*. For a scenario where there is a single unstable orbit before the bifurcation, which becomes stable afterwards as two new unstable orbits are born the parameters in Ref. [48] are $\sigma = +1$, $a < 0$, $\sigma_1 = -1$ and $\nu = \sigma_{A_6,r} = 6r$.

The global uniform approximation reads

$$\begin{aligned}\delta g^{un}_{A+L}(E) \;=\; & \Re e\,\frac{1}{\pi\hbar}\left|\frac{\pi\Delta S}{2\hbar}\right|^{1/2}\exp\left(\frac{i}{\hbar}S_+ - i3r\pi - i\frac{\pi}{4}\right)\times \\ & \times\left\{\overline{A}\left[\sigma_2 J_{1/4}\left(\frac{|\Delta S|}{\hbar}\right)e^{-i\frac{\pi}{8}} + J_{-1/4}\left(\frac{|\Delta S|}{\hbar}\right)e^{i\frac{\pi}{8}}\right] + \right. \\ & \left. +\Delta A\left[J_{3/4}\left(\frac{|\Delta S|}{\hbar}\right)e^{-3i\frac{\pi}{8}} + \sigma_2 J_{-3/4}\left(\frac{|\Delta S|}{\hbar}\right)e^{3i\frac{\pi}{8}}\right]\right\}. \quad (2.28)\end{aligned}$$

Here $\Delta A = (A_L - \sqrt{2}A_A)/2$, $\overline{A} = (A_L + \sqrt{2}A_A)/2$, $S_+ = (S_L + S_A)/2$, $\Delta S = (S_L - S_A)/2$, J_n are the Bessel functions of the first kind, $A_j(E)$ and $S_j(E)$ are the Gutzwiller amplitudes and actions of the isolated A and L orbits, respectively, away from the bifurcation, r is their repetition number, and $\sigma_2 = \mathrm{sign}(\alpha - \alpha_4)$. At the bifurcation ($\alpha = \alpha_4 = 10$), the local uniform approximation becomes

$$\delta g^{loc}_{A+L}(E) \;=\; \frac{T_A\Gamma(\frac{1}{4})}{2\pi\sqrt{2\pi}\,\hbar^{5/4}|a|^{1/4}r^{3/4}}\cos\left[\frac{S_A}{\hbar} - 3r\pi - \frac{\pi}{8}\right]. \quad (2.29)$$

Here $T_A(E)$ is the period of the primitive A orbit, and a is a normal form parameter which we determined numerically from the local expansion (cf. also Ref. [80, 48]).

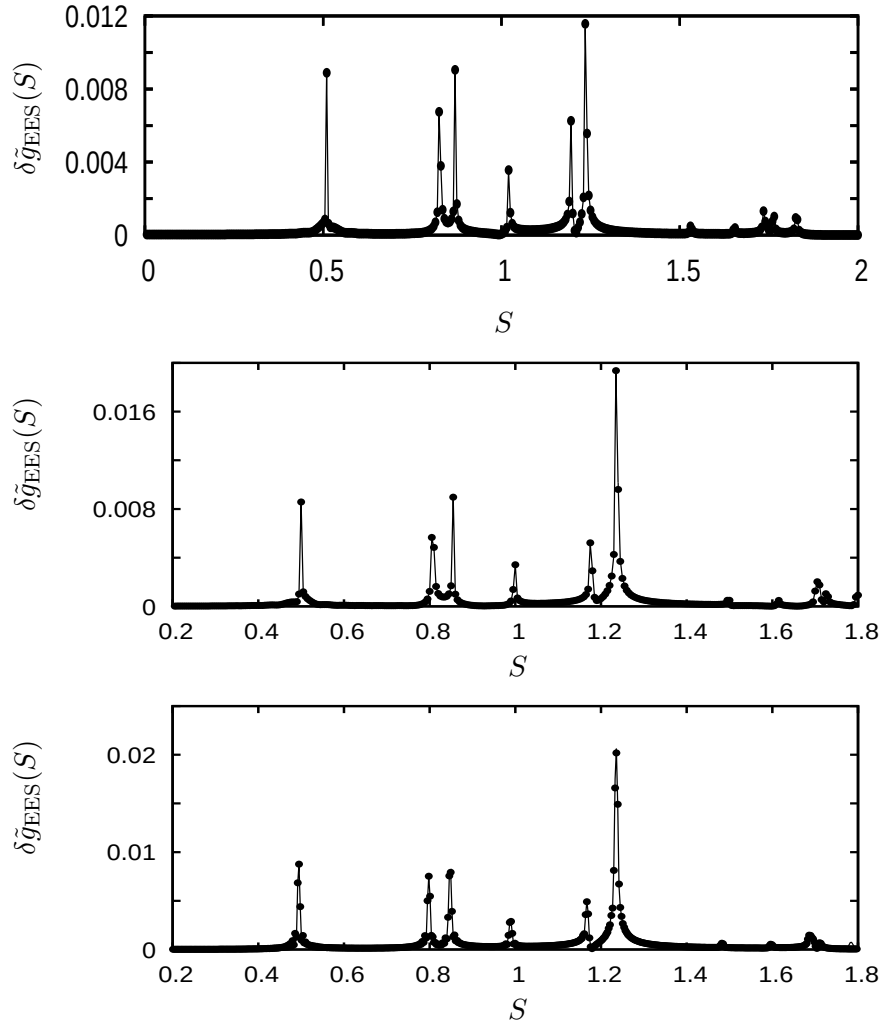

Figure 2.12: Action spectrum for the reduced density of states coarsed gained with $\gamma = 6$ ($\sim 8.4\bar{g}^{-1}$). Upper panel: the quantum mechanical (full line) and semiclassical (dots) comparison for $\alpha = 9$ with Eq. (2.27). Middle panel: QM and semiclassical for $\alpha = 10$ calculated from the Fourier transform of the local uniform approximation Eq. (2.31). Bottom: QM and semiclassical for $\alpha = 10.5$ using the global uniform approximation Eq. (2.30).

In order to calculate the corresponding symmetry-reduced density of states of a bifurcation orbit, we proceed in a similar way as for the case of isolated orbits. In this particular case, we take into account that the librational orbit A_6 is at the boundary of the fundamental domain. Therefore, it gives two contributions to the reduced density, each one corresponding to the two operators that leave each point of the orbit invariant: the identity and the reflection σ_1. In the first case the matrix D_I is the 2×2 identity matrix, the corresponding contribution has a prefactor $1/\sqrt{|\mathrm{Tra}\bar{M}_A - 2|}$, divergent at the bifurcation. In the second situation, the matrix D_{σ_1} is minus the identity matrix, yielding a contribution with an amplitude $1/\sqrt{|\mathrm{Tra}\bar{M}_A + 2|}$, which does not diverge at the bifurcation. This last term cancels out for the total density of states, since the sum over characters of the group operations related with the unfolding is equal to zero.

We replace the contribution corresponding to δg_{m} by eqs (2.28) and (2.29) with amplitudes and periods calculated in the fundamental domain, thus

$$\begin{aligned}
\delta g^{A+L}_{\mathrm{EES}}(E) \;=\; & \Re e\, \frac{1}{2\pi\hbar} \left| \frac{\pi \Delta S}{4\hbar} \right|^{1/2} \exp\left(\frac{i}{2\hbar} S_+ - i 3 r \frac{\pi}{2} - i \frac{\pi}{4} \right) \times \\
& \times \left\{ \frac{\overline{A}}{2} \left[\sigma_2 J_{1/4}\left(\frac{|\Delta S|}{2\hbar} \right) e^{-i\frac{\pi}{8}} + J_{-1/4}\left(\frac{|\Delta S|}{2\hbar} \right) e^{i\frac{\pi}{8}} \right] + \right. \\
& \left. + \frac{\Delta A}{2} \left[J_{3/4}\left(\frac{|\Delta S|}{2\hbar} \right) e^{-3i\frac{\pi}{8}} + \sigma_2 J_{-3/4}\left(\frac{|\Delta S|}{2\hbar} \right) e^{3i\frac{\pi}{8}} \right] \right\} \\
& + \frac{1}{4\pi\hbar} \frac{T_A}{\cos(r\bar{\theta})} \cos\left(\frac{r}{2\hbar} S_A - \bar{\sigma}_A \frac{\pi}{2} \right), \qquad (2.30)
\end{aligned}$$

where $\bar{\sigma}_A = r(\sigma_A - 1)/2 + 2[|r\bar{\theta}/\pi|]$, where $\bar{\theta}$ is the stability angle of the reduced orbit and $\sigma_A = 7$ after the bifurcation. The corresponding reduced local density of states will be given by

$$\begin{aligned}
\delta g^{loc}_{\mathrm{EES,A+L}}(E) \;=\; & \frac{T_A \Gamma(\frac{1}{4})}{8\pi\sqrt{2\pi}\,\hbar^{5/4} |\bar{a}|^{1/4} r^{3/4}} \cos\left[\frac{S_A}{2\hbar} - 3r\frac{\pi}{2} - \frac{\pi}{8} \right] \\
& + \frac{1}{4\pi\hbar} T_A \cos\left(\frac{r}{2\hbar} S_A - 3r\frac{\pi}{2} \right). \qquad (2.31)
\end{aligned}$$

A numerical comparison for the semiclassical power spectrum with the quantum calculation of the reduced density of states is shown in Fig. 2.12 for $\alpha = 9$, $\alpha = 10$ and 10.5. The highest peak (at $S \approx 1.2$) corresponds to the contribution of the $A + L$ orbits. We observe an excellent agreement with the semiclassical prediction. The contribution at α_4 is strongly enhanced by the bifurcation. This enhancement still persists at $\alpha = 10.5$, where Gutzwiller trace formula would predict a smaller amplitude. In the next chapter we will study the effect of this bifurcation in the spectral statistics of the QO, and see the relevance of the enhancement.

Chapter 3

Effect of pitchfork bifurcations in the spectral statistics

In the present chapter we study the role of pitchfork bifurcations on the spectral statistics in the QO. We show that bifurcations of short orbits have a considerable effect on the spectral rigidity and the spectral form factor respectively, even in the almost chaotic case. The spectral form factor has been the referred quantity to study spectral statistics in the context of quantum chaos. However, in a first semiclassical derivation of universal spectral properties, Berry in Ref. [19] considered the so-called rigidity or stiffness Δ [10]. This measure is closely related to the spectral form factor, but it is more appropriate to study non-universal features coming from short periodic orbits. We will mainly focus on this quantity and, at the end of the chapter, we will consider the form factor. We first introduce the rigidity and recall the semiclassical approximation for it. We then show numerical calculations for the QO oscillator for different regularity parameters. Afterwards we quantitatively analyze deviations of the spectral rigidity from universality employing uniform approximations. We show, in particular, that pairs of orbits with an action difference smaller than Planck's constant $\hbar$, born at a pitchfork bifurcation, yield important non-diagonal contributions to the spectral form factor and the rigidity. The deviations from the quantum chaotic universality are found to be most significant *after*, rather than *at* the bifurcation.

3.1 Spectral Rigidity

The spectral rigidity is defined as the local average of the mean-square deviation of the staircase function

$$N(E) = \sum_n \theta(E - E_n) \tag{3.1}$$

from its best-fit straight line over an energy range corresponding to L states with mean level spacing $\bar{g}$:

$$\Delta(L) = \Big\langle \min_{A,B} \frac{\bar{g}}{L} \int_{-L/2\bar{g}}^{L/2\bar{g}} \mathrm{d}\epsilon \, [N(E+\epsilon) - A - B\epsilon]^2 \Big\rangle. \tag{3.2}$$

The relation to the spectral form factor is given through

$$\Delta(L) = \frac{1}{2\pi^2} \int_0^\infty \frac{K(\tau)}{\tau^2} p(\pi L \tau) d\tau, \tag{3.3}$$

where $p(x)$ is a weight function that will be explicitly given in the next section, satisfying $p(0) = 0$ and $p(x) \approx 1$ as $x \to \infty$.

The quantity $\Delta(L)$ measures spectral correlations over energy distances of order L. For an uncorrelated Poisson spectrum the universal prediction is

$$\Delta^{\mathrm{Poisson}}(L) = L/15\,, \tag{3.4}$$

while for a chaotic system it is approximately given by

$$\Delta^{\mathrm{RMT}}(L) = \frac{\beta}{2\pi^2} \log L - D\,, \tag{3.5}$$

where D is a constant, $\beta = 1$ for systems without time reversal symmetry (GUE statistics) and $\beta = 2$ for systems with time reversal symmetry (GOE statistics). This universal behaviour has been observed up to correlation lengths $L < L_{\max} = 2\pi\hbar\bar{g}/T_{\min}$, where $T_{\min}$ is the period of the shortest orbit.

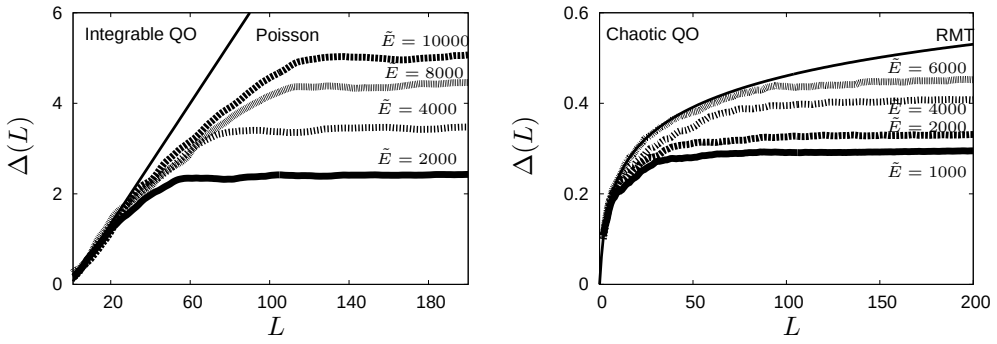

Figure 3.1: *Left panel*: Rigidity for $\alpha = 0$, where the QO is integrable. *Right Panel*: Rigidity for $\alpha = 9$, where the QO shows hard chaos. With increasing (unfolded) energy $\tilde{E}$ the numerical data converge to the universal Poisson (left panel) and random matrix predictions (right panel) marked as full lines.

In Fig. 3.1 we show the numerical results for the QO in an integrable and an almost chaotic regime, respectively, compared with the corresponding predictions Eqs. (3.4, 3.5). The L range, in which the numerical data coincide with the

universal predictions, increases with increasing energy, i.e., by approaching the semiclassical limit.

For a system with mixed classical dynamics it has been conjectured that the statistics will be a superposition of Poisson and RMT contributions [43, 44], parametrized as

$$\Delta(L) \approx \Delta^{\mathrm{Poisson}}((1-q)L) + \Delta^{\mathrm{RMT}}(qL), \tag{3.6}$$

were q is the the fraction of the phase space corresponding to the chaotic sea. Since both statistics are monotonously increasing functions, we expect that the more regular the system is, the larger is the rigidity. This approximation can work very well is some situations, as shown in Fig. 3.2. We will see in the following that it no longer holds when bifurcations of short periodic orbits take place.

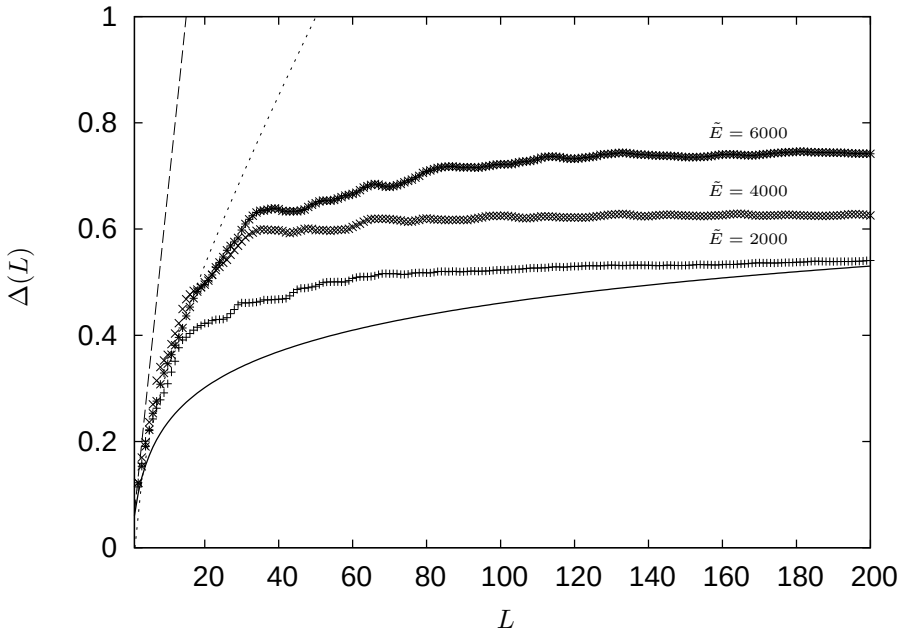

Figure 3.2: Rigidity for the mixed QO at $\alpha = 5$, RMT prediction (bold line), Poisson (dashed) and phase space sum rule Eq. (3.6) (dotted line).

3.2 Semiclassical theory for the spectral rigidity

The semiclassical theory for the rigidity was developed in Ref. [19] for the two limiting cases of complete chaoticity and full regularity (integrability). The procedure is the following: by energy integration of the semiclassical approximation

to the density of states, Eq. (1.15), one obtains an expression for the number of states. By inserting this expression into the definition of the rigidity one finds

$$\Delta(L) = \frac{1}{2\hbar^{2\mu}} \Big\langle \sum_j \sum_k \frac{A_j A_k}{T_j T_k} \cos\left[\frac{1}{\hbar}(S_j - S_k) + \frac{\pi}{2}(\sigma_j - \sigma_k)\right] G(y_j, y_k) \Big\rangle, \qquad (3.7)$$

where $T_j = dS_j/dE$ are the periods,

$$y_j = \frac{LT_j}{2\hbar\bar{g}} = \pi \frac{L}{L_{\max}} \frac{T_j}{T_{\min}}\,, \qquad (3.8)$$

and

$$G(x,y) = F(x-y) - F(x)F(y) - 3F'(x)F'(y), \qquad (3.9)$$

$$F(x) = \frac{1}{x}\sin x = j_0(x)\,. \qquad (3.10)$$

The main contributions come from pairs of orbits whose action difference is smaller than $\hbar$, so that y_j can be chosen to be equal to y_k in the argument of G:

$$\Delta(L) = \frac{1}{2\hbar^{2\mu}} \Big\langle \sum_j \sum_k \frac{A_j A_k}{T_j T_k} \exp\left[\frac{i}{\hbar}(S_j - S_k) + \frac{\pi}{2}(\sigma_j - \sigma_k)\right] p(\bar{y}_{j,k}) \Big\rangle, \qquad (3.11)$$

where $\bar{y}_{jk} = \frac{1}{2}(y_j + y_k)$ and $p(x) = G(x,x)$. The function $p(y)$ (see Fig. 3.3) selects

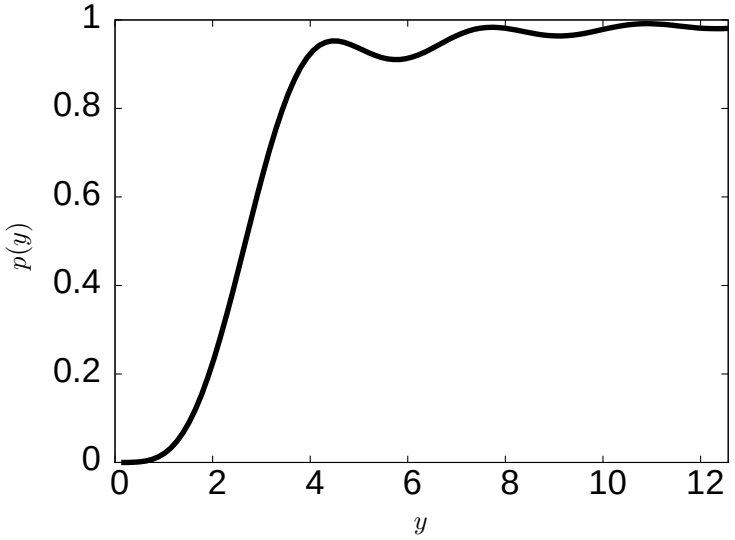

Figure 3.3: Window function $p(y)$, see text.

the orbits that contribute to the double sum. If $L \ll L_{\max}$ then $p(y)$ is almost unity only for long orbits, while for $L > L_{\max}$ the function is almost unity for all y, and the most important contributions to $\Delta(L)$ come from short orbits due to the

factor $1/T^2$. Since we are interested in studying the effects of a bifurcation of one of the shortest orbits, we are going to concentrate on the saturation behaviour, which corresponds basically to the first moment of the staircase function.

The semiclassical spectral rigidity as well as the spectral form factor is determined by a double sum over pairs of periodic orbits. The semiclassical limit $\hbar \to 0$ means that the typical classical actions of these paths are very large compared with $\hbar$, so that the energy average will strongly suppress the contributions of most pairs of orbits. The diagonal approximation was considered in Ref. [19]. For the following approach, the diagonal approximation together with the effect of bifurcations will be enough to reproduce the numerical quantum results.

3.3 Rigidity for the Integrable QO

For the QO at $\alpha = 0$, the tori amplitudes $A_{kx,ky}$ are given by

$$A_{kx,ky} = \left(\frac{\mathbf{K}}{\pi}\right)^{3/2} (4E)^{1/8} \frac{k_x k_y}{(k_x + k_y)^{5/8}} \tag{3.12}$$

for the irreducible representation EES. For integrable systems the contribution of the non-diagonal terms $j \neq k$ in the sum (3.7) will vanish after averaging, due to destructive interference. For this system, due to the degeneracy in the actions, the orbits that contribute to the double sum are those which satisfy $n_x^4 + n_y^4 = n_x'^4 + n_y'^4$. Inserting the amplitudes for the tori and summing only over terms with the same actions we have

$$\Delta(L) = \frac{(4E)^{3/4}}{2^4 \pi^3 \hbar \mathbf{K}} \sum_{k_x,k_y=1}^{\infty} \frac{k_x k_y}{l_k^7}\, p(\bar{y}_{k_x,k_y}) \sum_{n_x,n_y=1}^{\infty} n_x n_y \delta_{l_k - l_n}\,, \tag{3.13}$$

where $l_k = (k_x^4 + k_y^4)^{1/4}$, $l_n = (n_x^4 + n_y^4)^{1/4}$, and δ is the Kronecker delta.

With this expression, we can semiclassically reproduce very well the Δ statistics, as is shown in Fig. 3.4.

We have neglected here the contribution of the A orbit which undergoes a pitchfork bifurcation. We have checked that its contribution is negligible, since its amplitude in the PO expansion goes like $\hbar^{-5/4}$ (a power one quarter larger than an isolated orbit) compared with that ($\hbar^{-3/2}$) of the tori. For the saturation we can take $p(y_{k_x,k_y}) = 1$. Then the energy dependence of the saturation value Δ_∞ goes like $E^{3/4}$, as seen from Eq. (3.13).

In the left panel of Fig. 3.5 we depict the saturation value obtained from the quantum spectrum (dots), which is well reproduced by the semiclassical prediction (solid line). For the chaotic case, RMT gives a saturation value Δ_∞ that behaves

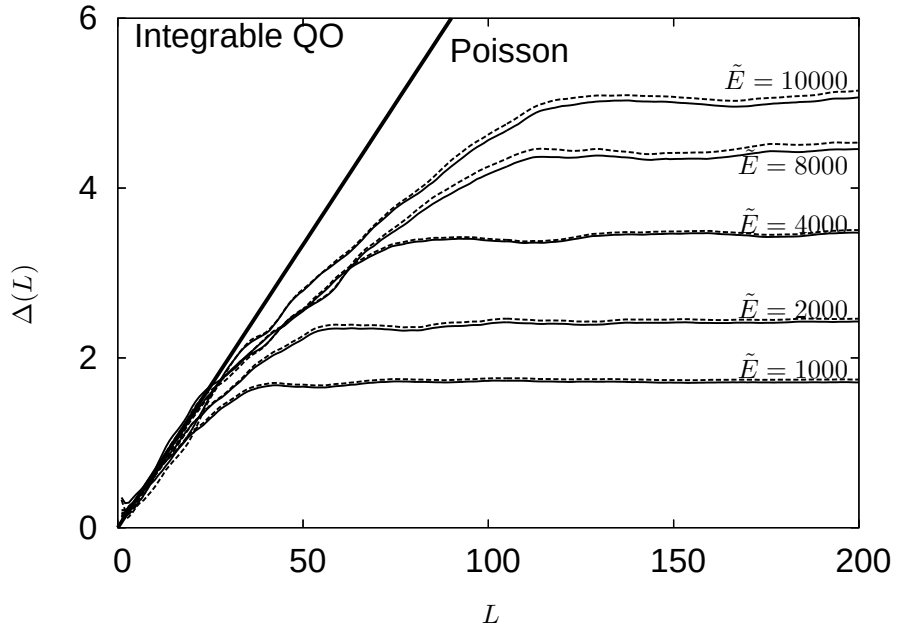

Figure 3.4: Semiclassical (dashed lines) and quantum results (solid lines) for the spectral rigidity $\Delta(L)$ for different values of $\tilde{E}$.

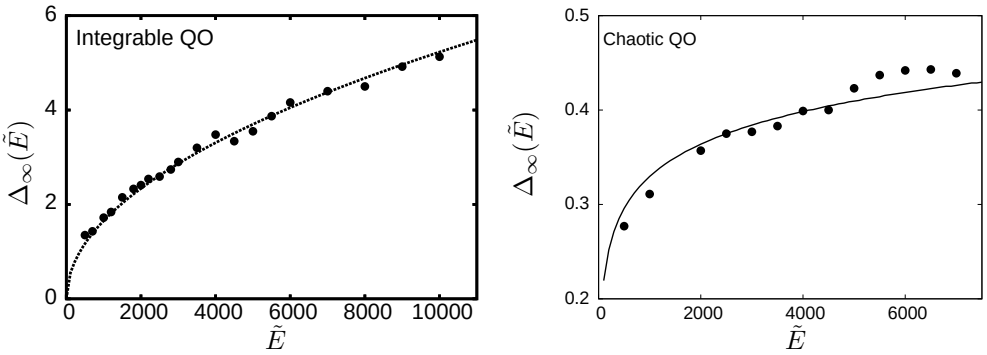

Figure 3.5: Saturation value Δ_∞, plotted versus unfolded energy $\tilde{E}$. The dots mark the quantum results. Left panel: integrable case ($\alpha = 0$); the solid line shows the semiclassical prediction. Right panel: Almost chaotic case ($\alpha = 9$). Here the solid line represents the GOE prediction.

as $\log(1/\hbar)$ which is obtained by replacing the form factor by its GOE prediction in Eq. (3.3). Though the exact saturation value is not universal, since it depends on the lower integration limit $\tau_{\min}$, its $\hbar$ dependence is. In the right panel of Fig. 3.5 we compare the quantum result with the GOE prediction evaluated for our value of $T_{\min}$ for $\alpha = 9$.

3.4 Bifurcation effects in the level statistics

It has been discussed in Ref. [49] that additional contributions to the long-range spectral correlations may arise from bifurcations of periodic orbits, and that this effect can be reproduced semiclassically. The authors of Ref. [49] investigated the cat map at a tangent bifurcation, and found that the number variance of the counting function shows a "lift off" reaching a much higher value than in the chaotic situation. We report here similar findings for the rigidity of the QO Hamiltonian for values of α near the pitchfork bifurcations of the A orbit at α_n. Moreover, we find that the increase of the saturation value Δ_∞ becomes even larger slightly above the bifurcations. This is illustrated in Fig. 3.6. In the

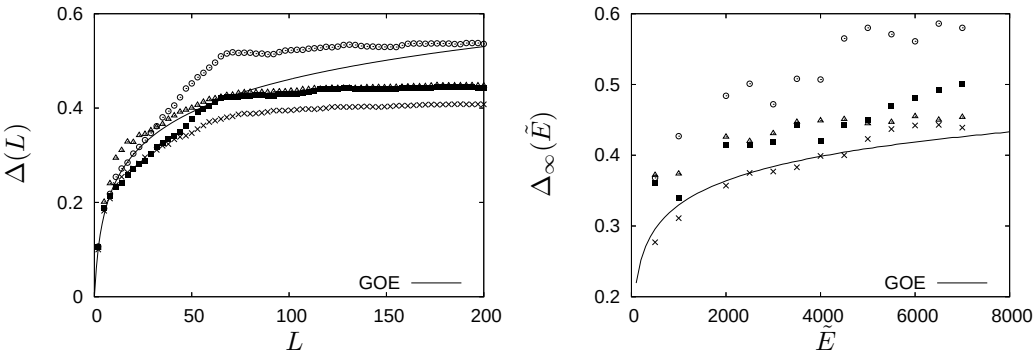

Figure 3.6: Left panel: spectral rigidity for $\alpha = 9$ (crosses), $\alpha = \alpha_4 = 10$ (filled squares), $\alpha = 10.5$ (circles), and $\alpha = 11$ (triangles) for $\tilde{E} = 4000$. Right panel: saturation value Δ_∞ versus $\tilde{E}$ before and after the bifurcation at $\alpha_4 = 10$. Although the phase space is barely affected, the saturation at $\alpha = 10.5$ is much larger than the saturation at $\alpha = 11$.

left panel we show the rigidity $\Delta(L)$ for four values of α around $\alpha = \alpha_4 = 10$ where such a bifurcation occurs. The rigidity at $\alpha_4 = 10$ exhibits a slightly larger saturation than at $\alpha = 9$ ("lift off"). However, the increase is even much more noticeable at $\alpha = 10.5$. Then the saturation goes down again for $\alpha = 11$, even though the system is more regular than at $\alpha = 10.5$.

The energy dependence of Δ_∞ is shown in the right panel of Fig. 3.6. We see that this effect exists over a large region of energies. As mentioned before, the phase space looks completely chaotic at the bifurcation at $\alpha = 10$; without

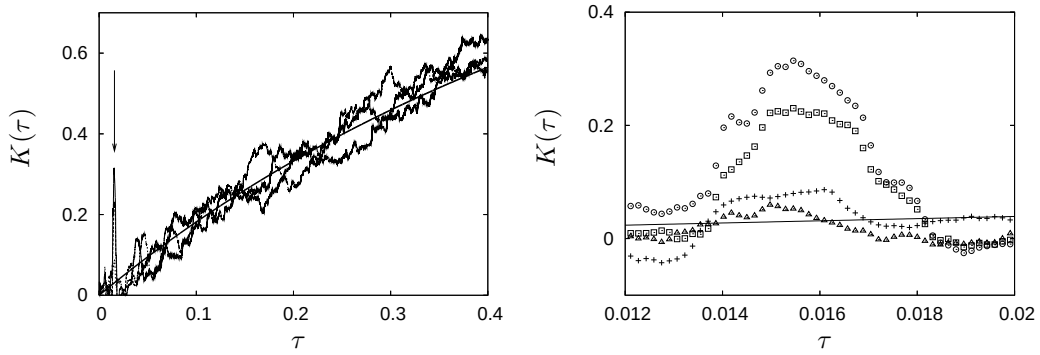

Figure 3.7: *Left panel:* Form factor at $\alpha = 9, 10$ and 10.5 compared with RMT (line). Note the strong peak at $\tau = \tau_{\rm A} \simeq 0.015$ (indicated by an arrow) coming from the bifurcating orbit. *Right panel:* Form factor at $\alpha = 9$ (crosses), $\alpha = 10$ (squares), $\alpha = 10.5$ (circles), and $\alpha = 11$ (triangles) in a zoomed region around $\tau \simeq \tau_{\rm A}$. For $\alpha = 10.5$: the amplitude of the peak is clearly larger than at the bifurcation.

knowledge of the bifurcation one would expect an almost universal behaviour. Above the bifurcation, a tiny regular island is seen at the center, which arises from orbit $\rm A_7$ that became stable. The island is slightly larger at $\alpha = 11$ than at $\alpha = 10.5$ (see Fig. 2.4).

Equivalently, in Fig. 3.7 we show that the effect is particularly pronounced in the spectral form factor. In the left panel we show $K(\tau)$ at $\alpha = 9, 10$ and 11. The results are consistent with the GOE prediction for almost all times, but we see a very large peak at a time that corresponds to the period of the libration orbit, $\tau_{\rm A}$. This is consistent with the results of Ref. [49]. However, the enhancement is even more noticeable at $\alpha = 10.5$ (right panel).

The exact calculation of the semiclassical rigidity for the QO in the chaotic regime is numerically impossible, since this would require an infinite number of periodic orbits, and there is no analytical way to calculate them. To reproduce the quantum result semiclassically, we calculate the coarse-grained reduced density of states defined analogously to Eq. (2.10) by

$$\delta g_\gamma^m(E) = \frac{d_m}{\hbar} \sum_l \frac{\overline{T}_l}{|K_l|} e^{-(\gamma \overline{T}_l/2)^2} \sum_r \frac{\chi_m(g_l^r)}{|\overline{\rm M}_l^r - {\rm D_l}|^{\frac{1}{2}}} \cos\Big[\frac{r}{\hbar}\overline{S}_l(E) - \frac{\pi}{2}\overline{\sigma}_{rl}\Big]. \qquad (3.14)$$

The longer orbits will be strongly suppressed assuring convergence, but, at the same time, affecting the universality. However, for the study of the saturation properties of $\Delta(L)$ as a probe for bifurcation effects, the information of the shorter orbits should be sufficient. In the following, we will drop the bars indicating that the orbits are in the fundamental domain, but all the numerical calculations were done taking this into account.

Consistently we also coarse-grain the quantum stair-case function, defining

$$N_\gamma(E) = \frac{1}{2}\sum_n \left[1 - \mathrm{erf}\left(\frac{E_n - E}{\gamma}\right)\right] . \tag{3.15}$$

Inserting $N_\gamma(E)$ into Eq. (3.2), we obtain a "smoothed" rigidity Δ_γ of the coarse-grained density of states. We find that even for relatively large values of γ, the bifurcation effects described above are still clearly visible, as shown in Fig. 3.8.

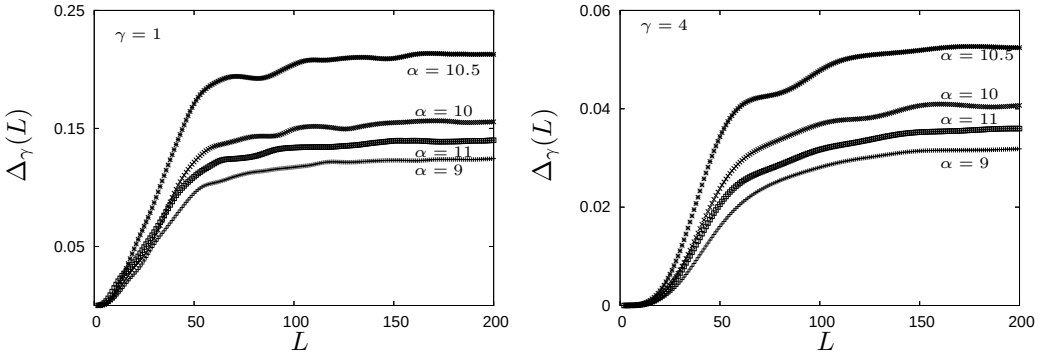

Figure 3.8: Same as Fig. 3.6, but after coarse-graining the reduced quantum spectrum by a Gaussian smoothing with width $\gamma = 1$ (left) and $\gamma = 4$ (right).

We calculate semiclassically the smooth rigidity $\Delta_\gamma(L)$, taking into account the bifurcation of the A orbit at $\alpha_4 = 10$, according to eqs. (2.28) and (2.29).

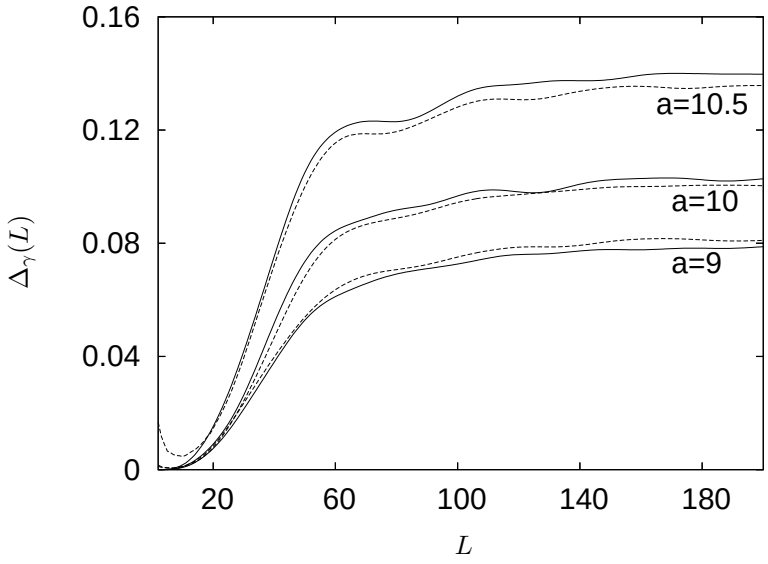

Figure 3.9: Smoothed rigidity for $\alpha = 9$, $\alpha = \alpha_4 = 10$ and $\alpha = 10.5$, obtained for $\gamma = 2$. The solid (dashed) curves represent the quantum mechanical (semiclassical) results.

In this way we can reproduce the quantum mechanical results near the bifurca-

tion semiclassically, as demonstrated in Fig. 3.9. As we have seen in the previous chapter from the action spectrum, the amplitudes and actions of most of the orbits do barely change, and the higher saturation for the smooth rigidity was mainly caused by the bifurcation.

Considering the rigidity without smoothing, we now assume that the contribution of the long orbits corresponds to and can be replaced by the universal RMT prediction, so that the differences in the saturation arise basically from the A and L orbits. Hence, we approximate the saturation value of Δ by

$$\begin{aligned}\Delta_\infty(E) &\simeq \Delta_\infty^{GOE} + \Delta_\infty^{A,L} \\ &\simeq \Delta^{GOE} + \frac{1}{2}\Big\langle \sum_{j,k=A,L} \frac{A_j A_k}{T_j T_k} \cos\left(\frac{S_j - S_k}{\hbar}\right)\Big\rangle . \end{aligned} \tag{3.16}$$

At the bifurcation, the second term corresponds to the diagonal contribution of (2.29), so that

$$\Delta_\infty^{A,L} = \frac{\Gamma^2(1/4)}{8\pi^3 |a|^{1/2}\hbar^{1/2}} , \tag{3.17}$$

and Δ_∞ behaves like

$$\Delta_\infty \;\propto\; \log(1/\hbar) + \frac{1}{\hbar^{1/2}}. \tag{3.18}$$

In the neighborhood of the bifurcation, i.e., when the action difference $|\Delta S|$ is smaller than $\hbar$, we can expand the actions and amplitudes around $\alpha = \alpha_4$ (cf. Ref. [48]):

$$\Delta S = \frac{S_A - S_L}{2} = \frac{\epsilon^2}{4a} + O(\epsilon^3) , \tag{3.19}$$

$$A_A = \frac{T_A}{\sqrt{2\epsilon}} , \qquad A_L = \frac{T_A}{\sqrt{\epsilon}} \left[1 + O(\epsilon)\right] , \tag{3.20}$$

where $\epsilon = c\,(\alpha - \alpha_4)$. Up to first order in ϵ this yields

$$\begin{aligned}\delta g_{A+L}^{un}(E) &\approx \frac{T_A}{\pi\sqrt{2\pi\hbar}}\, \Re e\, e^{i\bar{S}/\hbar - i3k\pi - i\pi/4} \times \\ &\quad \times \left[\frac{\sigma_2 \Gamma(3/4)}{|a\hbar|^{3/4}} \epsilon\, \mathrm{e}^{-i\pi/8} + \frac{\Gamma(1/4)}{2|a\hbar|^{1/4}}\, \mathrm{e}^{i\pi/8}\right]. \end{aligned} \tag{3.21}$$

Inserting this into the saturation value of the rigidity we obtain

$$\Delta_\infty^{A,L} \approx \frac{\Gamma^2(1/4)}{8\pi^3|a|^{1/2}\hbar^{1/2}} + \epsilon\, \frac{1}{2\pi^2|a|\hbar} + \epsilon^2\, \frac{\Gamma^2(3/4)}{2\pi^3|a|^{3/2}\hbar^{3/2}} . \tag{3.22}$$

In Fig. 3.10 we show the quantum results for Δ_∞ versus energy $\tilde{E}$ and for the form factor $K(\tau)$ near $\tau_{\rm A}$, for the three values $\alpha = 9$, 10 and 10.5 (as crosses, squares and circles, respectively). The solid line gives the universal GOE prediction, i.e., the first term in (3.18). It agrees well with the quantum result at $\alpha = 9$,

in line with the near chaoticity of the system below the bifurcation. The dashed and dotted lines show the prediction (3.22), which includes the bifurcating orbits A and L in the uniform approximation, and coincide well with the quantum results at and above the bifurcation. At the bifurcation ($\alpha = \alpha_4 = 10$) where $\epsilon = 0$, Eq. (3.22) is consistent with the diagonal approximation for the bifurcating orbits and thus the same as that used in Ref. [49].

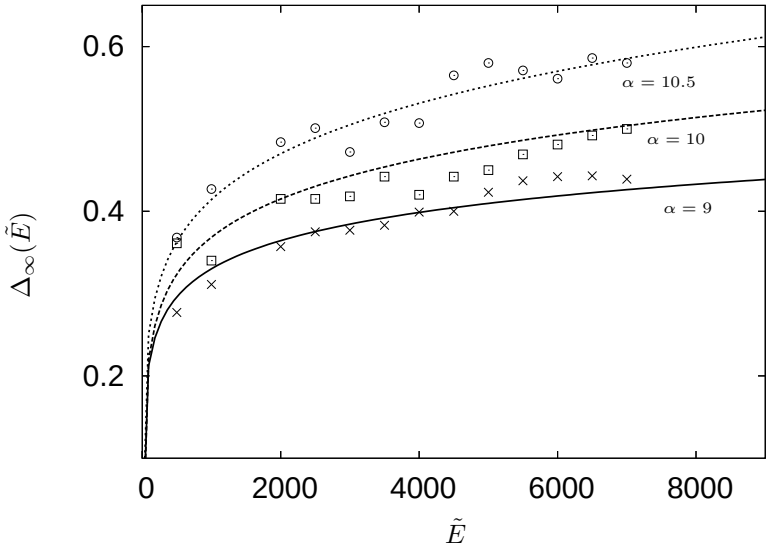

Figure 3.10: Saturation as a function of the energy. Crosses, squares and circles mark quantum-mechanical results for $\alpha = 9, 10$ and 10.5, respectively. Bold line: GOE result, dashed and dotted lines: Eq. (3.22).

Figure 3.10 moreover shows that slightly above the bifurcation, i.e. at $\alpha = 10.5$, the additional terms in Eq. (3.22), playing a role for $\epsilon \neq 0$, give a noticeable contribution, as seen by the dashed line. The main contribution comes from the term linear in ϵ which is the non-diagonal contribution of the pairs of separate orbits A and L above the bifurcation. To see this, we evaluate their non-diagonal contribution in the Gutzwiller approximation for isolated orbits, which would become

$$\Delta_{\infty(\mathrm{Gutz})}^{A.L(\mathrm{non-diag})} = 2\frac{A_L A_A}{\pi^2 T_A^2}\left\langle \sin\left(\frac{\Delta S}{\hbar}\right)\right\rangle \sin\left(\frac{\pi}{4}\right) \approx \frac{1}{\pi^2\epsilon}\frac{\Delta S}{\hbar} = \frac{\epsilon}{2\pi^2|a|\hbar}. \qquad (3.23)$$

The term $\sin\left(\frac{\pi}{4}\right)$ comes from the difference of phases between the two orbits, which is not yet a difference of one Maslov index. We see that although the diagonal contribution diverges at the bifurcation, the non-diagonal contribution stays finite there.

We therefore interpret the term in Eq.(3.22) as a non-diagonal contribution to the rigidity, which can actually be exactly reproduced by the Gutzwiller ap-

proximation, although this approximation is not yet valid for the evaluation of the individual contributions.

Note that the value of Δ_∞ is slightly enhanced also by the fact that the particular combination of Bessel functions in the uniform approximation (2.28) can be expressed as an Airy function and its derivative, cf. Ref. [48], which has its maximum slightly above the bifurcation. This effect is, however, not sufficient to explain the enhancement of Δ_∞ found in our results, so that we can argue that the non-diagonal contribution is substantial.

It is important to mention that this non-diagonal contribution exists as long as $\hbar$ remains finite. In the strict semiclassical limit $\hbar \to 0$, the global uniform approximation (2.28) merges into the Gutzwiller trace formula for non-zero ΔS, and $\sin(\Delta S/\hbar)$ oscillates very fast, so that after the energy average, the non-diagonal contribution will tend to zero. This is expected, since in the semiclassical approximation for mixed systems (Eq. 3.6), periodic orbits with different stability give rise to independent statistics.

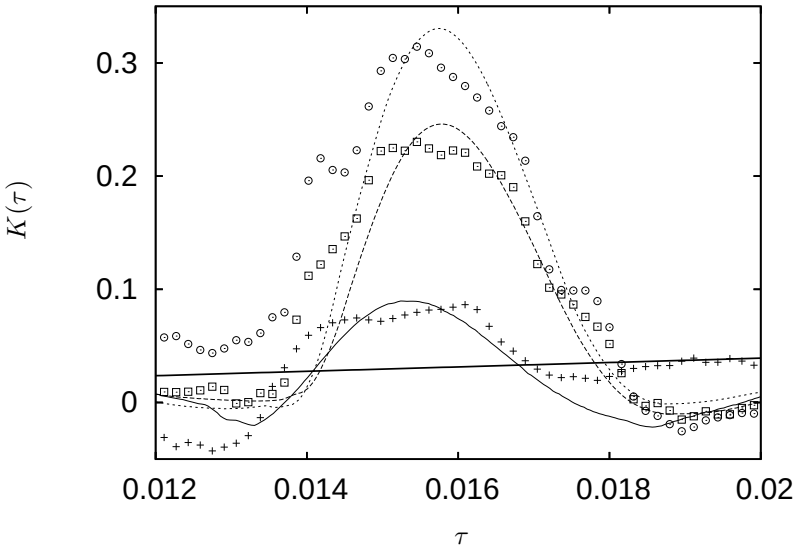

Figure 3.11: Form factor near $\tau_{\rm A}$. Crosses, squares and circles mark quantum-mechanical results for $\alpha = 9, 10$ and 10.5, respectively. Bold line: GOE result, dashed and dotted lines: Eq. (3.26).

An equivalent calculation can be done for the spectral form factor. For its semiclassical calculation we focus only on the contribution of the bifurcating orbit, $K_{\rm A}$. Thus we only reproduce the form factor for $\tau \sim \tau_{\rm A}$, using in (1.19) only the contributions of the A and L orbits. This yields for $\alpha = 9$

$$K_{\rm A}(\tau) = \frac{\tau_{\rm A}^2}{\pi^2(\mathrm{Tr}\,\mathrm{M_A} - 2)}\delta_{\Delta\tau}(\tau - \tau_{\rm A}), \tag{3.24}$$

for $\alpha = \alpha_4$

$$K_{\mathrm{A+L}}(\tau) = \frac{\Gamma^2(1/4)\tau_{\mathrm{A}}^2}{8\pi^3|a|^{1/2}\hbar^{1/2}}\,\delta_{\Delta\tau}(\tau-\tau_{\mathrm{A}}). \tag{3.25}$$

and in the neighborhood of the bifurcation,

$$K_{\mathrm{A+L}}(\tau) \approx \left(\frac{\Gamma^2(1/4)}{8\pi^3|a|^{1/2}\hbar^{1/2}} + \epsilon\,\frac{1}{2\pi^2|a|\hbar} + \epsilon^2\,\frac{\Gamma^2(3/4)}{2\pi^3|a|^{3/2}\hbar^{3/2}}\right)\tau_{\mathrm{A}}^2\delta_{\Delta\tau}(\tau-\tau_{\mathrm{A}})\,. \tag{3.26}$$

In Fig. 3.10b we show the quantum results for $K(\tau)$ near τ_{A} for the three values $\alpha = 9.0$, 10.0 and 10.5 (by crosses, squares and circles, respectively). The solid, dashed and dotted lines show the prediction (3.24), (3.25) and (3.26) respectively. In accordance with our results for the rigidity, we see a very good agreement with the semiclassical prediction. Moreover, the difference of the peak between $\alpha = 10$ and $\alpha = 10.5$ is about 25%, and can be explained again by a non-diagonal contribution of the orbits involved in the bifurcation.

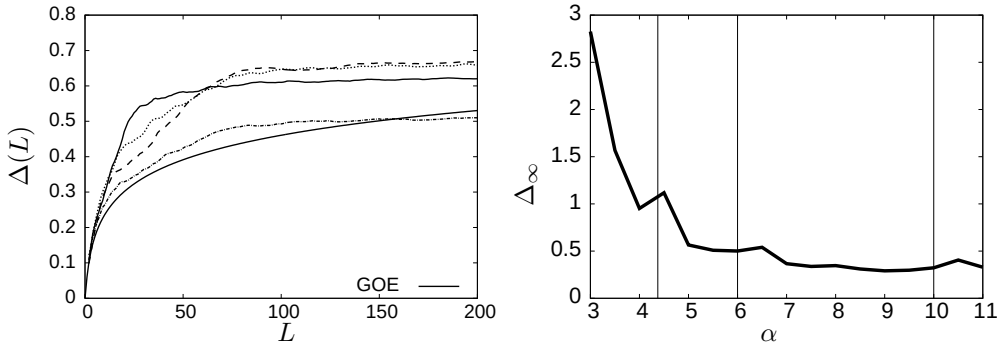

Figure 3.12: *Left panel:* rigidity for $\alpha = 5$ (full line), $\alpha = \alpha_3 = 6$ (dotted), $\alpha = 6.5$ (dashed) and $\alpha = 7$ (dot-dashed). A larger saturation is obtained near the bifurcation even when the system at $\alpha = 7$ is more regular that $\alpha = 6.5$. *Right panel:* Saturation as a function of α, the pitchfork bifurcations are indicated with the vertical lines.

It is important to point out that the results shown in this chapter are not particular for the parameter α that we have chosen, meaning that for other parameters where pitchfork bifurcations occur, we have also observed this strong enhancement of the saturation of the rigidity, being stronger after the bifurcation event. In Fig. 3.12 (left panel) we show another example, namely the case $\alpha = \alpha_3 = 6.0$. The saturation at $\alpha = 6.5$ (after the saturation) is extremely large in comparison with $\alpha = 7$, though the latter situation is more regular. Again the standard approximation for mixed systems Eq. (3.6) does not longer hold, and it is expected from our analysis, that apart from the different $\hbar$-scaling, a non-diagonal contribution plays an important role as before. In Fig. 3.12 (right panel) we show the saturation value as a function of the parameter α. The values of α

for which the libration orbit A has pitchfork bifurcations are indicated by vertical lines. It can be noticed that the saturation of the rigidity Δ_∞ shows a local maximum slightly after the bifurcation in all cases, consistent with our analysis. The parameter $\alpha_4 = 10$ was chosen for two reasons. First, we were interested in studying deviations from universality, and therefore we studied a situation near full chaoticity. The second was a practical one, as we have seen near $\alpha = 9$ we may assume that apart from the bifurcation of the A orbit all other contributions can be summed up with the help of ergodicity arguments, i.e. using the Hannay-de Almeida sum rule [18] and other possible bifurcations can be ignored.

Motivated by the dominant effect of bifurcations in spectral statistics we will follow, in the next chapter, a similar approach to the one shown here in a different physical context, namely transport properties in mesoscopic systems, where semiclassical methods have been successfully applied for clean chaotic systems. There the semiclassical expression involve double sums over trajectories which are no longer periodic, but satisfy another stationary condition. We are interested in a formal definition of a bifurcation scenario of these trajectories and its effect in the conductance.

Chapter 4

Semiclassical transport and open-orbits bifurcations

In this chapter we will define a bifurcation scenario for scattering orbits and calculate its contribution to the conductance. We will briefly recall the Landauer-Büttiker formalism for transport in mesoscopic systems and its semiclassical approximation. As mentioned in the introduction, the concept of bifurcations is attached to the task of describing the creation of stationary points upon small perturbations. In the case of periodic orbits, the definition is clear, since periodic orbits are stationary points of a Poincaré map. However, it is not clear how orbits that participate in the semiclassical description of transport in the scattering formalism are related with periodic orbits. Nevertheless it is possible to settle a definition of bifurcations in the case of open orbits, as we will see in this chapter. We will define a bifurcation scenario for scattering orbits and the corresponding uniform semiclassical approximation near two possible scenarios. Finally we will estimate the effect of a tangent and a pitchfork bifurcation in the conductance through a mesoscopic sample. In contrast to our previous result, in the case of conductance the different scaling of bifurcating open orbits is not enough to make them dominant over all other scattering orbits that give rise to universal properties.

4.1 Semiclassical transport through mesoscopic systems

Transport through mesoscopic systems has been intensively studied in the last decades [97, 98, 99, 100]. Mesoscopic devices, which are of the order of a micron in size, usually show classical and quantum signatures, and therefore are the kind

of systems where semiclassical methods can be implemented [101, 102]. A variety of effects has been studied theoretically and experimentally in such structures, e.g. conductance fluctuations [55], weak localization [56, 103] and Shubnikov-de Haas oscillations [104].

These systems can be built in such a way that impurity scattering is almost absent and the transport can be considered ballistic, i.e., the scattering comes from reflections at the boundaries of the confinement and the coherence length λ_ϕ and the elastic-mean free path are much larger than the system size, meaning that inelastic processes as well as impurity scattering are negligible. In semiclassical transport, the Fermi wavelength λ_F is the shortest length in the system.

The appropriate approach for the transport properties of systems satisfying such conditions is the so-called Landauer-Büttiker approach [98, 105], or scattering matrix approach. A corresponding semiclassical version has been developed by Baranger, Jalabert and Stone in Ref. [106].

Let us consider a two-probe device, as sketched in Fig. 4.1. The scattering description is based on an expansion in asymptotic states, assuming that the leads are free of disorder and with hard walls of width w_L (left) and w_R (right) in the y-direction and infinite in the x-direction. The asymptotic states can be written as a product of particle-in-a-box wave-functions and plane waves propagating in the longitudinal direction with wave vector k_n satisfying $k_n = n\pi/w_{L,R}$. The $(N_R + N_L) \times (N_R + N_L)$ scattering matrix S relates the incoming and outgoing fluxes and can be written in terms of the $N_i \times N_j$ $(i, j = L, R)$ reflection and transmission matrices r and t (r' and t') from the left (right) as

$$S = \begin{pmatrix} r & t' \\ t & r' \end{pmatrix}. \tag{4.1}$$

Current conservation implies that the incoming flux should be equal to the outgoing flux, and therefore S is unitary ($S^\dagger S = I$). The amplitudes t_{nm}, describing the transmission probability amplitude from the m channel at the left lead to the channel n at the right, can be written in terms of the projected Green function on the transversed modes in the leads as

$$t_{nm} = -i\hbar\sqrt{v_n v_m} \int_{\Sigma_x} dy \int_{\Sigma_{x'}} dy' \phi_n^*(y)\phi_m(y')G^+(x = L, y, x' = 0, y'; E_F), \tag{4.2}$$

where v_n denote the longitudinal velocities and the integrals take place at the transverse cross section $\Sigma_{x'}$ on the left (at $x = 0$) and Σ_x on the right lead ($x = L$). An intuitive interpretation of the above equation is a particle arriving at the cavity in mode m, propagating inside through the Green function and exiting in mode n.

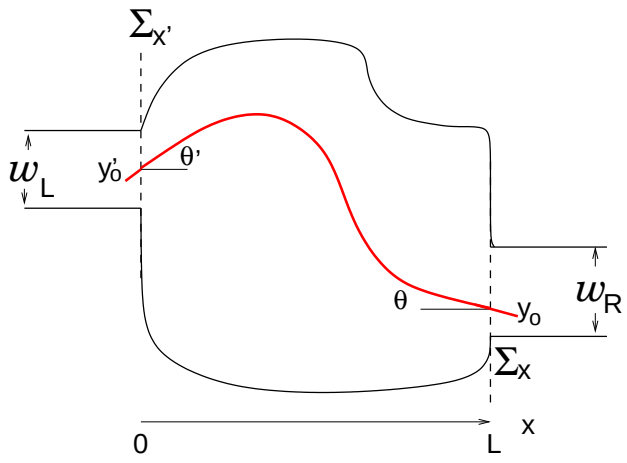

Figure 4.1: The simplest experimental set up is the two-probe measurement, where the sample is attached between two reservoirs whose electrochemical potentials differ by the value of the applied voltage V.

In this formalism the conductance G through the sample is proportional to the total transmission at the Fermi energy E_F (for zero temperature), for which N_L channels are open at the left and N_R at the right lead:

$$G = g_s \frac{e^2}{\hbar} T. \tag{4.3}$$

The factor g_s is counting for spin degeneracy, and $T = \sum_{n=1}^{N_R} \sum_{m=1}^{N_L} |t_{nm}|^2$ is the total transmission. For a review of the semiclassical approximation of ballistic quantum transport we recommend Refs. [102, 106]. Here we will briefly recall the main steps for its derivation. The semiclassical approximation to the transmission probability can be constructed by replacing the exact Green function in Eq. (4.2) by its semiclassical counterpart and evaluating the integrals over y and y' by stationary phase approximation. For leads with hard-wall boundaries the mode wave functions are simply $\phi_m^{\mathrm{L,R}}(y) = \sqrt{\frac{2}{w_{\mathrm{L,R}}}} \sin\left(\frac{m\pi y}{w_{\mathrm{L,R}}}\right)$.

The stationary phase condition will lead to contributions from classical trajectories whose transverse momentum at the leads match the wave vectors of the modes in the leads, i.e. trajectories for which $p_i = \pm m\pi\hbar/w_L$ (p_i stands for the initial momentum transversed to the left lead) and $p_f = \pm n\pi\hbar/w_R$ (p_f stands for the final momentum transversed to the right lead). Then, trajectories entering the cavity at $(0, y_o')$ with angle $\sin\theta' = \pm m\pi/kw_L$ and leaving at (L, y_o) with angle $\sin\theta = \pm n\pi/kw_R$ are the ones contributing to the transmission probability t_{nm}.

After the evaluation of the integral the semiclassical transmission coefficients

are given by

$$t_{mn}^{\rm sc} = -\sqrt{\frac{\pi i\hbar}{2w_L w_R}} \sum_{\gamma(\bar{n},\bar{m})} A_\gamma \,{\rm sgn}(\bar{m}){\rm sgn}(\bar{n}) \exp\left(\frac{i}{\hbar} S_\gamma^{\bar{n}\bar{m}}(E_F) - i\frac{\pi}{2}\bar{\mu}_\gamma\right), \qquad (4.4)$$

where $\bar{m} = \pm m$ and $S_\gamma^{\bar{n}\bar{m}}(E_F) = S_\gamma(L, y_o, 0, y_o'; E_F) + \hbar k y_o' \sin\theta' - \hbar k y_o \sin\theta$. The phases $\bar{\mu}_\gamma$ contain the Morse indices and additional phases arising from the integration over y and y'. The amplitudes are given by

$$A_\gamma = \left|\frac{\partial p_f}{\partial y'}\right|^{-1/2}_{\substack{y'=y_o' \\ y=y_o}} . \qquad (4.5)$$

As we notice, the procedure has been similar to that for the derivation of the semiclassical density of states, namely, the semiclassical approximation is done in two steps: first replacing the exact Green function by its semiclassical counterpart, and second evaluating the integrals by stationary phase approximation. The results are slightly different, since the semiclassical density of states implies a sum over classical periodic orbits, while the transmission coefficients are given by a sum over open trajectories. However, since both solutions correspond to stationary points, it should be possible to define a bifurcation scenario in the second context, similar to the well known bifurcation scenario of periodic orbits.

4.2 Open-orbits bifurcation theory

Periodic orbit bifurcation theory has been described by de Almeida and Hannay in Ref. [47], following the analysis of Meyer in Ref. [46]. The concept has been extend to non-periodic orbits in Ref. [107], in the context of photoabsorbtion spectrum, where the response function can be described in terms of orbits starting and going back to the nucleus, but not necessarily with the same momentum, i.e. the orbits giving some contribution are closed, but not periodic [108, 109]. We will here closely follow their approach, in order to define and discuss bifurcations of open orbits contributing to the transmission coefficients. The definitions are also valid to define a bifurcation scenario of reflection coefficients.

A fundamental concept in developing a bifurcation theory is the definition of a Poincaré surface of section in the neighborhood of the orbit, describing the dynamics of the degrees of freedom transverse to the orbit. For a periodic orbit it is defined by fixing a surface of section in phase space perpendicular to the orbit. For a point $\vec{y}$ on the surface of section, the trajectory is followed until it intersects the surface again at $P\vec{y}$, the image of $\vec{y}$ under the Poincaré map P. The periodic orbit itself returns to its original point, so that it appears as a fixed

point of the Poincaré map. Since open orbits do not return to their starting point, this definition has to be modified. We define two surfaces of section, one at the beginning of the orbit Σ_i, and the other one Σ_f, at the end of the orbit, in both cases perpendicular to the orbit. Orbits giving a contribution to the coefficient t_{nm} can be described as solutions of the equation $p_f(p_i = \hbar k \sin\theta_m, y_i) = \hbar k \sin\theta_n$. A particular solution is the orbit for which the construction was made. If $C = \partial p_f/\partial y_i$ is non-singular at $p_f = \hbar k \sin\theta_{\bar{n}}$, the solution is unique and will persist upon small variations of parameters. Therefore, the orbit can only go through a bifurcation when $\det C = 0$.

Type	Transformations	Regular matrix
$F_1(y_i, y_f)$	$p_i = +\partial F_1/\partial y_i$, $p_f = -\partial F_1/\partial y_f$	B
$F_2(y_i, p_f)$	$p_i = +\partial F_2/\partial y_i$, $p_f = +\partial F_2/\partial p_f$	D
$F_3(p_i, y_f)$	$y_i = -\partial F_3/\partial p_i$, $p_f = -\partial F_3/\partial y_f$	A
$F_4(p_i, p_f)$	$y_i = -\partial F_4/\partial p_i$, $p_f = +\partial F_4/\partial p_f$	C

Table 4.1: Different types of generating functions. The regular matrices satisfy the linear symplectic map $y_f = Ay_i + Bp_i$, $p_f = Cy_i + Dp_i$ and the conditions: AC, BD, AB and CD are self-adjoint and $A^\dagger D - C^\dagger B = 1$.

It is convenient at this stage to represent the open-orbit Poincaré map by a generating function [110]. We will also adopt here the same convention as in [110] for denoting the different types of generation functions, summarized in the table 4.1.

For convenience, we will choose the following generating function

$$\Phi(y_i, y_f) = F_1(y_i, y_f) + y_i \hbar k \sin\theta_m - y_f \hbar k \sin\theta_n. \tag{4.6}$$

The transformation equations for this type of generating function read

$$p_i = \frac{\partial \Phi}{\partial y_i} = \frac{\partial F_1}{\partial y_i} + \hbar k \sin\theta m = \tilde{p}_i + \hbar k \sin\theta m, \tag{4.7}$$

$$p_f = -\frac{\partial \Phi}{\partial y_f} = -\frac{\partial F_1}{\partial y_f} + \hbar k \sin\theta n = \tilde{p}_f + \hbar k \sin\theta n. \tag{4.8}$$

Open orbit contributions to the scattering matrix are those for which $p_i = \hbar k \sin\theta m$ and $p_f = \hbar k \sin\theta n$; they agree therefore with the stationary points of F_1. *The classification of bifurcations for open orbits corresponds to determining how the stationary points of a real function change upon the variation of parameters.* Catastrophe theory [45] is a local theory that studies the stability of a single stationary point and the pattern of stationary points that can be generated by a small perturbation.

A fundamental definition for this purpose is the concept of structurally stable stationary points, quoting Ref. [107]: *Two real-valued functions $f(\mathbf{x})$ and $\tilde{f}(\mathbf{x})$, defined in a neighborhood of the origin in an n-dimensional configuration space, are said to be equivalent, if there exists a diffeomorphism $\psi(\mathbf{x})$ such that*

$$\tilde{f}(\mathbf{x}) = f(\psi(\mathbf{x})). \tag{4.9}$$

The coordinate transformation ψ maps the stationary points of $\tilde{f}$ to those of f. f is said to be structurally stable if any small perturbation $\tilde{f}(\mathbf{x}) = f(\mathbf{x}) + \epsilon g(\mathbf{x})$ of $f(\mathbf{x})$, for a smooth function g and small ϵ, is equivalent to f.

A structurally stable stationary point of F_1 is a stationary point that is preserved under small variations of parameters and therefore corresponds to a non-bifurcating open orbit. Structurally stable fixed points are characterized by a non-singular Hessian matrix.

The determinant of the Hessian of F_1 can be written as $-\frac{\det C \det A}{\det B}$ and it is singular if either $C = \partial\tilde{p}_f/\partial y_i = \partial p_f/\partial y_i$ or $A = \partial y_f/\partial y_i$ is singular. Only the first situation can be associated with bifurcations of open orbits. If $\det C = 0$ new fixed points are born, while if $\det A = 0$ the Lagrangian manifold is tangent to the plane $\tilde{p}_i = 0$ and after variation it can acquire additional intersections with the plane $y_f = 0$, but there are no new solutions (no new intersection with the plane $\tilde{p}_f = 0$). This latter situation is accounted for in the semiclassical treatment by the phases $\bar{\mu}_\gamma$.

Let us consider the case $\det C = 0$. The splitting lemma of catastrophe theory states that *if the dimension of the configuration space is n and a function f on that space has a stationary point at the origin whose Hessian has rank $n - m$, a coordinate system $x_1, ..., x_n$ can be introduced in a neighborhood of the stationary point, so that*

$$f(x_1, ..., x_n) = g(x_1, ..., x_m) + h(x_{m+1}, ..., x_n), \tag{4.10}$$

where h is a non-degenerate quadratic form of $n - m$ variables, and g has a stationary point with zero Hessian matrix at the origin. Since h has structurally stable stationary points, the behaviour of the stationary points of f under small perturbations are determined by g.

In general, a degenerate stationary point of f will be splitted into several distinct stationary points after a perturbation (bifurcation).*The generic situation corresponds to bifurcations of finite codimension. This means that there is a finite number of smooth functions $g_1(\mathbf{x}), ..., g_k(\mathbf{x})$ so that*

$$F(\mathbf{x}) = f(\mathbf{x}) + \alpha_1 g_1(\mathbf{x}) + ... + \alpha_k g_k(\mathbf{x}), \tag{4.11}$$

with suitable constants α_i. The minimum number of such functions k is defined as the codimension, and F is called an unfolding of f. F contains the information of the stationary points created through the perturbation and their stability. It is usually argued that only bifurcations of codimension smaller than the number of external parameters are structurally stable, and these are the type of bifurcations that generically happen. The external parameters can describe, for example, the shape of the cavity, a magnetic field or the Fermi energy. By "generic" bifurcations one means that these are the typical situations. A rigorous definition depends on the bifurcation scenario and for different cases can be found in Ref. [111]. In our discussion, bifurcations of codimension 1 are generic if A can be taken as non-singular when C is singular, which is the general situation in the absence of special symmetries.

A list of catastrophes of codimensions up to 6 for generic functions is available in Ref. [45]. We will consider that there is only one external parameter varied, so the important bifurcations are those of codimension 1. In the absence of symmetries there is only one generic bifurcation of codimension 1: the tangent bifurcation. In the presence of discrete symmetries, pitchfork bifurcations are also generic with a single variation parameter.

4.3 Uniform approximation for the transmission coefficient

In the evaluation of the integrals in Eq. (4.2) by stationary phase approximation, it is assumed that scattering trajectories contributing to transport are isolated. As already mentioned in Chapter 2, uniform approximations give the correct description of the collective contribution of orbits involved in a bifurcation. As we have just seen, we can also define a bifurcation scenario in the context of transmission trajectories, whenever $C = \frac{\partial p_f}{\partial y_i} = 0$, which will modify the result in Eq.(4.4).

4.3.1 Uniform approximation for a tangent bifurcation

In this section we will calculate the contribution for the only bifurcation of codimension one in the absence of symmetries, namely a tangent bifurcation. We will follow the approach in Ref. [112] again in the context of open orbits, to calculate such a contribution.

The main requirement of a "global" uniform approximation is that it must asymptotically go to Eq.(4.4) far away from the bifurcation. We will assume that the integral over y can be done by stationary phase approximation, meaning that

the generation function can be written as $F_1(y,y') = f_1(y') + f_2(y)$, where $f_2(y)$ is a non-degenerate quadratic form of y and f_1 is going to be replaced by a normal form, unfolding the fixed points born at the bifurcation.

The integration over y by stationary phase approximation yields

$$t_{nm}^{\rm sc} = -\frac{1}{2\sqrt{w_L w_R}} \sum_{\gamma(\bar{n},y')} {\rm sgn}(\bar{n}){\rm sgn}(\bar{m}) {\rm e}^{-iky_o \sin\theta_{\bar{n}}} I_\gamma {\rm e}^{-i\frac{\pi}{2}\bar{\mu}_\gamma}, \tag{4.12}$$

where

$$I_\gamma = \int dy' g(y') {\rm e}^{\frac{i}{\hbar}(S_\gamma(y_o,y',E) + \hbar k y' \sin\theta_{\bar{m}})}, \tag{4.13}$$

with $g(y') = \left|\frac{\partial y'}{\partial y}\right|^{-1/2}_{y=y_o}$.

We will make the ansatz for a bifurcating orbits ξ:

$$S_\xi(y_o,y',E_F) = S_{0,\xi}(y_o,y'_o,E_F) + f_1(y'),$$

where y'_o is the central stationary point of S_ξ. The evaluation of this integral by stationary phase approximation would lead to

$$I_\xi = {\rm e}^{\frac{i}{\hbar}S_{0,\xi}(y_o,y'_o,E_F) + iky'_i \sin\theta_{\bar{m}}} \sum_i \sqrt{2\pi\hbar} {\rm e}^{i\frac{\pi}{4}{\rm sgn}(f_1''(y'_i))} A_i {\rm e}^{\frac{i}{\hbar}f_1(y'_i)}, \tag{4.14}$$

with $A_i = \frac{g(y'_i)}{\sqrt{|f_1''(y'_i)|}}$ and the sum is over the stationary points y'_i of $f_1(y')$, and the asymptotic values of A_i correspond to Eq.(4.5). The normal form for the tangent bifurcation is given by [46]

$$f_1(y') = \frac{1}{3}y'^3 - \epsilon y', \tag{4.15}$$

where ϵ is the bifurcation parameter. The stationary points are given by

$$y'_i = \pm\sqrt{\epsilon}, \tag{4.16}$$

where it assumes the values

$$f_1(y'_i) = \mp\frac{2}{3}\epsilon^{3/2} \tag{4.17}$$

and there stability is given by

$$f_1''(y'_i) = \pm 2\sqrt{\epsilon}. \tag{4.18}$$

When $\epsilon < 0$ the two solutions are imaginary, and there are no real open orbits satisfying the stationary condition. At $\epsilon = 0$ a tangent bifurcation occur, the two solutions become real, with opposite stability, and they move apart as $\sqrt{\epsilon}$.

According to Eq.(4.14) then

$$A_1 = \frac{g\left(\sqrt{\epsilon}\right)}{\sqrt{2}|\epsilon|^{1/4}} \tag{4.19}$$

and

$$A_2 = \frac{g\left(-\sqrt{\epsilon}\right)}{\sqrt{2}|\epsilon|^{1/4}}. \tag{4.20}$$

Here we make the standard ansatz $g(y') = p_0 + p_1 y'$ [112], where p_o, p_1 are system specific parameters. In terms of the amplitudes, then p_0 and p_1 are given by:

$$p_0 = (A_1 + A_2)\frac{|\epsilon|^{1/4}}{\sqrt{2}}, \tag{4.21}$$

$$p_1 = (A_1 - A_2)\frac{1}{|\epsilon|^{1/4}\sqrt{2}}. \tag{4.22}$$

Going back to the original integral in Eq.(4.13), we have an integral of the form $\int dy'(p_o + p_1 y')\mathrm{e}^{\frac{i}{\hbar}(y'^3/3 - \epsilon y')}$, which can be written as

$$I_\xi = \mathrm{e}^{\frac{i}{\hbar}S_{0,\xi}(y_o, y'_o, E_F) + iky'_i \sin\theta_{\bar{m}}} \left(p_0 + p_1 i\hbar\frac{d}{d\epsilon}\right) \int_{-\infty}^{\infty} dy' \mathrm{e}^{\frac{i}{\hbar}(y'^3/3 - \epsilon y')}, \tag{4.23}$$

whose solution is given in terms of Airy functions [113] using:

$$\int_0^\infty dy' \cos(ay'^3 - \epsilon y') = \frac{1}{(3a)^{1/3}}\pi \mathrm{Ai}[-(3a)^{-1/3}x]. \tag{4.24}$$

Expressing the Airy functions $\mathrm{Ai}(x)$ in terms of Bessel functions of the first kind $J_n(x)$ one has

$$\begin{aligned} I_\xi &= \frac{2\pi}{3}\mathrm{e}^{\frac{i}{\hbar}S_{0,\xi}(y_o, y'_o, E_F) + iky'_i \sin\theta_{\bar{m}}} \\ &\times \left(p_0 + p_1 i\hbar\frac{d}{d\epsilon}\right)\left\{\sqrt{\epsilon}\left(J_{1/3}\left(\frac{2\epsilon^{3/2}}{3\hbar}\right) + J_{-1/3}\left(\frac{2\epsilon^{3/2}}{3\hbar}\right)\right)\right\}. \end{aligned} \tag{4.25}$$

The final result is

$$\begin{aligned} I_\xi &= 2\frac{\pi\sqrt{\hbar}}{\sqrt{3}}\mathrm{e}^{\frac{i}{\hbar}S_{0,\xi}(y_o, y'_o, E_F) + iky'_i \sin\theta_{\bar{m}}} \\ &\times\sqrt{\left|\frac{\Delta S}{\hbar}\right|}\left\{\bar{A}\left[J_{1/3}\left(\left|\frac{\Delta S}{\hbar}\right|\right) + J_{-1/3}\left(\left|\frac{\Delta S}{\hbar}\right|\right)\right]\right. \\ &\left. + i\Delta A\left[J_{-2/3}\left(\left|\frac{\Delta S}{\hbar}\right|\right) - J_{2/3}\left(\left|\frac{\Delta S}{\hbar}\right|\right)\right]\right\}, \end{aligned} \tag{4.26}$$

with $\bar{A} = \frac{1}{2}(A_1 + A_2)$, $\Delta A = \frac{1}{2}(A_1 - A_2)$ and $\Delta S = S_1 - S_2$.

Therefore, the contribution to the transmission coefficient t^ξ_{nm} of the orbits born at a tangent bifurcation will be

$$\begin{aligned} t^\xi_{nm} &= -\sqrt{\frac{\pi^2}{3w_L w_R}}\mathrm{sgn}(\bar{m})\mathrm{sgn}(\bar{n})\mathrm{e}^{\frac{i}{\hbar}S^{nm}_\xi(E) - i\frac{\pi}{2}\mu_\xi} \\ &\times\sqrt{|\Delta S|}\left\{\bar{A}\left[J_{1/3}\left(\frac{|\Delta S|}{\hbar}\right) + J_{-1/3}\left(\frac{|\Delta S|}{\hbar}\right)\right]\right. \\ &\left. \times i\Delta A\left[J_{-2/3}\left(\frac{|\Delta S|}{\hbar}\right) - J_{2/3}\left(\frac{|\Delta S|}{\hbar}\right)\right]\right\}. \end{aligned} \tag{4.27}$$

If we take the limit $\epsilon \to \infty$ we recover, as expected, Eq.(4.4) and the contribution of each of the two orbits scales like $\sqrt{\hbar}$.

On the other hand, taking the limit $\epsilon \to 0$ we obtain the local uniform approximation by taking the asymptotic expression for $J_n(x)$ ($J_n(x) \approx x^n/\Gamma(n+1)$, $x \ll 1$), thus

$$t_{nm}^{\xi,\mathrm{loc}} = -\frac{(3)^{2/3} p_0 \hbar^{1/3} \pi}{2^{1/3}\Gamma(2/3)\sqrt{w_L w_R}} \mathrm{sgn}(\bar{m})\mathrm{sgn}(\bar{n}) \mathrm{e}^{\frac{i}{\hbar} S_\xi^{nm}(E) - i\frac{\pi}{2}\mu_\xi}. \tag{4.28}$$

A second term also appears, which scales as $\hbar^{2/3}$, which we will neglect since its semiclassical weight is even smaller than that of isolated orbits. We see from Eq. (4.28) that bifurcating scattering orbits, have a stronger semiclassical weight than isolated ones and the difference in the $\hbar$-scaling between the two types of contributions is the same as in the density of states.

4.3.2 Uniform approximation for a pitchfork bifurcation

In the case of a system with discrete symmetries, it is possible to find bifurcations of higher codimensions that are still generic when the number of parameters to vary is smaller than the codimension. An example is the case of pitchfork bifurcations. Pitchfork bifurcations are usually of codimension 2, but in presence of discrete symmetries, they can take place as if they were of codimension 1, like we have seen before in the case of the QO and periodic orbit bifurcations.

The normal form of such a bifurcation is given by [46]

$$f_1(y') = \frac{1}{4}y'^4 - \frac{1}{2}\epsilon y'^2, \tag{4.29}$$

with stationary points

$$y'_o = 0, \qquad y'_{1,2} = \pm\sqrt{\epsilon}, \tag{4.30}$$

if $\epsilon > 0$, two symmetry - related stationary points are created, which are going to be counted with a single amplitude A_1 in Eq. (4.14).

The action difference between the central orbit and the new one is given by

$$\Delta S = \frac{1}{4}\epsilon^2. \tag{4.31}$$

The standard ansatz for the amplitudes in Eq. (4.19) and Eq.(4.20) is given by $g(y') = p_0 + p_2 t^2$, since it must be an even function of t [112]. The parameters p_0 and p_2 depend of the potential. According to Eq. (4.14) these are related to the asymptotic amplitudes as

$$p_0 = \sqrt{\epsilon} A_0, \tag{4.32}$$

$$p_2 = \frac{1}{\sqrt{2\epsilon}}(A_1 - \sqrt{2}A_0). \tag{4.33}$$

The integrals $\int dy'(p_0 + p_0 y'^2) e^{if(y')/\hbar}$ can be expressed as

$$I_\xi = \mathrm{e}^{\frac{i}{\hbar}S_{0,\xi}(y_o,y'_o,E_F)+iky'_i\sin\theta_{\bar{m}}}\left(p_0 + 2p_2 i\hbar\frac{d}{d\epsilon}\right)\int_{-\infty}^{\infty} dy' \mathrm{e}^{\frac{i}{\hbar}(y'^4/4-\epsilon y'^2/2)}, \quad (4.34)$$

with solutions given in term of Bessel functions of the first kind [113]:

$$\begin{aligned} I_\xi &= \frac{\pi}{2}\mathrm{e}^{\frac{i}{\hbar}S_{0,\xi}(y_o,y'_o,E_F)+iky'_i\sin\theta_{\bar{m}}} \quad (4.35)\\ &\times \left(p_0 + 2p_2 i\hbar\frac{d}{d\epsilon}\right)\left\{\sqrt{\epsilon}e^{-i\epsilon^2/8\hbar}\left(e^{i\pi/8}J_{-1/4}\left(\frac{\epsilon^2}{8\hbar}\right) + e^{-i\pi/8}J_{1/4}\left(\frac{\epsilon^2}{8\hbar}\right)\right)\right\}, \end{aligned}$$

for $\epsilon \geq 0$.

The final result for the transmission coefficient is given by

$$\begin{aligned} t^\xi_{nm} &= -\frac{1}{\sqrt{w_L w_R}}\mathrm{sgn}(\bar{m})\mathrm{sgn}(\bar{n})\mathrm{e}^{\frac{i}{\hbar}S^{nm}_\xi(E)-i\frac{\pi}{2}\mu_\xi-i\frac{\pi}{4}}\left|\frac{\pi\Delta S}{2}\right|^{1/2}\\ &\times\left\{\overline{A}\left[J_{1/4}\left(\frac{|\Delta S|}{\hbar}\right)e^{-i\frac{\pi}{8}} + J_{-1/4}\left(\frac{|\Delta S|}{\hbar}\right)e^{i\frac{\pi}{8}}\right] +\right.\\ &\left.+\Delta A\left[J_{3/4}\left(\frac{|\Delta S|}{\hbar}\right)e^{-3i\frac{\pi}{8}} + J_{-3/4}\left(\frac{|\Delta S|}{\hbar}\right)e^{3i\frac{\pi}{8}}\right]\right\}. \quad (4.36) \end{aligned}$$

Here $\Delta A = \frac{A_1}{2} - \frac{A_0}{\sqrt{2}}$, $\overline{A} = \frac{A_1}{2} + \frac{A_0}{\sqrt{2}}$,$\overline{S} = (S_0 + S_1)/2$ and $\Delta S = (S_1 - S_0)/2$. With a local value given by

$$t^\xi_{nm} = -\frac{(2\hbar)^{1/4}p_0}{2\Gamma(3/4)\sqrt{w_L w_R}}\mathrm{sgn}(\bar{m})\mathrm{sgn}(\bar{n})\mathrm{e}^{\frac{i}{\hbar}S^{nm}_\xi(E)-i\frac{\pi}{2}\mu_\xi-i\frac{\pi}{8}}. \quad (4.37)$$

The expressions given above for the tangent and pitchfork bifurcation are analogous to the corresponding expressions for the contribution of periodic orbits bifurcations to the density of states derived in [48] or for the photo-absorption spectrum in [112], since the normal forms are the same. The difference between them is the physical meaning of the stationary condition that the trajectories satisfy.

4.4 Conductance and open-orbits bifurcations

As we have seen, for a single transmission coefficient, bifurcating open orbits have a higher semiclassical weight than isolated ones. In analogy to our previous approach in spectral statistics, we are going to study deviations of the conductance from universality coming from a single bifurcation event. Therefore we assume that the rest of the orbits contributing to transport can be treated in the standard way in open chaotic systems.

Let us denote the two orbits born in a tangent bifurcation by ξ and ξ', which contribute to the transmission from channel α to β. At the bifurcation they give

a collective contribution to the transmission given by Eq. (4.28). We are mainly interested in the $\hbar$-dependence of the contribution. Therefore, we write the total transmission amplitudes in a short form as

$$t_{nm}^{\rm sc} = \frac{1}{\sqrt{t_H}} \sum_{\gamma(n,m)} A_\gamma {\rm e}^{\frac{i}{\hbar}S_\gamma} + \frac{1}{t_H^{1/3}} \delta_{n,\beta}\delta_{m,\alpha} \tilde{A}_\xi {\rm e}^{\frac{i}{\hbar}S_\xi}, \tag{4.38}$$

where we have hidden all other prefactors and phases in the amplitudes A_γ and $\tilde{A}_\xi$.

The mean transmission is given by substituting Eq.(4.38) in Eq.(4.3):

$$\langle T \rangle = \langle {\rm Tr}(tt^\dagger) \rangle = \left\langle \frac{1}{t_H} \sum_{n,m} \sum_{\substack{\gamma(n,m) \\ \gamma'(n,m)}} A_\gamma A_{\gamma'}^* {\rm e}^{\frac{i}{\hbar}(S_\gamma - S_{\gamma'})} \right\rangle \tag{4.39}$$

$$+ \left\langle \frac{1}{t_H^{5/6}} \sum_{\gamma(\beta,\alpha)} \left(A_\gamma A_\xi^* {\rm e}^{\frac{i}{\hbar}(S_\gamma - S_\xi)} + c.c. \right) + \frac{1}{t_H^{2/3}} |\tilde{A}_\xi|^2 \right\rangle .$$

As in the previous chapter, we have a double sum with a rapidly oscillating phase, most of the contributions will cancel out in the semiclassical limit after the average in energy. A semiclassical derivation for the transmission in the diagonal approximation, i.e., taking only terms $\gamma = \gamma'$ in Eq.(4.39), was done first in Ref. [106].

In the diagonal approximation the first double sum can be replaced by the sum rule for open systems [114], leading to

$$\begin{aligned} T_{\rm u}^{\rm diag} &= \left\langle \frac{1}{t_H} \sum_{n,m} \sum_{\gamma(n,m)} |A_\gamma|^2 \right\rangle \\ &= \frac{1}{t_H} \sum_{n,m} \int_0^\infty dt e^{-(N_L+N_R)t/t_H} = \frac{N_L N_R}{N_L + N_R}, \end{aligned} \tag{4.40}$$

where $(N_L+N_R)/t_H = 1/\tau_d$ is the classical escape rate of the system with openings of size w_L and w_R.

The second sum in Eq.(4.39) does not give any contribution, since the sum over γ does not contain the trajectory ξ and therefore the phase cannot be cancelled out or be systematically smaller than $\hbar$.

The total contribution to T at the bifurcation is then given in the diagonal approximation by

$$\langle T \rangle^{\rm diag} = \frac{N_L N_R}{N} + \frac{\tilde{a}}{N^{2/3}}, \tag{4.41}$$

where we have written t_H is terms of $N = N_L + N_R$ and τ_d, and all other constants and potential-dependent parameters are hidden in $\tilde{a}$. The semiclassical limit corresponds to $\hbar \to 0$ or equivalently $N \to \infty$. It is clear that the contribution from

the bifurcation goes to zero in that limit. This lets us conclude that even when for a single transmission coefficient a bifurcation can be dominant, upon summing over all possible scattering trajectories the contribution is negligible, since the sum over channel gives a term N^2, that dominates over the different $\hbar$ scaling.

We have seen in the previous chapter that the effect of bifurcations can be stronger slightly after the bifurcations, and that this can be associated with a non-diagonal contribution of the orbits born at the bifurcations. Let us consider here the non-diagonal contribution of ξ and ξ' for $0 < \epsilon < \hbar^{2/3}$. Since the standard semiclassical approximation for the non-diagonal contribution of the orbits born at a bifurcation does not diverge, we will use it to calculate this contribution. Thus,

$$T_{\xi\xi'}^{\mathrm{off-d}} = 2A_\xi A_{\xi'}^* \sin\left(\frac{2\epsilon^{3/2}}{3\hbar}\right) \approx \frac{\pi p_0^2 \epsilon}{3 w_L w_R}. \tag{4.42}$$

Off-diagonal contributions to T has been considered semiclassically to leading order in Ref. [115] and up to all orders in Ref. [116]. Trajectories giving a contribution are similar to those presented in the introduction in the spectral statistics, but they are not periodic. The trajectories come close to their time-reversed in phase space, i.e., they have a self-crossing in configuration space or in momentum space, the partner trajectory avoids such a self-crossing. It can be shown that the difference in action can be systematically smaller than $\hbar$, as for the spectral statistics. For the transmission through a cavity the first quantum correction to the double sum in Eq.(4.38) is

$$T_{\mathrm{u}}^{\mathrm{off-d}} = -\frac{N_L N_R}{N^2}. \tag{4.43}$$

As we can notice, the non-diagonal contribution of the orbits born at the bifurcation also scales also like $N^{-2/3}$ (since it only exist for $\epsilon < \hbar^{2/3}$), therefore it is not only negligible in comparison to the diagonal contribution of chaotic orbits, but also in comparison with the weak localization correction, which is of order 1.

A similar analysis can be done for a pitchfork bifurcation. In this case the $\hbar$ scaling of the transmission is $\hbar^{1/4}$, and then the diagonal and off-diagonal contributions of the bifurcating orbits go like $N^{-1/2}$, vanishing in the semiclassical limit. A remaining open question is the implications of bifurcations of transmission trajectories on the reflection coefficients, in order to preserved unitarity when these effects are taken into account.

We have seen in this chapter that bifurcation scenarios for scattering trajectories can be defined, and that for a single transmission (or reflection) coefficient they can be dominant, but when considering the full transmission their effect goes

to zero in the semiclassical limit. This is because, although they have a different $\hbar$-dependence than isolated orbits, if they happen as single events, they can be ignored when summing up all possible channel contributions. For other kinds of bifurcations the scaling is different, depending on the type of bifurcation [51]. The amplitude of the contribution of isolated orbits scales as $\hbar^{1/2}$, while that of bifurcating orbits goes as $\hbar^{1/2-\nu}$ with $\nu \leq 1/2$. In the total transmission the contribution of isolated orbits scales as $\hbar^{-1}$ (for the two-probe set up) due to the factor $\hbar^{-2}$ coming from the sum over all possible channels. This is always dominant in comparison with $\hbar^{1-2\nu}$ with $1-2\nu \geq 0$ coming from a single bifurcating trajectory. We conclude then, that open-orbit bifurcations, as defined in this chapter, are not significant for total transmission in the semiclassical approximation to coherent transport, in contrast to the spectral statistics.

However, bifurcations of periodic orbits that are inside the system do, apparently, play a rôle according to Ref. [117], where it was studied the effect of bifurcations in the conductance moments in antidot lattices. These bifurcations are of periodic orbits, and they enter into play in the semiclassical description of transport within the Kubo formalism [118]. The equivalence between the scattering approach and the Kubo formalism has been shown quantum-mechanically in Ref. [106], but this result has not been shown so far to be preserved within the semiclassical approximation (a more detailed discussion will be given in the outlook).

Though we do not pretend to give an answer to this question, this has been a motivation to study the preservation of unitarity in the semiclassical approximation for open chaotic systems. In the next chapter, we will consider the decay problem in an open chaotic system. In the semiclassical consideration of decay two features are interesting. First of all, the standard semiclassical tools for evaluating double sums fails in preserving unitarity, as shown in Ref. [73] and have to be improved by introducing new diagrams. And second, Ehrenfest time effects can be of importance.

Chapter 5

Semiclassical approximation to the decay

In this chapter we will consider the semiclassical approximation to the survival probability for an open chaotic system, i.e., the probability to find a particle inside a certain volume at a certain time. We will compare the analytical results with numerical simulations and study a different class of deviations from the universal RMT prediction, compared to bifurcations, coming from Ehrenfest-time effects. First, we will introduce the system and the method of wave-function propagation that we consider in the numerical analysis. Then we will discuss the semiclassical approach to the survival probability and the leading quantum corrections for systems with time reversal symmetry. Finally, we will study Ehrenfest-time dependence of these corrections and compare with the numerical results.

5.1 Model system and important time scales

Billiards are typical model systems in the study of classical signatures in quantum systems [122]. They correspond to a bounded domain, where the dynamics is free apart from specular bounces at the boundaries. The shape of the boundary determines the nature of the dynamics.

For the numerical calculations presented in this chapter we will consider the desymmetrized diamond (DD) billiard, defined as the fundamental domain of the area confined by four intersecting disks centered at the vertices of a square (see Fig. 5.1(a)). The DD billiard is chaotic in the classical limit according to [123], and can be characterized by the disk radius R, and the length L of the longest straight segment of the boundary. In Fig. 5.1(b) we see the evolution of a single trajectory inside the billiard, showing the complexity of the dynamics.

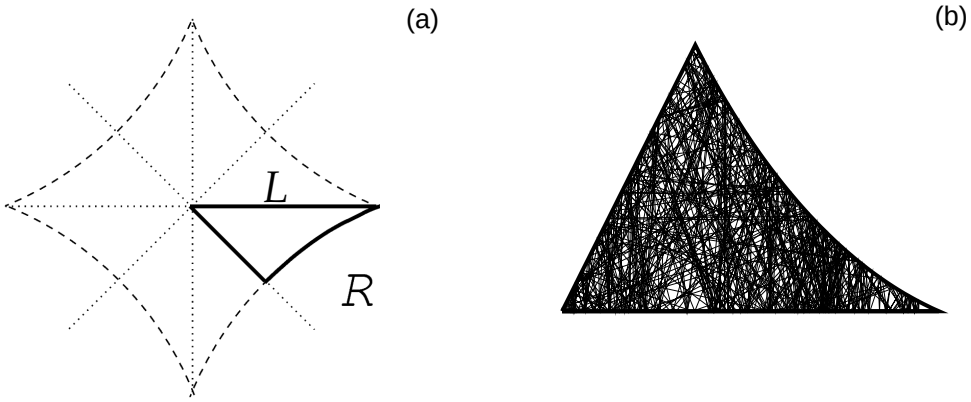

Figure 5.1: (a) Desymmetrized diamond (DD) billiard. (b) A classical trajectory in the DD billiard after 500 bounces, it fills the area of the billiard homogeneously, the phase space shows also the ergodicity of the dynamics.

Let us introduce the time scales that are important for our forthcoming analysis. The typical time that a trajectory travels between bounces is called the flight time t_f, and can be calculated for 2-dimensional chaotic billiards as

$$t_f = \frac{m\pi A}{p\mathcal{P}}, \tag{5.1}$$

where p is the magnitude of the momentum of the particles, m is the mass, A and $\mathcal{P}$ are the area and the perimeter of the billiard, respectively.

We will consider that at the boundary of the billiard there is an opening of size $w \ll \mathcal{P}$, so the dynamics inside the billiard is not strongly affect by the opening, and the main properties of closed chaotic systems are preserved. The dwell time τ_d is the typical time that a classical trajectory remains inside the system. At energy $E = H(\mathbf{r}, \mathbf{p})$ it is given by

$$\tau_d = \frac{\Omega(E)}{2wp}, \tag{5.2}$$

for a 2-dimensional system, recalling that $\Omega(E) = \int d\mathbf{r}' d\mathbf{p}' \delta(E - H(\mathbf{r}', \mathbf{p}'))$. For 2-dimensional billiards the integrals can be calculated easily yielding $\Omega(E) = \Omega = 2\pi m A$, independent of the energy. For which the dwell time reduces to

$$\tau_d = \frac{m\pi A}{wp} = \frac{\mathcal{P}}{w} t_f. \tag{5.3}$$

The ratio between the two classical time scales t_f and τ_d is energy independent, the two scales depend themselves on energy through p. The third classical scale of importance is the inverse of the Lyapunov exponent λ. The parameters that we have chosen were $L = 500$, $R = 655$ and $w = 80$, for which the ratio τ_d/t_f is

about 15, i.e., a classical particle bounces about 15 times against the boundary of the billiard before leaving. For the chosen parameter we have that $\lambda \approx \frac{1}{3t_f}$, which means that a typical classical trajectory can be considered ergodic after about three bounces.

The most important quantum scale is the Heisenberg time given for a 2-dimensional billiard by

$$t_H = \frac{mA}{\hbar}, \tag{5.4}$$

independent of the energy, since the mean density of states is energy-independent. The number of open channels is

$$N = \left[\!\left[\frac{2w}{\lambda_B}\right]\!\right], \tag{5.5}$$

where $\lambda_B = 2\pi\hbar/p$ is the de Broglie wave length. Typical experiments and numerical simulations in billiards are in the regime of $N \approx 10$, which is also the regime of our numerical simulations. Another important quantum time scale is the Ehrenfest time. As mentioned in the introduction, the Ehrenfest time τ_E [34] separates the short-time quantum dynamics where it follows the classical one, from a long-time regime, where the dynamics is dominated by wave interference. It is the time that two classical trajectories separated a distance of the de Broglie wavelength (a "quantum" distance), need to have a distance of the order of the system size (a "classical" distance). In a chaotic system one may use the fact that distances increase exponentially in order to estimate such a time. Different kind of "classical" scales can be used depending on the problem of consideration. According to Ref. [33] three different Ehrenfest time scales can be define: the closed-system τ_E^c, the transport τ_E^o and the escape τ_E^e Ehrenfest times. Quoting Ref. [33]: *the difference between these Ehrenfest times can be attributed to the additional splitting of a wave packet into partially transmitted and partially reflected waves at each encounter with an opening.* The definitions of the three times in terms of the typical size of the billiard $\mathcal{L}$, the opening w and the de Broglie wave-length λ_B are [40]:

i) the closed-system Ehrenfest time is defined as the time necessary for two trajectories initially separated by λ_B to have a separation of the typical system size $\mathcal{L}$:

$$\tau_E^{\mathrm{c}} = \frac{1}{\lambda} \ln\left(\frac{\mathcal{L}}{\lambda_B}\right). \tag{5.6}$$

For a two-dimensional billiard $\mathcal{L} \sim \sqrt{A}$.

ii) The transport Ehrenfest time is given by

$$\tau_E^{\mathrm{o}} = \frac{1}{\lambda} \ln\left(\frac{w^2}{\mathcal{L}\lambda_B}\right), \tag{5.7}$$

related with the opening w.

iii) The escape Ehrenfest time is given by

$$\tau_E^{\mathrm{e}} = \frac{1}{\lambda} \ln\left(\frac{w}{\lambda_B}\right). \tag{5.8}$$

Notice that $\tau_E^{\mathrm{e}} = (\tau_E^{\mathrm{c}} + \tau_E^{\mathrm{o}})/2$.

It is usually assumed that $\tau_d \gg \tau_E^{\mathrm{x}}$, so that quantum effects are noticeable before the particle leaves the system. When the two scales are comparable, deviations from RMT can show up, us we will see in this chapter.

5.2 Numerical simulation

For the study of the survival probability we need to compute the quantum time evolution of a given initial state localized inside the DD billiard at $t = 0$, and the classical time evolution of an ensemble of classical trajectories. For the classical evolution we use a routine in C++ to calculate the propagation for each individual initial condition. The propagation was done as following: free propagation until the particle reaches the boundary of the billiard plus specular reflection at the boundary. This procedure was repeated until the particle had escaped through the opening.

The quantum time evolution of the wave packet was performed with a Trotter-Suzuki algorithm provided by the author of Ref. [119]. Its basic idea is to decomposed the evolution operator by a finite product of evolution operators where each one can be solved analytically. We recommend to check Ref. [120] for a detailed review of the method. We will briefly recall the basic ideas for its implementation in this section.

The solution of the Schrödinger equation for a time independent Hamiltonian can be written as

$$|\psi(t)\rangle = \mathrm{e}^{-i\frac{\hat{H}}{\hbar}t}|\psi(0)\rangle. \tag{5.9}$$

Consider a one dimensional problem of a confined particle between $0 < x < a$, with a Hamiltonian in position representation given by

$$H(x) = -\frac{\hbar^2}{2m}\frac{d}{dx^2} + V(x). \tag{5.10}$$

In order to calculate numerically the wave function at a time t in position representation we need to discretize the continuum space, so we choose a grid of $M+1$ mesh points of size δ. The discretized Schrödinger equation can be written as

$$i\frac{\partial}{\partial t}\psi_l(t) = -\delta^{-2}(\psi_{l+1}(t) + \psi_{l-1}(t)) + (V(l\delta) + 2\delta^{-2})\psi_l(t), \tag{5.11}$$

for $l = 1, ..., M+1$, with $\hbar = 1$, $m = 1$ and $\psi_l(t) = 0$ for $l \leq 0$ or $l > M+1$. This is completely equivalent to consider a particle moving on a chain with $M+1$ lattice sites, described by the tight-binding Hamiltonian

$$\hat{H} = v \sum_{l=1}^{M} (\hat{c}_l^\dagger \hat{c}_{l+1} + \hat{c}_{l+1}^\dagger \hat{c}_l) + w \sum_{l=1}^{M+1} \epsilon_l \hat{n}_l, \tag{5.12}$$

where $\hat{c}_l^\dagger$ ($\hat{c}_l$) creates (annihilates) a particle at the site l, $n_l = \hat{c}_l^\dagger \hat{c}_l$ counts the number of particles at site l, v is the kinetic energy scale and $w\epsilon_l$ is the potential at site l felt by the particle. We need to set $v = -\delta^{-2}$ and $w\epsilon_l = V(l\delta) + 2\delta^{-2}$, in order to have the equivalence between both formulations.

The method is based in writing the Hamiltonian as a sum of other Hamiltonians that can be easily diagonalized. If $\hat{H} = \hat{H}_O + \hat{H}_E$ one can approximate for short times τ

$$e^{-i\tau\hat{H}} = e^{-i\tau(\hat{H}_O + \hat{H}_E)} \approx e^{-i\tau\hat{H}_O} e^{-i\tau\hat{H}_E} \equiv \hat{U}_1(\tau). \tag{5.13}$$

The error in this approximation can be shown to scale as τ^2 [120].

Let us recall the example given in Ref. [120] of a free particle moving on an open-ended chain of $M+1$ sites, with a Hamiltonian give by Eq. (5.12) with $w\epsilon_l = 0$ (denoted by $\hat{K}$ in the following). Assuming M even for convenience, $\hat{K}$ can be decomposed as $\hat{K} = \hat{K}_O + \hat{K}_E$ where O and E refer to odd and even sub-lattices, respectively, and are given by

$$\hat{K}_0 = v \sum_{l=0}^{M/2-1} (\hat{c}_{2l+1}^\dagger \hat{c}_{2l+2} + \hat{c}_{2l+2}^\dagger \hat{c}_{2l+1}) \tag{5.14}$$

and

$$\hat{K}_E = v \sum_{l=0}^{M/2-1} (\hat{c}_{2l+2}^\dagger \hat{c}_{2l+3} + \hat{c}_{2l+3}^\dagger \hat{c}_{2l+2}). \tag{5.15}$$

This leads to

$$\hat{U}_1(\tau) = \left(\prod_{l=0}^{L/2-1} e^{-i\tau K_{2l+1}} \right) \left(\prod_{l=0}^{L/2-1} e^{-i\tau K_{2l+2}} \right), \tag{5.16}$$

where $K_l \equiv v(\hat{c}_l^\dagger \hat{c}_{l+1} + \hat{c}_{l+1}^\dagger \hat{c}_l)$.

Eq. (5.16) shows how the propagation is ordered as a sequence of two-site systems. Each of the two-site propagators can be easily calculated and one can finally write

$$e^{-i\tau K_l} \begin{pmatrix} \Phi_l(t) \\ \Phi_{l+1}(t) \end{pmatrix} = \begin{pmatrix} \cos(\tau v) & -i\sin(\tau v) \\ -i\sin(\tau v) & \cos(\tau v) \end{pmatrix} \begin{pmatrix} \Phi_l(t) \\ \Phi_{l+1}(t) \end{pmatrix}. \tag{5.17}$$

The procedure can be generalized for $w\epsilon_l \neq 0$, taking $\hat{H} = \hat{K} + \hat{U}$ with $\hat{U} = w\sum_{l=1}^{M+1} \epsilon_l \hat{n}_l$ and making the approximation $\mathrm{e}^{-i\hat{H}\tau} = \mathrm{e}^{-i\hat{K}\tau/2}\mathrm{e}^{-i\hat{U}\tau}\mathrm{e}^{-i\hat{K}\tau/2}$. The propagation with $\mathrm{e}^{-i\hat{U}\tau}$ is trivial: each component $\Phi_l(t)$ has to be multiplied by a phase $\mathrm{e}^{-i\tau w\epsilon_l}$.

A second order approximation can be built from the first order approximation as

$$\hat{U}_2(\tau) = \hat{U}_1^T(\tau/2)\hat{U}_1(\tau/2), \tag{5.18}$$

where $\hat{U}_1^T$ is the transpose of $\hat{U}_1$. In a similar way, an approximation that is correct up to fourth-order in the time step can be constructed from the previous approximation algorithm as

$$\hat{U}_4(\tau) = \hat{U}_2(s\tau)\hat{U}_2(s\tau)\hat{U}_2((1-4s)\tau)\hat{U}_2(s\tau)\hat{U}_2(s\tau), \tag{5.19}$$

with $s = 1/(4 - 4^{\frac{1}{3}})$ (the subindices 4 and 2 indicate the order of the approximation).

The calculation for a 2-dimensional billiard is straight-forward, the propagator can be written as the product of the free propagation in one direction, times the free propagation in the other. The 2-dimensional discretized wave function can be written as a vector with components $\psi_{lk}(t)$ (with $\psi_{lk}(t) = 0$ if $(l\delta, k\delta)$ are outside the billiard). The second order propagator for the two dimensional problem can be written as

$$\begin{aligned} \hat{U}_2(t) &= e^{-i\hat{K}_{O,x}\tau/2}e^{-i\hat{K}_{O,y}\tau/2}e^{-i\hat{K}_{E,x}\tau/2}e^{-i\hat{K}_{E,y}\tau/2} \\ &\quad \times e^{-iU\tau}e^{-i\hat{K}_{E,y}\tau/2}e^{-i\hat{K}_{E,x}\tau/2}e^{-i\hat{K}_{O,y}\tau/2}e^{-i\hat{K}_{O,x}\tau/2}, \end{aligned} \tag{5.20}$$

where $\hat{K}_{O,x}$ ($\hat{K}_{O,y}$) and $\hat{K}_{E,x}$ ($\hat{K}_{E,y}$) are given by Eqs. (5.14) and (5.15), acting on the first (second) subindex of $\psi_{lk}(t)$ according to Eqs. (5.16), (5.17). The numerical propagation was done as an implementation on Fortran of the fourth-order propagator Eq. (5.19), taking into account Eqs. (5.20), (5.16) and (5.17).

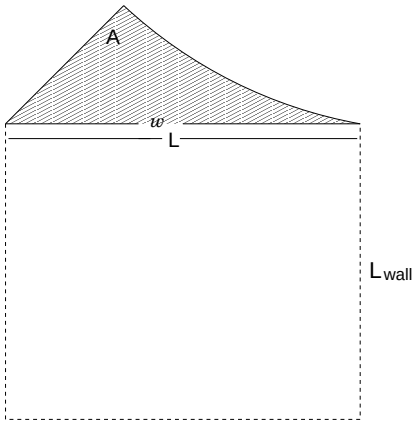

Figure 5.2: Open DD billiard (filled) attached to a rectangular guide.

As we notice this method applies for unitary propagation. In order to consider an open system, it was attached to the lower part of the billiard a guide as sketched in Fig. 5.2 and performed the propagation of the full system as a closed system (within the previous description). The outer box was

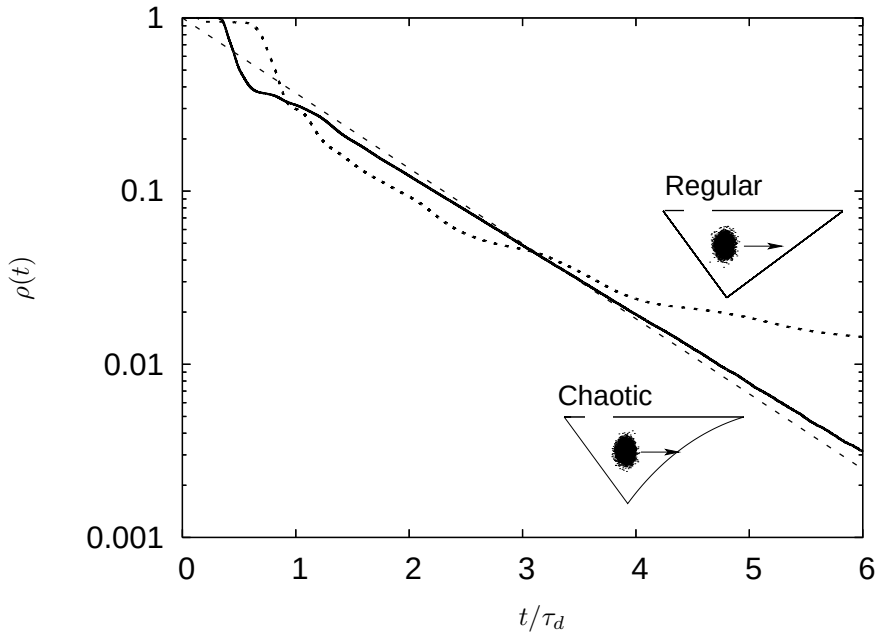

Figure 5.3: Classical survival probability for an ensemble of particles with a Gaussian distribution in phase space (as depicted in the inset billiards) inside the DD billiard (full line) and for a triangular billiard (dotted line), together with Eq. (5.21) (dashed). The DD billiard shows the expected exponential decay, while the triangular billiard, for which the dynamics is regular, shows a slower decay.

chosen big enough in order to avoid back reflections, therefore the size L_{wall} was selected such that $2mL_{\text{wall}}/p > t_H$, i.e., the minimal time for a classical trajectory to bounce and go back into the DD billiard was larger that the Heisenberg time of the closed DD-billiard. Therefore the time at which back reflections start being important was much larger than our range of interest (which is $t < \sqrt{t_H \tau_d}$). For $L = 500$ we have taken $L_{\text{wall}} = 3500$. This method of propagation requires a lot of numerical effort, mainly due to the attached box. A single propagation of a Gaussian initial state up to $t = 6\tau_d$ takes almost 3 weeks of computation.

5.3 Survival probability

Physical phenomena involving decay processes have been addressed in many physical contexts. As mentioned in the introduction, they play a central role in the study of excitation relaxation in semiconductors quantum dots and wires [58, 59], ionization of molecular Rydberg states [121], atoms in optically generated lattices [62, 63, 64, 65] and optical micro-cavities [66], to name a few examples.

The survival probability is the probability of finding a particle inside the system

at a certain time. Classically, once the initial conditions of a single particle are given we know exactly when the particle is going to be outside the volume A, so this probability must be understood as an average quantity, i.e., from an ensemble of classical particles with a given energy how many will remain after a certain time when the system is open. When the dynamics is chaotic (and this is preserved after opening the system) the classical survival probability decays exponentially in time

$$\rho^c(t) = e^{-t/\tau_d}, \tag{5.21}$$

while for mixed or integrable systems the decay is usually algebraic. We depict in Fig. 5.3 an example comparing the decay for the above mentioned DD billiard with the case of a billiard of triangular shape, which is regular. We see that Eq.(5.21) describes very accurately the chaotic situation for times $t > \lambda^{-1}$. Numerical results confirming Eq.(5.21) have been extensively done; moreover, it has also been confirmed experimentally, e.g. in Ref. [64] experimental measurements for the decay of atoms in optically generated lattices were shown, revealing the fast exponential decay for chaotic dynamics in contrast with the slower algebraic decay for regular shapes.

Theoretical calculations with supersymmetry techniques [124, 125] however reveal that the quantum survival probability, defined as

$$\rho\,(t) = \int_A d\mathbf{r}\psi(\mathbf{r},t)\psi^*(\mathbf{r},t), \tag{5.22}$$

deviates from the classical one at times comparable to $t^* = \sqrt{\tau_d t_H}$. The quantum decay was considered as well in Ref. [126] where these deviations were observed.

The RMT predictions are universal functions, which only depend on the general symmetries of the system, the classical life time and the Heisenberg time. A successful semiclassical approach to derive the RMT prediction in the context of quantum graphs was performed in Ref. [127], reproducing RMT up to first order corrections for networks with and without time-reversal symmetry. In Ref. [73] a semiclassical calculation for the decay of an initially localized wave function inside an arbitrary chaotic system was developed. In the analysis a unitarity problem was encountered when using standard semiclassical techniques to evaluate the contribution of pairs of interfering trajectories starting and ending inside the system. Therefore a new kind of diagrams was introduced, which are crucial to ensure unitarity in any problem involving open trajectories connecting two arbitrary points in the bulk, as we will see in the following.

5.4 Semiclassical approximation to the survival probability

The survival probability can be written in terms of the propagator as

$$\rho\left(t\right)=\int_{A}d\mathbf{r}d\mathbf{r}'d\mathbf{r}''K(\mathbf{r},\mathbf{r}',t)K^{*}(\mathbf{r},\mathbf{r}'',t)\psi_{o}(\mathbf{r}')\psi_{o}^{*}(\mathbf{r}''),\tag{5.23}$$

where $\psi_o(\mathbf{r})$ is the wave function at $t=0$. For a closed system $\rho(t)=\langle\psi(t)|\psi(t)\rangle=1$, while for an open system this does not longer hold and $\rho(t)$ decays in time.
In order to calculate the semiclassical expression for this quantity, we replace the exact quantum propagator $K(\mathbf{r},\mathbf{r}',t)$ with the semiclassical Van Vleck propagator Eq. (1.7). The semiclassical survival probability is given by

$$\rho^{\mathrm{sc}}(t)=\frac{1}{(2\pi\hbar)^{2}}\int_{A}d\mathbf{r}d\mathbf{r}'d\mathbf{r}''\sum_{\substack{\tilde{\gamma}(\mathbf{r}'\to\mathbf{r},t)\\ \tilde{\gamma}'(\mathbf{r}''\to\mathbf{r},t)}}D_{\tilde{\gamma}}D_{\tilde{\gamma}'}^{*}\mathrm{e}^{\frac{i}{\hbar}(S_{\tilde{\gamma}}-S_{\tilde{\gamma}'})}\psi_{o}(\mathbf{r}')\psi_{o}^{*}(\mathbf{r}''),\tag{5.24}$$

where we have hidden the Maslov indices into the amplitudes $D_{\tilde{\gamma}}$.
Let us consider a smoothed survival probability

$$\tilde{\rho}(t)=\langle\rho^{\mathrm{sc}}(t)\rangle_{\Delta t}=\frac{1}{\Delta t}\int_{t-\Delta t/2}^{t+\Delta t/2}\rho^{\mathrm{sc}}(t')dt',\tag{5.25}$$

with $\Delta t\ll t$. We will see, later on, that apart from corrections of order $\hbar$, $\tilde{\rho}(t)\approx\rho(t)$ in the semiclassical limit, generalizing the result in Ref. [73] to non-localized wave functions.

The phase of the double sum in Eq. (5.24) is rapidly oscillating unless trajectories are correlated. Therefore most of the contributions will disappear due to the average in time. The contributions that remain are from pairs of trajectories with action differences of the order of $\hbar$, which implies that the trajectories $\tilde{\gamma}$ and $\tilde{\gamma}'$ should be "similar". This restricts the initial points of the trajectories, i.e. they must be almost the same. We expand trajectories $\tilde{\gamma}$ (or $\tilde{\gamma}'$) going from $\mathbf{r}'$ (or $\mathbf{r}''$) to $\mathbf{r}$ in a time t around trajectories γ (or γ') going from $\mathbf{r}_o=(\mathbf{r}'+\mathbf{r}'')/2$ to $\mathbf{r}$ in a time t. The expansion will contain terms up to zero order in the prefactor and terms up to the first order in the exponential, because the latter is more sensitive to small changes in the argument. The expansion of the actions yields

$$S_{\tilde{\gamma}}\left(\mathbf{r},\mathbf{r}',t\right)\approx S_{\gamma}\left(\mathbf{r},\mathbf{r}_{o},t\right)-\frac{1}{2}\mathbf{q}\cdot\mathbf{p}_{\gamma,o},\tag{5.26}$$

$$S_{\tilde{\gamma}'}\left(\mathbf{r},\mathbf{r}'',t\right)\approx S_{\gamma'}\left(\mathbf{r},\mathbf{r}_{o},t\right)+\frac{1}{2}\mathbf{q}\cdot\mathbf{p}_{\gamma',o},\tag{5.27}$$

where $\mathbf{q}=\mathbf{r}'-\mathbf{r}''$ and $\mathbf{p}_{\gamma,o}$ ($\mathbf{p}_{\gamma',o}$) is the initial momentum of the trajectory γ (γ'). Here we have approximated $D_{\tilde{\gamma}}\left(\mathbf{r},\mathbf{r}',t\right)\approx D_{\gamma}\left(\mathbf{r},\mathbf{r}_{o},t\right)$, and $D_{\tilde{\gamma}'}\left(\mathbf{r},\mathbf{r}'',t\right)\approx$

$D_{\gamma'}(\mathbf{r}, \mathbf{r}_o, t)$, then

$$\tilde{\rho}(t) = \left\langle \frac{1}{(2\pi\hbar)^2} \int d\mathbf{r} d\mathbf{r}_o d\mathbf{q} \psi_o \left(\mathbf{r}_o + \frac{\mathbf{q}}{2}\right) \psi_o^* \left(\mathbf{r}_o - \frac{\mathbf{q}}{2}\right) \times \sum_{\gamma,\gamma'(\mathbf{r}_o \to \mathbf{r}, t)} D_\gamma D_{\gamma'}^* e^{\frac{i}{\hbar}(S_\gamma - S_{\gamma'})} \mathrm{e}^{-\frac{i}{\hbar}(\mathbf{p}_{\gamma,o} + \mathbf{p}_{\gamma',o}) \cdot \frac{\mathbf{q}}{2}} \right\rangle_{\Delta t}. \tag{5.28}$$

For an initial coherent state, the integrals over $\mathbf{r}_0$ and $\mathbf{q}$ can easily be done and the result is consistent with Ref. [128].
We recognized that the integral over $\mathbf{q}$ gives the Wigner function of the initial states, therefore we can write

$$\tilde{\rho}(t) = \left\langle \frac{1}{(2\pi\hbar)^2} \int d\mathbf{r} d\mathbf{r}_o \sum_{\gamma,\gamma'(\mathbf{r}_o \to \mathbf{r}, t)} D_\gamma D_{\gamma'}^* e^{\frac{i}{\hbar}(S_\gamma - S_{\gamma'})} \rho_W(\mathbf{r}_o, \bar{\mathbf{p}}_{\gamma\gamma',o}) \right\rangle_{\Delta t}, \tag{5.29}$$

where $\bar{\mathbf{p}}_{\gamma\gamma',o} = (\mathbf{p}_{\gamma,o} + \mathbf{p}_{\gamma',o})/2$ and

$$\rho_W(\mathbf{r}, \mathbf{p}) = \int d\mathbf{r}' \psi_o \left(\mathbf{r} + \frac{\mathbf{r}'}{2}\right) \psi_o^* \left(\mathbf{r} - \frac{\mathbf{r}'}{2}\right) \mathrm{e}^{-\frac{i}{\hbar}\mathbf{r}' \cdot \mathbf{p}} \tag{5.30}$$

is the Wigner transformation of $\psi_o(\mathbf{r})$.

5.4.1 Diagonal approximation

In Eq. (5.29) we still have a fast oscillating phase and most of the contributions will cancel out due to the time average, unless the trajectories are systematically correlated. The main contribution corresponds to the diagonal approximation, i.e. $\gamma = \gamma'$, which gives the classical survival probability:

$$\tilde{\rho}(t) = \left\langle \frac{1}{(2\pi\hbar)^2} \int d\mathbf{r} d\mathbf{r}_o \sum_{\gamma(\mathbf{r}_o \to \mathbf{r}, t)} |D_\gamma|^2 \rho_W(\mathbf{r}_o, \bar{\mathbf{p}}_{\gamma\gamma',o}) \right\rangle_{\Delta t}. \tag{5.31}$$

Together with the following sum rule for open systems [114]:

$$\int d\mathbf{r} \sum_{\gamma(\mathbf{r}_o \to \mathbf{r}, t)} |D_\gamma|^2 (...) = \int d\mathbf{p}_o \mathrm{e}^{-t/\tau_d} (...), \tag{5.32}$$

Eq. (5.31) yields

$$\tilde{\rho}^{\mathrm{diag}}(t) = \langle \mathrm{e}^{-t/\tau_d} \rangle_{\mathbf{r},\mathbf{p}}, \tag{5.33}$$

where $\langle ... \rangle_{\mathbf{r},\mathbf{p}}$ indicates a phase space average,

$$\langle F \rangle_{\mathbf{r},\mathbf{p}} = \frac{1}{(2\pi\hbar)^2} \int d\mathbf{r} d\mathbf{p} F(\mathbf{r}, \mathbf{p}) \rho_W(\mathbf{r}, \mathbf{p}). \tag{5.34}$$

Since τ_d is energy dependent, in Eq. (5.33) it is calculated at $E = H(\mathbf{r}, \mathbf{p})$. For initial states that are localized in energy, the exponential can be taken out of the

brackets and the remaining integral is equal to 1 due to normalization. We also observe that at the diagonal approximation, which corresponds to the classical decay, the probability is equal to one for $t = 0$ and for the limit of a closed system $\tau_d \to \infty$, reflecting that classically the conservation of particles is also fulfilled.

Eq. (5.33) has two restrictions. First of all, we have supposed that at time t the trajectories can already be considered ergodic. This is a good assumption as long as $t\lambda \gg 1$. Secondly, we have supposed that the ergodicity of the corresponding closed system is not affected by the opening, meaning, classically the opening should be small $\tau_d\lambda \gg 1$ (though quantum mechanically it is very large $\tau_d \ll t_H$ in the semiclassical limit).

Let us compare Eq. (5.33) with the numerical simulations for the quantum propagation. For this purpose we will consider an Gaussian wave packet, given by

$$\psi_o\left(\mathbf{r}\right) = \left(\frac{1}{\pi\sigma^2}\right)^{1/2} \exp\left(\frac{i}{\hbar}\mathbf{p}_o\cdot\left(\mathbf{r}-\mathbf{r}_o\right) - \frac{1}{2\sigma^2}\left(\mathbf{r}-\mathbf{r}_o\right)^2\right), \tag{5.35}$$

where $\sigma \ll \sqrt{A}$ so that it is normalized in A: $\int_A d\mathbf{r}|\psi_0(\mathbf{r})|^2 = 1$. The corresponding Wigner transformation can be easily calculated given this condition:

$$\rho_W(\mathbf{r},\mathbf{p}) = 4\exp\left(-\frac{1}{\sigma^2}\left(\mathbf{r}-\mathbf{r}_o\right)^2\right)\exp\left(-\frac{\sigma^2}{\hbar^2}\left(\mathbf{p}-\mathbf{p}_o\right)^2\right), \tag{5.36}$$

so that Eq. (5.33) can be written as

$$\tilde{\rho}^{\mathrm{diag}}_{\psi_o}(t) = 2\mathrm{e}^{-\frac{1}{a^2}}\int_0^\infty du\, u\, \mathrm{e}^{-u^2-aut/\tau_d^o} I_o\left(\frac{2u}{a}\right), \tag{5.37}$$

where $a = \hbar/(\sigma p_o)$ and $\tau_d^o = \tau_d(p_o)$ is the dwell time for $p_o = |\mathbf{p}_o|$ and $I_0(x)$ is the modified Bessel function of the first kind.

The advantage of working with a Gaussian wave packet is that the classical counterpart of Eq. (5.35) has a direct translation: given that the Wigner function is always positive in this case, it can be taken as a probability distribution. For the classical simulation we choose an ensemble of trajectories with an initial distribution is phase space given by Eq. (5.36) and simulate the dynamics inside the DD billiard.

The chosen parameters for the wave function are $\sigma = 15$ and $\lambda_B = 2\pi\hbar/p_o = 15$. The way of choosing the parameters σ and λ_B has to be careful. On one hand, numerical limitations does not allow one to choose λ_B smaller than 12. On the other hand, to be on the semiclassical limit the number of channels must be much larger than one, yielding the condition

$$\lambda_B^{-1} < \frac{\sigma}{\sigma^2 + w^2}. \tag{5.38}$$

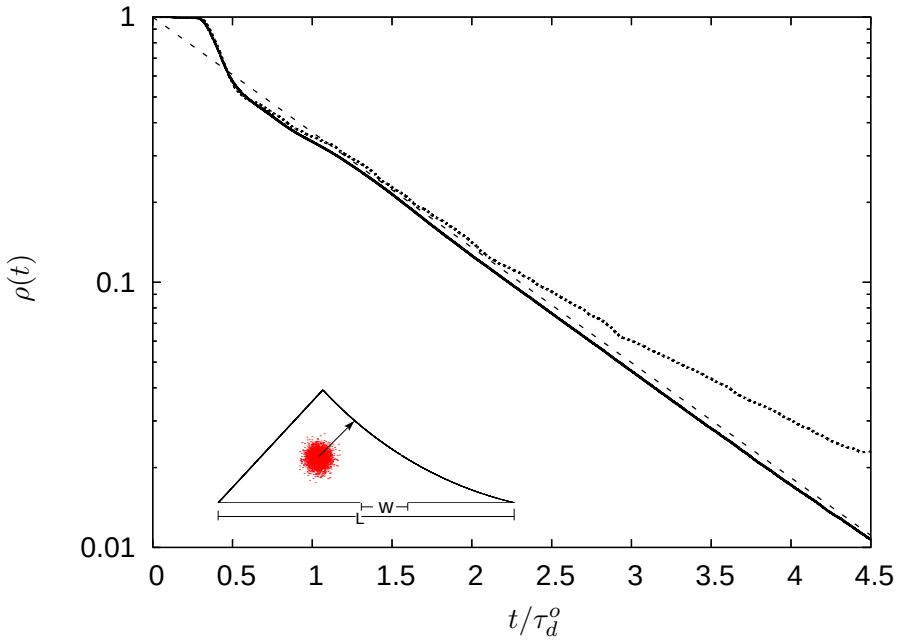

Figure 5.4: Comparison between quantum mechanical decay (dotted line) with the classical decay (full line) for the DD billiard and Eq. (5.37) (dashed line). The time in given in units of τ_d^o, the data showed in the plot is for a single numerical realization with $\mathbf{r}_o = (0.34L, 0.14L)$, the momentum direction $\theta_o = \pi/4$ and the opening starting at $0.48L$ (inset).

There is a restriction as well for the validity of the expansion of the actions Eq.(5.26) and Eq. (5.27). According to Ref. [129] this is $\sigma^2 m\lambda \ll \hbar$. This condition is a requirement for the linearization of all the trajectories around a single starting point r_o, i.e, the second term in the expansion should be smaller than $\hbar$. In our approach, we are not linearizing all the trajectories around a single starting point, but we are neglecting contributions of pairs of trajectories whose starting points are very different, since their contribution will be rapidly oscillating and cancelled out by the time average. This requires a weaker condition, it is sufficient that the second term in the expansion is smaller than the first one, which corresponds to take $\lambda t_f \mathcal{P} < 2\pi\sqrt{A}$. In Fig. 5.4 we show a comparison between the classical and the quantum simulation for the decay inside the DD billiard together with Eq. (5.37), evaluated numerically. The classical curve agrees very well with the diagonal approximation Eq. (5.37). The quantum mechanical curve follows the classical one for short times and starts to deviate at times comparable with $2\tau_d^o$.

Eq. (5.37) is independent of $\mathbf{r}_o$, of the direction of $\mathbf{p}_o$ and of the exact position of the leads. In the numerical simulations this is not strictly so, since for short time these conditions are all important, and lead to some corrections to Eq. (5.37) which are system specific. These non-universal corrections are of classical

"nature", in the sense that they appear already in the classical decay, as revealed by the numerical simulations. As we can observe, $\rho(t)$ is a sufficiently smooth curve, therefore we did not perform any local time average in the data shown. In the next section, for a more precise comparison of the quantum corrections we will introduce an average. For chaotic systems averages can be interchanged. So we can instead of performing a time average, perform an average over the initial localization, positions of the leads and direction of the momentum.

5.4.2 Leading quantum corrections to the decay

The first non-diagonal contribution to the semiclassical expression in Eq.(5.29) comes from trajectories coming "close" to their time-reversed version as sketched in Fig. 5.5. These are the kind of trajectories giving rise to weak localization in the context of transport [115]. In the case of open trajectories that are not attached to the opening, special care must be taken, as shown in Ref. [73], and new diagrams have to be considered.

Two-leg-loops contribution

Let us first consider the contribution of the standard loops sketched in Fig. 5.5, denoted here by 2ll (two-leg-loops). We follow the phase space approach introduced in Ref. [31] and used in Ref. [73] to describe such a contribution to the survival probability.

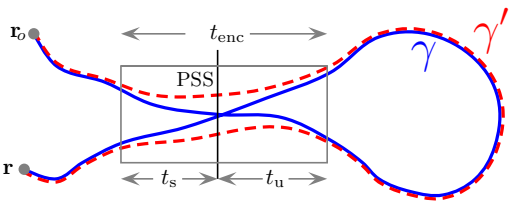

Figure 5.5: Sketch of orbits with a self encounter, giving off-diagonal contribution for systems with time reversal symmetry.

As explained in the introduction, in each loop pair the trajectory γ contains an encounter region, where two stretches of the same trajectory are sufficiently close, such that they are mutually linearizable. The time where this linearization is valid is defined as the encounter time $t_{\rm enc}$. Along γ the two stretches are separated from each other and from the initial and final point by three links. The partner trajectory γ' is distinguished from the original by differently connecting these links inside the encounter. In order to calculate the probability of these encounters, we define a Poincaré surface of section (PSS) perpendicular to γ inside the encounter region, at some point P. The trajectory pierces P first at time t_1 and then at t_2. The probability that a trajectory pierces a fixed Poincaré surface of section in a time $(t_2, t_2 + dt_2)$ with coordinates between (u, s) and $(u + du, s + ds)$ is uniform in chaotic systems and is given by the Liouville measure $dt_2 du ds/\Omega$.

To find the contribution of the two-leg-loops we need to integrate this probability over t_2 to get all the possible piercings at t_2, and also over all t_1, to count the possible sections P along γ. The density of these encounters is then given by

$$w^{2\mathrm{ll}}(u,s,t) = \int_0^{t-2t_{\mathrm{enc}}} dt_1 \int_0^{t-t_1-2t_{\mathrm{enc}}} dt_2 \frac{1}{\Omega t_{\mathrm{enc}}(u,s)} = \frac{(t-2t_{\mathrm{enc}})^2}{2\Omega t_{\mathrm{enc}}}, \qquad (5.39)$$

where the encounter time is given by $t_{\mathrm{enc}} = \lambda^{-1}\ln(c^2/|us|)$. The factor $1/t_{\mathrm{enc}}$ comes from the fact that we have weighted each encounter by t_{enc} when integrating over t_1, since P may be placed over any point inside the encounter itself. The limits of integration arise from the requirement that all the times t_1, t_2 and $t_1+t_2+2t_{\mathrm{enc}}$ must be positive.

The double sum is replaced by the sum rule together with integrals over the stable and unstable manifolds along γ weighted by the density of 2-encounters in a orbit of length t, $w^{2\mathrm{ll}}(u,s,t)$, giving rise to a difference in action $\Delta S(u,s) = us$ smaller than a classical value c^2:

$$\tilde{\rho}^{2\mathrm{ll}}(t) = \left\langle \frac{1}{(2\pi\hbar)^2} \int d\mathbf{r} d\mathbf{r}_o \sum_{\gamma(\mathbf{r}_o\to\mathbf{r},t)} \int_{-c}^{c} duds |D_\gamma|^2 \rho_W(\mathbf{r}_o, \bar{\mathbf{p}}_{\gamma\gamma',o}) w^{2\mathrm{ll}}(u,s,t) \mathrm{e}^{\frac{i}{\hbar}us} \right\rangle_{\Delta t},$$

where c is a typical classical action up to which the two stretches are linearizable. As we have seen in the diagonal contribution the sum rule contains a factor e^{-t/τ_d} giving the classical probability of staying. When a trajectory has a self encounter this probability is modified by a factor $\mathrm{e}^{t_{\mathrm{enc}}/\tau_d}$, coming from the fact that the trajectory γ during the encounter region is so close to itself that if the first stretch is inside the system, the second one must be also inside [115, 116]. We have then the following expression:

$$\begin{aligned} \tilde{\rho}^{2\mathrm{ll}}(t) &= \frac{1}{(2\pi\hbar)^2} \int d\mathbf{q} d\mathbf{p} \mathrm{e}^{-t/\tau_d} \rho_W(\mathbf{q},\mathbf{p}) \int_{-c}^{c} duds e^{t_{\mathrm{enc}}/\tau_d} w^{2\mathrm{ll}}(u,s,t) \mathrm{e}^{\frac{i}{\hbar}us} \\ &= \left\langle \mathrm{e}^{-t/\tau_d} \int_{-c}^{c} duds e^{t_{\mathrm{enc}}/\tau_d} \frac{(t-2t_{\mathrm{enc}})^2}{2\Omega t_{\mathrm{enc}}} \mathrm{e}^{\frac{i}{\hbar}us} \right\rangle_{\mathbf{q},\mathbf{p}}. \end{aligned} \qquad (5.40)$$

The integration can be done by making the change of variables $x = su/c^2$, $\sigma = c/u$ as in Ref. [39], thus

$$\begin{aligned} \tilde{\rho}^{2\mathrm{ll}}(t) &= \left\langle \mathrm{e}^{-t/\tau_d} \frac{\lambda r}{\pi t_H} \int_0^1 dx (t - 2\tau_d \alpha \ln x)^2 x^\alpha \cos(rx) \right\rangle_{\mathbf{q},\mathbf{p}}, \\ &= \left\langle \mathrm{e}^{-t/\tau_d} \frac{\lambda r}{\pi t_H} \left(t^2 - 4\tau_d t\alpha \frac{d}{d\alpha} + 4\alpha^2\tau_d^2 \frac{d^2}{d\alpha^2} \right) \int_0^1 dx x^\alpha \cos(rx) \right\rangle_{\mathbf{q},\mathbf{p}} \end{aligned} \qquad (5.41)$$

where $\alpha = -\frac{1}{\lambda\tau_d}$ and $r = c^2/\hbar$. We can perform the remaining integral by partial integration taking $\alpha \to 0$ and $r \to \infty$, and neglecting highly oscillating terms

which cancel out due to the average [39]:

$$\begin{aligned}\int_0^1 dx x^\alpha \cos(rx) &= r^{-1-\alpha}\int_0^r dy y^\alpha \cos(y) \\ &= \frac{\sin(y)}{r}\Big|_0^\infty - \frac{\alpha}{r}\int_0^r dy \frac{\sin(y)}{y} \\ &\approx -\frac{\alpha}{r}\frac{\pi}{2}. \end{aligned} \tag{5.42}$$

Substituting in Eq. (5.41), we have

$$\tilde{\rho}^{2\text{ll}}(t) = \left\langle e^{-t/\tau_d}\left(\frac{t^2}{2\tau_d t_H} - 2\frac{t}{t_H}\right)\right\rangle_{\mathbf{q},\mathbf{p}}. \tag{5.43}$$

The quadratic term corresponds to the first order quantum correction according to RMT [124], while the linear term damages normalization and therefore unitarity, i.e. when the system is closed, then $\tau_d \to \infty$ we should recover $\rho(t) = \tilde{\rho}(t) = 1$, but this does not happen. As shown in Ref. [73] another diagram has to be considered in order to solve this problem.

One-leg-loops contribution

Two possible diagrams have not yet been considered. The first one is the case where the points $\mathbf{r}_o$ and $\mathbf{r}$ are close together inside the encounter region. This type of correlation leads to coherent back-scattering (CBS) in the context of semi-classical transport [40].

The second one is where only one of the two stretches is inside the encounter region, as shown in Fig. 5.6 b,c. Clearly, the latter only exists for initial and final points inside the cavity, since, at the openings the exit of one stretch of the encounter implies the exit of the other one (with perfect coupling). To evaluate

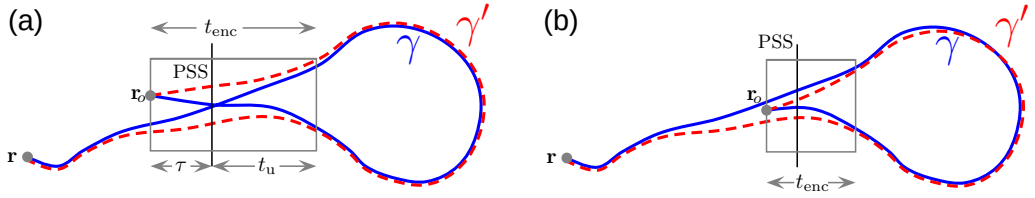

Figure 5.6: Sketch of trajectories with a self-encounter at the beginning or at the end. (b) is a configuration without a self-crossing of any of the two trajectories.

this two contributions we define a Poincaré surface of section at some time τ from the end or beginning of the trajectory [39].

The encounter time will be given by

$$t_{\text{enc}}(\tau, u) = \tau + \frac{1}{\lambda}\ln(c/|u|),$$

with the restriction $\tau < \frac{1}{\lambda}\ln(c/|s|)$.

The density of such encounters is given by

$$\begin{aligned} w^{1\mathrm{ll}}(u,s,t) &= 2\int_0^{\frac{1}{\lambda}\ln(c/|s|)} d\tau \int_0^{t-2t_{\mathrm{enc}}} dt_2 \frac{1}{\Omega(E) t_{\mathrm{enc}}(\tau,u)} \\ &= 2\int_0^{\frac{1}{\lambda}\ln(c/|s|)} d\tau \frac{t-2t_{\mathrm{enc}}(\tau,u)}{\Omega(E) t_{\mathrm{enc}}(\tau,u)}. \end{aligned} \tag{5.44}$$

The factor two is due to the possibility of having the encounter at the beginning of the trajectory or at the end. The difference in action will be $\Delta S = us$ at any point of the Poincaré surface of section. We can now proceed to calculate this contribution to the survival probability, in the same way as before, replacing $w^{1\mathrm{ll}}(u,s,t)$ instead of $w^{2\mathrm{ll}}(u,s,t)$ in Eq.(5.40). In order to evaluate the integrals, we make the following change of variables [39]

$$t' = \tau + \frac{1}{\lambda}\ln\left(\frac{c}{|u|}\right), \qquad u = c/\sigma, \qquad s = cx\sigma, \tag{5.45}$$

with an integration domain $-1 < x < 1$, $1 < \sigma < e^{\lambda t'}$ and $0 < t' < \frac{1}{\lambda}\ln\left(\frac{1}{|x|}\right)$. Here is important to notice, that the limits of t' are counting also the situation when $\tau \approx t_{\mathrm{enc}}$ (the point at which the orbits start is after a possible self-crossing), that means, it is not necessary to have a self-crossing in configuration space in order to give some contribution of this kind.

After the change of variables the integrals over u, s can be written as

$$\begin{aligned} I &= 2\int_{-c}^{c} du \int_{-c}^{c} ds \int_0^{\frac{1}{\lambda}\ln(c/|s|)} d\tau \frac{t-2t_{\mathrm{enc}}(\tau,u)}{\Omega t_{\mathrm{enc}}(\tau,u)} \mathrm{e}^{\frac{i}{\hbar}us} \mathrm{e}^{t_{\mathrm{enc}}/\tau_d} \\ &= \frac{4r}{\pi t_H}\int_0^1 dx \cos(rx) \int_0^{\frac{1}{\lambda}\ln(1/x)} dt' \left(\frac{t-2t'}{t'}\right) \mathrm{e}^{t'/\tau_d} \int_1^{e^{\lambda t'}} \frac{d\sigma}{\sigma} \\ &= \frac{4r\lambda}{\pi t_H}\int_0^1 dx \cos(rx) \int_0^{\frac{1}{\lambda}\ln(1/x)} dt''(t-2t')\mathrm{e}^{t'/\tau_d} \\ &= \left(t - 2\frac{d}{d\tau_d^{-1}}\right) \frac{4r\lambda\tau_d}{\pi t_H}\int_0^1 dx \cos(rx) x^{-\frac{1}{\lambda\tau_d}}, \end{aligned} \tag{5.46}$$

where $r = c^2/\hbar$ and $\tilde{\rho}^{1\mathrm{ll}}(t) = \langle \mathrm{e}^{-t/\tau_d} I\rangle_{\mathbf{r},\mathbf{p}}$. Replacing the result for the integration obtained in Eq.(5.42) the final result for the 1lls contribution to the decay is

$$\tilde{\rho}^{1\mathrm{ll}}(t) = \left\langle 2\frac{t}{t_H} e^{-t/\tau_d} \right\rangle_{\mathbf{q},\mathbf{p}}. \tag{5.47}$$

This term is exactly minus the linear term coming from the loop contribution, recovering unitarity and the first quantum correction (quadratic in time) for the

survival probability:

$$\tilde{\rho}^{2\mathrm{ll}+1\mathrm{ll}} = \left\langle e^{-t/\tau_d}\left(1+\frac{t^2}{2\tau_d t_H}\right)\right\rangle_{\mathbf{q},\mathbf{p}}, \tag{5.48}$$

this result agrees with an expansion of the the RMT prediction [124] for $t < \sqrt{t_H \tau_d}$.

For a detailed numerical analysis of the quantum deviations we consider the ratio

$$R(t) \equiv \frac{\tilde{\rho}(t) - \tilde{\rho}^{\mathrm{diag}}(t)}{\tilde{\rho}^{\mathrm{diag}}(t)}. \tag{5.49}$$

According to Eq. (5.48) the semiclassical prediction is

$$R^{\mathrm{sc}}(t) = \frac{t^2}{2t_H^2}\frac{\left\langle N e^{-t/\tau_d}\right\rangle_{\mathbf{q},\mathbf{p}}}{\left\langle e^{-t/\tau_d}\right\rangle_{\mathbf{q},\mathbf{p}}}. \tag{5.50}$$

For the numerical evaluation of $R(t)$ we have taken the classical simulation instead of $\tilde{\rho}^{\mathrm{diag}}(t)$ in order to get rid of the system specific features appearing at short times, which are in both, the classical and the quantum simulations, so

$$R^{\mathrm{n}}(t) \equiv \frac{\rho^{\mathrm{qn}}(t) - \rho^{\mathrm{cn}}(t)}{\rho^{\mathrm{cn}}(t)}, \tag{5.51}$$

where qn and cn stand for the quantum and classical numerical results respectively. In Fig. 5.7 we show $R^{\mathrm{n}}(t)$ for two simulations without any averaging. The full line shows the numerical results when the center of the Gaussian is $\mathbf{r}_o = (0.34L, 0.14L)$, the momentum direction $\theta_o = \pi/4$ and the opening starts at $0.5L$ ($w = 80 = 0.16L$ in all simulations). The second one (dotted line) corresponds to a packet centered at $\mathbf{r}_o = (0.34L, 0.14L)$, with $\theta_o = 4\pi/5$ and opening at $0.1L$. The semiclassical prediction Eq. (5.50) (dashed line), evaluated numerically for the Gaussian initial state, predicts larger quantum deviations than observed.

In Fig. 5.7 we show also the results after averaging over 27 different Gaussian distributions and positions of the opening (same as in Fig. 5.9, where the standard deviation is also shown). We have avoided choosing extreme positions, e.g., the center of the wave packet near the opening, or the opening very close to the corners; since they usually present strong system-specific features already at the classical level, not predictable in our previous approach. As we notice in Fig. 5.7 Eq. (5.50) (dashed line) overestimates the numerical result. The quantum decay follows the classical one for larger times than expected according to our semiclassical prediction. One possible explanation for such a shift in the quantum corrections is the finiteness of the Ehrenfest time. Up to now we have not considered them, in order to show a formal derivation of RMT predictions for specific systems. But a calculation of the Ehrenfest times at p_o leads to $\tau_E^c \sim 0.5\tau_d$ and $\tau_E^o \sim 0.27\tau_d$.

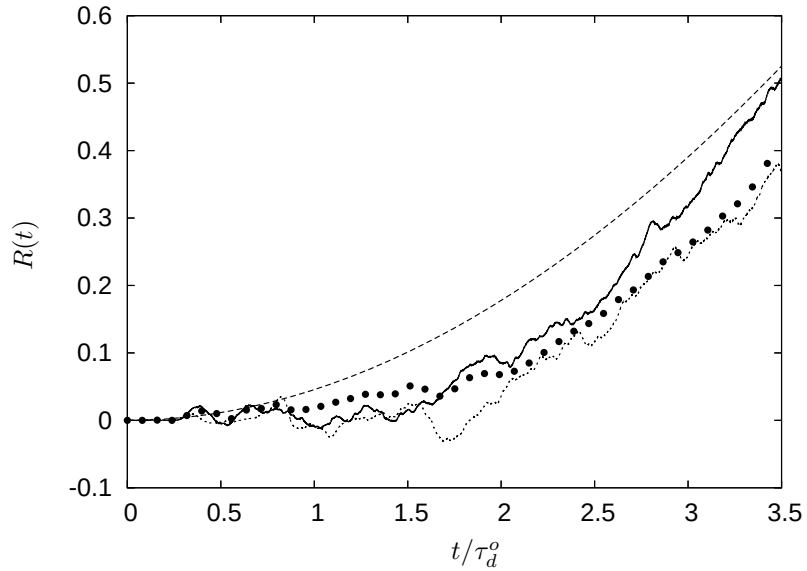

Figure 5.7: Numerical and semiclassical evaluation of the quantum corrections Eq. (5.49). The dashed line corresponds to the semiclassical prediction of the leading quantum corrections Eq. (5.50). *Full line*: $R(t)$ for a wave packet with $\mathbf{r}_o = (0.34L, 0.14L)$, the momentum direction $\theta_o = \pi/4$ and the opening starting at $0.5L$. *Dotted line*: $\mathbf{r}_o = (0.34L, 0.14L)$, $\theta_o = 4\pi/5$, opening starting at $0.1L$. The dots correspond to an average over 27 different distributions and positions of the opening.

Therefore in our range of parameters Ehrenfest time effects are not negligible and therefore RMT is not applicable. In the next section, we will consider the semiclassical approach taking into account this corrections, going beyond the RMT approach.

5.5 Ehrenfest time effects

Ehrenfest time effects have been mainly considered for stationary processes in chaotic systems involving time integration [35, 36, 37, 38, 39, 40]. In Refs. [41, 71] it is pointed out that these signatures should be even more noticeable in the time domain.

We will follow the approach in Ref. [41] to calculate the Ehrenfest time dependence of the first quantum correction to the survival probability. However we consider as in Ref. [40] the difference between the Ehrenfest time of the closed system $\tau_E^{\rm c} = \lambda^{-1}\ln(\mathcal{L}/\lambda_B)$, and the open-system Ehrenfest time $\tau_E^{\rm o} = \lambda^{-1}\ln(w^2/(\mathcal{L}\lambda_B))$, related to the width w of the opening.

We will consider the Laplace transform of the 2ll and 1ll contributions to the

survival probability:

$$\rho_{\tau_E}^{1,2\mathrm{ll}+1\mathrm{ll}}(s) = \int_0^\infty \mathrm{e}^{-st}\tilde{\rho}^{1,2\mathrm{ll}+1\mathrm{ll}}(t)dt. \tag{5.52}$$

The densities Eqs. (5.39) and (5.44) have to be multiplied by a Heaviside function ensuring that these contributions exist only if the time is larger than twice the encounter time. This has been ignored before since we have supposed that all Ehrenfest time scales are negligible in comparison with the dwell time.

Only trajectories that are closer than a distance w to themselves will have an enhanced probability of staying. Correlated trajectories should come closer to themselves than a distance c^2 in phase space related to the opening, i.e. we place the PSS only in the region were the stretches are closer than a distance w. Moreover, on the right hand side of the encounter, the stretches should separate at least a distance $\mathcal{L}$ in order to close themselves. The time when the trajectory pierce again the PSS is therefore at least $2t_{\mathrm{enc}} + 2t_{WL}$, where $t_{\mathrm{WL}} = \lambda^{-1}\ln(\mathcal{L}/w)$ is the time it takes the stretches to be separated at a distance $\mathcal{L}$ when they are initially separated a distance w. The weight function is slightly modified by this minimal time and by ensuring that the time is long enough in order to have such an encounter, thus

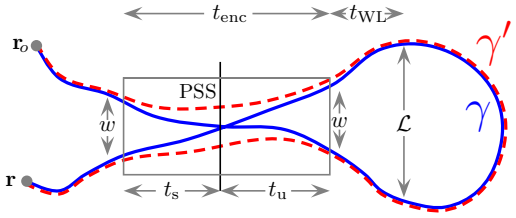

Figure 5.8: Sketch of the 2ll for the semiclassical calculation with finite Ehrenfest time.

$$w^{2\mathrm{ll}}(u,s,t) = \frac{(t-2(t_{\mathrm{enc}}+t_{\mathrm{WL}}))^2}{2\Omega t_{\mathrm{enc}}}\theta(t-2t_{\mathrm{enc}}-2t_{\mathrm{WL}}), \tag{5.53}$$

with $t_{\mathrm{enc}} = \lambda^{-1}\ln(c/|s|) + \lambda^{-1}\ln(c/|u|)$ and for the 1lls

$$w^{1\mathrm{ll}}(u,s,t) = 2\int_0^{\lambda^{-1}\ln(c/|s|)} dt' \frac{(t-2(t_{\mathrm{enc}}+t_{\mathrm{WL}}))}{\Omega t_{\mathrm{enc}}}\theta(t-2t_{\mathrm{enc}}-2t_{\mathrm{WL}}), \tag{5.54}$$

with $t_{\mathrm{enc}} = t' + \lambda^{-1}\ln(c/|u|)$. For both situations the classical survival probability is modified by a factor $\mathrm{e}^{t_{\mathrm{enc}}/\tau_d}$ as before. After replacing Eqs. (5.53) and (5.54) in Eq. (5.52) and shifting the integrals over time by $2t_{\mathrm{enc}} + 2t_{\mathrm{WL}}$ we have that

$$\rho_{\tau_E}^{1,2\mathrm{ll}}(s) = \frac{2}{t_H}\int_0^\infty t^2\,\mathrm{e}^{-(1+s\tau_d)(t+2t_{\mathrm{WL}})/\tau_d} I^{2\mathrm{ll}}(s)dt, \tag{5.55}$$

where,

$$I^{2\mathrm{ll}}(s) = \frac{1}{\pi\hbar}\int_0^c du \int_0^c ds \frac{e^{\frac{i}{\hbar}us}}{t_{\mathrm{enc}}}\mathrm{e}^{t_{\mathrm{enc}}/\tau_d}\mathrm{e}^{-2(1+s\tau_d)t_{\mathrm{enc}}/\tau_d}. \tag{5.56}$$

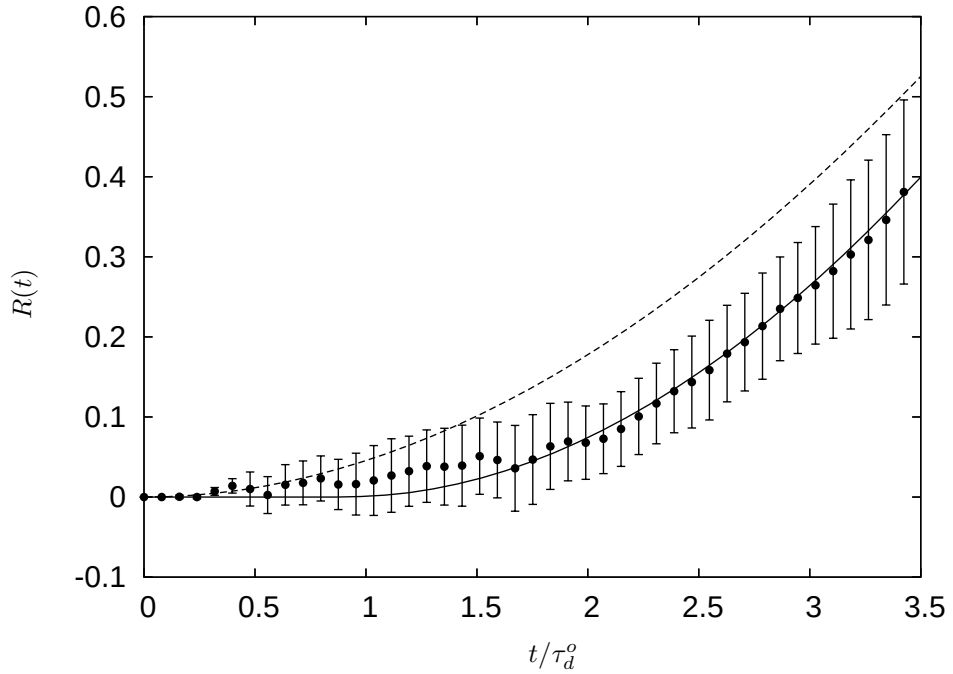

Figure 5.9: Eq. (5.49) for the numerical simulation averaged over 27 packages (dots). The analytical prediction with finite Ehrenfest time corresponds to the bold line. Our previous result neglecting the Ehrenfest time is the dashed line.

And for the 1ll's:

$$\rho^{1,1\mathrm{ll}}_{\tau_E}(s) = \frac{8}{t_H}\int_0^\infty t\,\mathrm{e}^{-(1+s\tau_d)(t+2t_{WL})/\tau_d} I^{1\mathrm{ll}}(s)dt, \tag{5.57}$$

with

$$I^{1\mathrm{ll}}(s) = \frac{1}{\pi\hbar}\int_0^c du\int_0^c ds\int_0^{\lambda^{-1}\ln(c/|s|)} dt'\frac{e^{\frac{i}{\hbar}us}}{t_{\mathrm{enc}}}\mathrm{e}^{t_{\mathrm{enc}}/\tau_d}\mathrm{e}^{-2(1+s\tau_d)t_{\mathrm{enc}}/\tau_d}. \tag{5.58}$$

The evaluation of the integrals can be done as before, and it is found in appendix B. By taking the inverse Laplace transform we obtain

$$\tilde{\rho}^{2\mathrm{ll}+1\mathrm{ll}}(t) = \left\langle e^{-t/\tau_d}e^{\tau_E^o/\tau_d}\frac{(t-2\tau_E^e)^2}{2\tau_d t_H}\theta(t-2\tau_E^e)\right\rangle_{\mathbf{q},\mathbf{p}}. \tag{5.59}$$

Here we see two competing effects. On one hand if the Ehrenfest time is too large, loops can not be formed before the trajectories escape, then $\theta(t-2\tau_E^e)=0$ and there are no quantum contributions. On the other hand, for those trajectories that have not escaped after $2\tau_E^e$ and have a self encounter, the probability of staying is enhanced by a factor $e^{\tau_E^o/\tau_d}$, revealing the enhanced classical survival probability due to the encounter.

In Fig. 5.9 we show the numerical results (red dots) in comparison with Eq. (5.59) (bold line) and Eq. (5.50) (dashed line). As we notice, the finiteness of the

Ehrenfest time shifts the quantum corrections, and therefore they appear later, as also revealed by the numerical simulations. The simulated average escape agrees with Eq. (5.59), implying that that τ_E-effects may indeed play a rôle. However, we cannot rule out other non-universal effects, like diffraction effects or fluctuations of the effective τ_d [126], that may also yield to time shifts. Furthermore the individual numerical traces $R(t)$ exhibit strong fluctuations as reflected in the large standard deviation in Fig. 5.9. A numerical confirmation of the $\log(1/\hbar)$-dependence of τ_E seems to date impossible for billiards, since it requires to increase the size of the billiards exponentially and the computation would take a disproportionate amount of time.

5.6 Variance of the survival probability

In section 2 we have introduced a local time average, in order to select from the trajectories contributing to Eq. (5.24) those that have almost the same action. In order to compare deviations of $\tilde{\rho}(t)$ from $\rho(t)$ let us consider the mean variance of $\rho(t)$.

$$\langle \mathrm{var}\rho(t)\rangle_{\Delta t} = \left\langle (\rho(t) - \tilde{\rho}(t))^2 \right\rangle_{\Delta t} . \tag{5.60}$$

Introducing Eq. (5.24) in Eq. (5.60), we can write it as

$$\begin{aligned} \langle \mathrm{var}\rho(t)\rangle_{\Delta t} &= \Big\langle \frac{1}{(2\pi\hbar)^4} \int_A \prod_{i=1}^{6} d\mathbf{r}_i \sum_{\substack{\tilde{\gamma}_1(\mathbf{r}_1\to\mathbf{r}_3,t)\\ \tilde{\gamma}_2(\mathbf{r}_2\to\mathbf{r}_3,t)}} \sum_{\substack{\tilde{\gamma}_3(\mathbf{r}_4\to\mathbf{r}_6,t)\\ \tilde{\gamma}_4(\mathbf{r}_5\to\mathbf{r}_6,t)}} D_{\tilde{\gamma}_1} D^*_{\tilde{\gamma}_2} D_{\tilde{\gamma}_3} D^*_{\tilde{\gamma}_4} \\ &\quad \times \mathrm{e}^{\frac{i}{\hbar}(S_{\tilde{\gamma}_1} - S_{\tilde{\gamma}_2} + S_{\tilde{\gamma}_3} - S_{\tilde{\gamma}_4})} \psi_o(\mathbf{r}_1)\psi_o^*(\mathbf{r}_2)\psi_o(\mathbf{r}_4)\psi_o^*(\mathbf{r}_5) \Big\rangle_{\Delta t}, \end{aligned} \tag{5.61}$$

where the configurations $\mathbf{r}_1 \approx \mathbf{r}_2$ and $\mathbf{r}_4 \approx \mathbf{r}_5$ have to be subtracted since they are taken into account in $\tilde{\rho}(t)^2$, therefore they do not have to be considered in Eq. (5.61). Due to the average most of the contributions to Eq. (5.61) will cancel out, the configuration of the points $\mathbf{r}_i$ must be such that the phase cancels out.

We will only consider the diagonal approximation here, which corresponds to take $\tilde{\gamma}_1 \approx \tilde{\gamma}_4$ and $\tilde{\gamma}_2 \approx \tilde{\gamma}_3$, and is the leading contribution for short times. This requires that $\mathbf{r}_1 \approx \mathbf{r}_5$, $\mathbf{r}_2 \approx \mathbf{r}_4$, and $\mathbf{r}_3 \approx \mathbf{r}_6$. We expand the trajectories $\tilde{\gamma}_1$ and $\tilde{\gamma}_4$ around trajectories γ_1 and γ_4 going from $\mathbf{q}_1 = (\mathbf{r}_1 + \mathbf{r}_5)/2$ to $\mathbf{q}_3 = (\mathbf{r}_3 + \mathbf{r}_6)/2$ and trajectories $\tilde{\gamma}_2$ and $\tilde{\gamma}_3$ around trajectories γ_2 and γ_3 going from $\mathbf{q}_2 = (\mathbf{r}_2 + \mathbf{r}_4)/2$ to $\mathbf{q}_3$. We can make the integrals over $\mathbf{r}_1 - \mathbf{r}_5$ and $\mathbf{r}_2 - \mathbf{r}_4$, and write the variance

in terms of the Wigner function of the initial state:

$$\begin{aligned}\langle \mathrm{var}\rho(t)\rangle_{\Delta t} &= \Big\langle \frac{1}{(2\pi\hbar)^4}\int\prod_{i=1}^{4}d\mathbf{q}_i \sum_{\substack{\gamma_1,\gamma_4(\mathbf{q}_1\to\mathbf{q}_3,t)\\ \gamma_2,\gamma_3(\mathbf{q}_2\to\mathbf{q}_3,t)}} D_{\gamma_1}D^*_{\gamma_2}D_{\gamma_3}D^*_{\gamma_4}\mathrm{e}^{i\Delta S/\hbar} \\ &\quad\times\rho^*_W\left(\mathbf{q}_1,\frac{\mathbf{p}_{\gamma_1,o}+\mathbf{p}_{\gamma_4,o}}{2}\right)\rho_W\left(\mathbf{q}_2,\frac{\mathbf{p}_{\gamma_2,o}+\mathbf{p}_{\gamma_3,o}}{2}\right)\Big\rangle_{\Delta t}, \end{aligned} \tag{5.62}$$

with

$$\Delta S = S_{\gamma_1}-S_{\gamma_2}+S_{\gamma_3}-S_{\gamma_4}+(\mathbf{p}_{\gamma_1,f}-\mathbf{p}_{\gamma_2,f}-\mathbf{p}_{\gamma_3,f}+\mathbf{p}_{\gamma_4,f})\cdot\frac{\mathbf{q}_4}{2}, \tag{5.63}$$

$\mathbf{p}_{\gamma_i,f}$ standing for the final momentum of the trajectory γ_i and $\mathbf{q}_4=\mathbf{r}_3-\mathbf{r}_6$.

The dominant contribution will come from the diagonal approximation $\gamma_1=\gamma=4$ and $\gamma_2=\gamma_3$ this leads to

$$\begin{aligned}\langle \mathrm{var}\rho(t)\rangle^{\mathrm{d}}_{\Delta t} &= \Big\langle \frac{1}{(2\pi\hbar)^4}\int\prod_{i=1}^{4}d\mathbf{q}_i \sum_{\substack{\gamma_1(\mathbf{q}_1\to\mathbf{q}_3,t)\\ \gamma_2(\mathbf{q}_2\to\mathbf{q}_3,t)}} |D_{\gamma_1}|^2|D_{\gamma_2}|^2\mathrm{e}^{\frac{i}{\hbar}(\mathbf{p}_{\gamma_1,f}-\mathbf{p}_{\gamma_2,f})\cdot\mathbf{q}_4} \\ &\quad\times\rho^*_W\left(\mathbf{q}_1,\mathbf{p}_{\gamma_1,o}\right)\rho_W\left(\mathbf{q}_2,\mathbf{p}_{\gamma_2,o}\right)\Big\rangle_{\Delta t}, \end{aligned} \tag{5.64}$$

In appendix C we show that we can write this for a two dimensional cavity as

$$\langle \mathrm{var}\rho(t)\rangle^{\mathrm{d}}_{\Delta t} = \Big\langle \frac{1}{(2\pi\hbar)^2 A}\int dk\left|\int d\mathbf{r}\int d\mathbf{p}\mathrm{e}^{-t/\tau_d}\mathrm{e}^{ikp^2}\rho_W(\mathbf{r},\mathbf{p})\right|^2\Big\rangle. \tag{5.65}$$

For a Gaussian initial state, the integrals can be done neglecting the p dependence of the dwell time in the integrand (see appendix C). We obtain for $\lambda t\gg 1$

$$\langle \mathrm{var}\rho(t)\rangle^{\mathrm{d}}_{\Delta t}\approx e^{-2t/\tau^o_d}\frac{\sqrt{2\pi}\sigma\hbar}{Ap_o}\approx e^{-2t/\tau^o_d}\frac{1}{M}, \tag{5.66}$$

where σ is the dispersion in position of the initial state and p_o is the magnitude of the mean momentum, and $M=Ap_o/(\pi\hbar\sigma)$ is approximately the number of eigenstates (of the closed billiard) occupied by the initial wave function. This contribution goes to zero in the semiclassical limit. Higher order contributions can be neglected for $t\ll t_H$.

For the DD billiard and the parameters chosen here we have that

$$\frac{\langle \mathrm{var}\rho(t)\rangle^{\mathrm{d}}}{(\rho^c(t))^2}\approx 2.4\times 10^{-3}. \tag{5.67}$$

The square of the standard deviation in Fig. 5.9 fluctuates between 10^{-3} and 0.4×10^{-3} for $\tau^c_E<t<\sqrt{\tau_d t_H}$, consistent with order of magnitude in Eq. (5.67). Due to the numerical effort in each simulation we could not increase the size of the ensemble in our average (27), which can improve these results.

We have seen in this chapter how the semiclassical approach has to be modified when one is considering trajectories that are open, like in chapter 4, but not attached to leads, where unitary problems can be solved by taking into account new diagrams. We have studied the importance of Ehrenfest time effects, which appears in the numerical simulation as a shift in the quantum corrections. The semiclassical approximation can give a quantitative estimation of this effect, which explains our data for a chaotic billiard. Typical examples of decay processes are molecular photo-dissociation or atomic photo-ionization. In the next chapter we will study the semiclassical approximation for such processes introducing the diagrams discussed here, as well as Ehrenfest time effects.

Chapter 6

Semiclassical approximation to photo-dissociation statistics

The purpose of this chapter is to develop a semiclassical approach to determine the leading contributions to photo-dissociation statistics for systems with time reversal symmetry. We follow the diagrammatic approach introduced in Ref. [131], and calculate the leading quantum corrections. We will see that the corresponding form factor of the cross section auto-correlation function can be related to the survival probability and the spectral form factor given by the periodic orbits that remain trapped inside the system. We also calculate the Ehrenfest-time dependence of the leading quantum corrections.

6.1 Photo-dissociation statistics

Typical examples of quantum decay processes are molecular photo-dissociation [132, 133, 134] or atomic photo-ionization [135], there the molecule (atom) absorbs a photon, which excites it to an energy region that allows the dissociation or ionization of the system [136].

In indirect processes the dissociation proceeds through excited intermediate resonance states. These resonance states are directly coupled to the continuum states that describe possible breakup channels of the molecule into fragments [136]. In Fig. 6.1 an schematic representation of the photo-dissociation of a molecule is shown. The energy surfaces e_o and e_{ef} correspond to a cut of the potential surfaces of the ground and excited electronic state, respectively. $|g\rangle$ is the ground electronic state of the molecule. We suppose, as in Ref. [137, 138], that the effective Hamiltonian of the excited molecule can be written as a "binding" potential coupled to the continuum (in the following, when we refer to properties of the "correspond-

ing" closed system, we mean the binding part of the effective Hamiltonian of the excited molecule). The number N of possible dissociation states of the molecule (dissociation channels) is assumed to be large and the complexity of e_b is assumed to lead to chaotic dynamics. In the classical approach to photo-dissociation the study of the fragmentation of the molecules is essentially done by *placing "billiard balls" on the electronic energy surfaces and follow their trajectories towards one of the exit channels* [136], similar to the study of decay in an open cavity. This analogy will be kept in our further analysis.

Due to the complexity of the system, it is justified to described such processes quantum mechanically within the Random Matrix Theory [137, 138], which has been shown to reproduce the statistics of the fluctuations of the photo-dissociation cross section of neutron scattering [139] and atomic systems [140].

Another possible approach, applicable for individual systems, is the semiclassical theory, which can also reveal the limits of RMT. A first semiclassical approach to the auto-correlation function of the photo-dissociation cross section was done in Refs. [131] and [141], were only diagonal (classical) contributions where considered.

In this chapter, we will develop a semiclassical approach for the leading quantum corrections to the photo-dissociation cross section for system with time reversal symmetry, following the diagrammatic approach in Ref. [131] and our previous analysis of the semiclassical approximation to the survival probability, introducing 2lls and 1lls in order to calculate the leading quantum corrections.

The quantity describing the probability of those processes is the photo-dissociation cross section, which in the dipole approximation is given by

$$\sigma(E) = Im\mathrm{Tr}\{\hat{A}G^{-}(E)\} = Im\int d\mathbf{r}\int d\mathbf{r}' A(\mathbf{r},\mathbf{r}')G^{-}(\mathbf{r}',\mathbf{r},E), \qquad (6.1)$$

where $G^{-}(E)$ is the retarded Green function of the molecule, $\hat{A}$ is a projection operator, given by

$$\hat{A} = \eta|\phi\rangle\langle\phi|, \qquad |\phi\rangle = D|g\rangle, \qquad (6.2)$$

where $D = \mathbf{d}\cdot\hat{\mathbf{e}}$ is the projection of the electronic dipole moment operator of the molecule on the polarization of the absorbed light (with polarization $\hat{\mathbf{e}}$) and $\eta = E/c\hbar\epsilon_o$.
The two-point correlation function of the cross section is defined as

$$C(\omega) \equiv \frac{\langle\sigma(E+\hbar\omega/2)\sigma(E-\hbar\omega/2)\rangle - \langle\sigma(E)\rangle^2}{\langle\sigma(E)\rangle^2}, \qquad (6.3)$$

where $\langle ...\rangle$ denotes in this case an energy average over an energy window ΔE around E, such that $1/\bar{g} \ll \Delta E \ll E$, with $\bar{g}$ the mean density of states of the

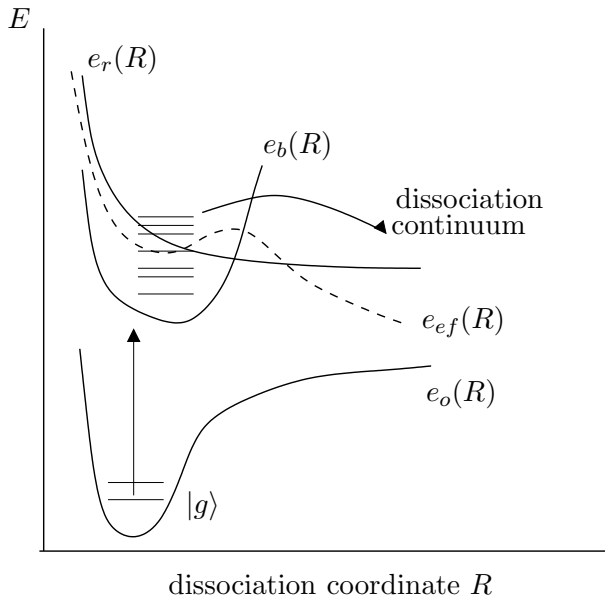

Figure 6.1: Sketch of an indirect molecular photo-dissociation process. The electronic surfaces shown are: the ground state surface e_o (where $|g\rangle$ resides), and the effective electronic surface e_{ef} (dashed line), which is approximately the sum of a binding surface e_b with a repulsive surface e_r.

corresponding closed system. $\langle\sigma(E)\rangle$ is the mean cross section. In the semiclassical limit

$$\langle\sigma(E)\rangle \approx \bar{\sigma}(E) \equiv \frac{\pi}{(2\pi\hbar)^2}\int d\mathbf{r}d\mathbf{p}\, A_W(\mathbf{r},\mathbf{p})\delta(E-H(\mathbf{r},\mathbf{p})), \tag{6.4}$$

with

$$A_W(\mathbf{r},\mathbf{p}) = \int d\mathbf{r}'\langle\mathbf{r}+\mathbf{r}'/2|\hat{A}|\mathbf{r}-\mathbf{r}'/2\rangle \mathrm{e}^{-i\frac{\mathbf{r}'\cdot\mathbf{p}}{\hbar}} \tag{6.5}$$

the Weyl representation of the $\hat{A}$ operator (which corresponds to the Wigner representation of $\phi(\mathbf{r})$).
We consider the Fourier transform of the two-point correlation function of the cross section:

$$Z(t) = \frac{t_H}{2\pi}\int_{-\infty}^{\infty} d\omega e^{i\omega t}C(\omega). \tag{6.6}$$

As $C(\omega) = C(-\omega)$ then $Z(t)$ is real and even. We consider $Z(t)$ for $t > 0$ and we can calculate $C(\omega)$ from $C(\omega) = \frac{2}{t_H}\int_0^\infty Z(t)\cos(\omega t)dt$.

6.2 Semiclassical approximation to the cross-section form factor

In order to calculate the semiclassical expression for this quantity, we replace the exact Green function by its semiclassical counterpart Eq. (1.10). The semiclassical

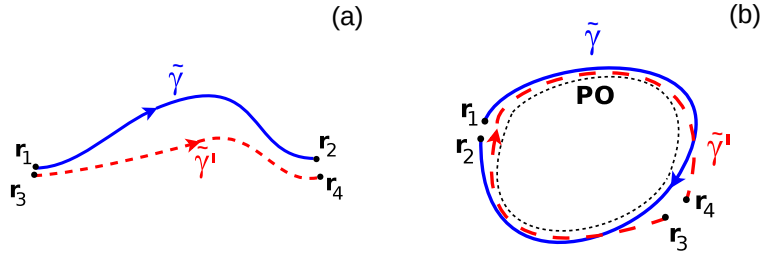

Figure 6.2: Scheme of configurations given some contribution to $Z(t)$. (a) Open trajectory (OT) configurations counted in $Z^1(t)$. (b) Configuration with $\tilde{\gamma}$ and $\tilde{\gamma}'$ surrounding a periodic orbit (PO), accounted in $Z^2(t)$.

cross-section form factor is then given by

$$Z^{\rm sc}(t) = \frac{t_H}{8\pi\hbar^3\bar{\sigma}^2}{\rm Re}\left\langle \int \prod_{i=1}^{4} d\mathbf{r}_i A(\mathbf{r}_1,\mathbf{r}_2)A^*(\mathbf{r}_3,\mathbf{r}_4) \right. \tag{6.7}$$
$$\left. \sum_{\substack{\tilde{\gamma}(\mathbf{r}_1\to\mathbf{r}_2,E)\\ \tilde{\gamma}'(\mathbf{r}_3\to\mathbf{r}_4,E)}} \tilde{D}_{\tilde{\gamma}}\tilde{D}^*_{\tilde{\gamma}'} \exp\left(\frac{i}{\hbar}(S_{\tilde{\gamma}}-S_{\tilde{\gamma}'})\right)\delta\left(t-\frac{(t_{\tilde{\gamma}}+t_{\tilde{\gamma}'})}{2}\right)\right\rangle .$$

The term containing the action difference is a rapidly oscillating function, so due to the energy average most of the contributions will cancel out. Only trajectories with similar actions will give some contribution, which imposes conditions on the possible configuration of the points $\mathbf{r}_i$. There are two possible configurations, as depicted in Fig. 6.2, following the analysis in Ref. [131]: (a) open trajectory (OT) contributions (that we will denote by $Z^1(t)$) where $\mathbf{r}_1 \approx \mathbf{r}_3$ and $\mathbf{r}_2 \approx \mathbf{r}_4$, or additionally, in case of time reversal symmetry, $\mathbf{r}_1 \approx \mathbf{r}_4$ and $\mathbf{r}_2 \approx \mathbf{r}_3$ (this gives a factor of two, taking into account that in case of time reversal symmetry $\phi(\mathbf{r})$ is real), (b) periodic orbit (PO) contributions ($Z^2(t)$), with $\mathbf{r}_1 \approx \mathbf{r}_2$ and $\mathbf{r}_3 \approx \mathbf{r}_4$ and both trajectories surrounding a periodic orbit.

6.2.1 Open trajectory contributions

Let us consider the contributions of OT's. For this purpose we expand the trajectories $\tilde{\gamma}$ and $\tilde{\gamma}'$ along trajectories γ and γ' connecting $\mathbf{q} = (\mathbf{r}_1+\mathbf{r}_3)/2$ and $\mathbf{Q} = (\mathbf{r}_2+\mathbf{r}_4)/2$. Thus

$$Z^1(t) = \frac{\kappa t_H}{8\pi\hbar^3\bar{\sigma}^2}{\rm Re}\left\langle \int d\mathbf{Q}d\mathbf{Q}'d\mathbf{q}d\mathbf{q}' \sum_{\gamma,\gamma'(\mathbf{q}\to\mathbf{Q},E)} \tilde{D}_\gamma\tilde{D}^*_{\gamma'}\delta\left(t-\frac{(t_\gamma+t_{\gamma'})}{2}\right)\right. \tag{6.8}$$
$$A(\mathbf{q}+\mathbf{q}'/2,\mathbf{Q}+\mathbf{Q}'/2)A^*(\mathbf{q}-\mathbf{q}'/2,\mathbf{Q}-\mathbf{Q}'/2)$$
$$\left.\exp\left(\frac{i}{\hbar}(S_\gamma-S_{\gamma'})-\frac{i}{\hbar}\mathbf{q}'\cdot\frac{(\mathbf{p}_{\gamma,i}+\mathbf{p}_{\gamma',i})}{2}+\frac{i}{\hbar}\mathbf{Q}'\cdot\frac{(\mathbf{p}_{\gamma,f}+\mathbf{p}_{\gamma',f})}{2}\right)\right\rangle .$$

where $\mathbf{q}' = \mathbf{r}_1 - \mathbf{r}_2$ and $\mathbf{Q}' = \mathbf{r}_2 - \mathbf{r}_4$ and $\kappa = 1$ in the absence of time reversal symmetry and 2 with time reversal symmetry.
Considering the diagonal approximation $\gamma = \gamma'$, we will use the following sum rule [142]

$$\sum_{\gamma(\mathbf{r}\to\mathbf{r}',E)} |\tilde{D}_\gamma|^2(...)\delta(t_\gamma - t) = \int d\mathbf{p} \int d\mathbf{p}' f(\mathbf{r},\mathbf{p},\mathbf{r}',\mathbf{p}',t)\delta(E - H(\mathbf{r},\mathbf{p}))(...), \quad (6.9)$$

where

$$f(\mathbf{r},\mathbf{p},\mathbf{r}',\mathbf{p}',t) = \delta(\mathbf{r}(t) - \mathbf{r}')\delta(\mathbf{p}(t) - \mathbf{p}') \quad (6.10)$$

is the classical probability of going from a point $(\mathbf{r},\mathbf{p})$ in phase space to a point $(\mathbf{r}',\mathbf{p}')$ in a time t, with the evolution given by H. In the case of classical ergodic dynamics we can replace this classical probability, for sufficiently large times ($t\lambda \gg 1$), with its phase space average. For an open chaotic system this average is given by

$$\overline{f(\mathbf{r},\mathbf{p},\mathbf{r}',\mathbf{p}',t)} = \mathrm{e}^{-t/\tau_d} \frac{\delta(H(\mathbf{r}',\mathbf{p}') - H(\mathbf{r},\mathbf{p}))}{\Omega(H(\mathbf{r},\mathbf{p}))}. \quad (6.11)$$

Substituting into Eq. (6.8) and using Eq. (6.4) we have

$$\begin{aligned} Z^{1,\mathrm{diag}}(t) &= \kappa \frac{e^{-t/\tau_d}}{16\pi^2\hbar^4\bar{\sigma}^2} \mathrm{Re} \int d\mathbf{q} \int d\mathbf{p} d\mathbf{q}' \eta\phi(\mathbf{q} + \mathbf{q}'/2)\phi^*(\mathbf{q} - \mathbf{q}'/2) \quad (6.12) \\ &\quad \times \exp(-i\mathbf{q}'\cdot\mathbf{p}/\hbar)\delta(E - H(\mathbf{q},\mathbf{p})) \int d\mathbf{Q} d\mathbf{Q}' d\mathbf{P} \\ &\quad \eta\phi^*(\mathbf{Q} + \mathbf{Q}'/2)\phi(\mathbf{Q} - \mathbf{Q}'/2)\exp(i\mathbf{Q}'\cdot\mathbf{P}/\hbar)\delta(E - H(\mathbf{Q},\mathbf{P})), \end{aligned}$$

where τ_d in the dwell time at the energy E. The integrals over $\mathbf{q},\mathbf{p},\mathbf{q}'$ are independent of the integrals over $\mathbf{Q},\mathbf{P},\mathbf{Q}'$ and each one gives the mean cross section correlation, according to Eq. (6.4), therefore

$$Z^{1,\mathrm{diag}}(t) = \kappa e^{-t/\tau_d}, \quad (6.13)$$

here $\tau_d = \tau_d(E)$.

We can calculate the 2ll contribution to $Z^1(t)$ for $\kappa = 2$, as in Chapter 5. The double sum is replaced by the sum rule and an integral counting the encounters along γ. The classical survival probability is modified again by a factor $\mathrm{e}^{t_{\mathrm{enc}}/\tau_d}$. We assume that the stability amplitudes of the two trajectories are the same, so the calculation of the integral over $\mathbf{q}_i$ and $\mathbf{p}_i$ can be performed as for the diagonal approximation. Then,

$$\begin{aligned} Z^{1,2\mathrm{ll}}(t) &= 2\int du ds\, \mathrm{e}^{\frac{i}{\hbar}su} w^{2\mathrm{ll}}(u,s,t) e^{-(t-t_{\mathrm{enc}})/\tau_d} \quad (6.14) \\ &= 2e^{-t/\tau_d}\left(\frac{t^2}{2\tau_d t_H} - 2\frac{t}{t_H}\right). \end{aligned}$$

As shown before in the semiclassical evaluation of double sums of OT connecting points inside a system 'one-leg-loop' (1ll) diagrams have to be considered. The result for the integrals in this case is

$$Z^{1,1\mathrm{ll}}(t) = 4\frac{t}{t_H}e^{-t/\tau_d}, \tag{6.15}$$

cancelling the linear contribution in Eq. (6.14).
We notice that this contribution can be written as $Z^1(t) = 2\rho(t)$, where $\rho(t)$ is the survival probability of the state $\phi(\mathbf{r})$, i.e. $\rho(t) = \int_A d\mathbf{r}|\phi(\mathbf{r},t)|^2$ (if its Wigner function is localized in energy at E). Here the area of integration A entering in the decay corresponds to the area allowed to be explored by the binding potential.

6.2.2 Periodic orbit contributions

Let us now consider the contributions of diagrams like Fig. 6.2 (b). We first calculate the contribution of periodic orbits to the cross section, following a similar procedure as for the semiclassical trace formula. Replacing the semiclassical Green function into the definition of the photo-dissociation cross-section σ we can write the oscillatory part of it as

$$\begin{aligned}\sigma(E) &= Im\frac{2\pi}{(2\pi i\hbar)^{3/2}}\int d\mathbf{r}\int d\mathbf{r}' A\left(\mathbf{r}+\frac{\mathbf{r}'}{2},\mathbf{r}-\frac{\mathbf{r}'}{2}\right) \\ &\quad \sum_\gamma \tilde{D}_\gamma \exp\left(\frac{i}{\hbar}S_\gamma\left(\mathbf{r}+\frac{\mathbf{r}'}{2},\mathbf{r}-\frac{\mathbf{r}'}{2},E\right)\right)\end{aligned} \tag{6.16}$$

where the trajectories γ are going from $\mathbf{r}-\frac{\mathbf{r}'}{2}$ to $\mathbf{r}+\frac{\mathbf{r}'}{2}$. Since we are considering orbits near periodic orbits we can expand the actions for small $\mathbf{r}'$

$$\begin{aligned}\sigma^{\mathrm{PO}}(E) &= Im\frac{2\pi}{(2\pi i\hbar)^{3/2}}\int d\mathbf{r}\int d\mathbf{r}' A(\mathbf{r}+\mathbf{r}'/2,\mathbf{r}-\mathbf{r}'/2) \\ &\quad \sum_{\gamma(\mathbf{r}\to\mathbf{r},E)} \tilde{D}_\gamma \exp\left(\frac{i}{\hbar}S_\gamma(\mathbf{r},\mathbf{r},E)-\frac{i}{\hbar}\mathbf{r}'\cdot(\mathbf{p}_{\gamma,i}+\mathbf{p}_{\gamma,f})/2\right).\end{aligned} \tag{6.17}$$

The integral can be performed via a stationary phase approximation [141], yielding

$$\sigma^{\mathrm{PO}}(E) = \frac{1}{\hbar}Re\sum_{\mathrm{j}}\tilde{D}_{\mathrm{j}}\exp\left(\frac{i}{\hbar}S_{\mathrm{j}}(E)\right)\int_0^{T_{\mathrm{pj}}} dt\, A_W(\mathbf{q}_{\mathrm{j}},\mathbf{p}_{\mathrm{j}}), \tag{6.18}$$

where the sum is over trapped periodic orbits j, and pj refers to the primitive periodic orbit.

$\tilde{D}_{\mathrm{j}} = e^{i\nu_{\mathrm{j}}\pi/2}/\sqrt{|\mathrm{Tr}M_{\mathrm{j}}-2|}$ is the stability amplitude of the PO together with the Maslov index ν_{j}, and M_{j} is the monodromy matrix describing the linearization around the PO. Long enough trajectories will be uniformly distributed in phase

space if the system is ergodic. Then, the integral over time can be replaced by a phase space average:

$$\int_0^{T_{\rm pj}} dt A_W(\mathbf{q}_{\rm j},\mathbf{p}_{\rm j}) \approx T_{\rm pj}\int d\mathbf{r}d\mathbf{p}A_W(\mathbf{r},\mathbf{p})\delta(E-H(\mathbf{r},\mathbf{p}))/\Omega(E), \tag{6.19}$$

and

$$\sigma^{\rm PO}(E) \approx \frac{2\langle\sigma(E)\rangle}{t_H} Re\sum_{\rm j} T_{\rm pj}\tilde{D}_{\rm j}\exp\left(\frac{i}{\hbar}S_{\rm po}(E)\right) \approx \frac{\bar{\sigma}(E)}{\bar{g}(E)}g^{\rm osc}(E), \tag{6.20}$$

where $g^{\rm osc}(E)$ refers to the oscillatory part of the density of states, and $\bar{g}(E)$ to its smooth part (Thomas Fermi). We recognize here that the contribution of periodic orbits to the cross-section form factor $Z^2(t)$ corresponds to the spectral form factor of the open system. Substituting Eq. (6.20) in Eq. (6.3) we have

$$Z^2(t) = K_{\rm open}(t) = \frac{1}{t_H}{\rm Re}\Big\langle \sum_{\rm j,j'} T_{\rm pj}T_{\rm pj'}\tilde{D}_{\rm j}\tilde{D}^*_{\rm j'}{\rm e}^{\frac{i}{\hbar}(S_{\rm j}(E)-S_{\rm j'}(E))}\delta\left(t-\bar{T}_{\rm jj'}\right)\Big\rangle, \tag{6.21}$$

where $\bar{T}_{\rm jj'} = (T_{\rm j}+T_{\rm j'})/2$. We recognize here Eq. (1.17), but the orbits entering into the sums are those that are trapped inside the system. The expression given in Eq. (6.21) has been calculated as an expansion in t/t_H in Ref. [143] up to 8th order for the unitary case and up to 7th order for the orthogonal case.

The diagonal approximation can be calculated by using the Ozorio-de Almeida sum rule [18] modified for open systems, thus

$$Z^{2,\rm diag}(t) = \frac{2t}{t_H}{\rm e}^{-t/\tau_d}. \tag{6.22}$$

The first order quantum corrections corresponds to periodic orbits with a self-crossing as depicted in Fig. 1.2 (denoted in the following by $(2)^1$). The calculation is similar as for the spectral form factor of the closed system, but in addition the enhanced probability of staying has to be taken into account. The weight function can be written as

$$w^{(2)^1}(u,s,t) = \frac{t(t-2t_{\rm enc})}{2\Omega t_{\rm enc}}, \tag{6.23}$$

then

$$\begin{aligned} Z^{2,(2)^1}(t) &= \frac{2}{t_H}\int dt' t' e^{-t/\tau_d}\delta(t-t')\int ds\int du\frac{t'(t'-2t_{\rm enc})}{2\Omega t_{\rm enc}}e^{t_{\rm enc}/\tau_d} \\ &= e^{-t/\tau_d}\left(-\frac{2t^2}{t_H^2}+\frac{t^3}{t_H^2\tau_d}\right). \end{aligned} \tag{6.24}$$

Up to quadratic term in time, the form factor of the open and closed system coincide, τ_d enters in higher order corrections. In this context, 1ll's do not play

a role, since on both sides of the encounter a minimal time is required, as the deviation from the almost parallel momenta of the two stretches of j has to grow until they are in opposite direction in order to close both sides of the trajectory forming a periodic orbit.

Summing up the two contributions $Z^1(t)$ and $Z^2(t)$, we can generally write

$$Z(t) = K_{\text{open}}(t) + \kappa\rho(t), \tag{6.25}$$

where $K_{\text{open}}(t)$ is the spectral form factor of the open system. This corresponds for systems with time reversal symmetry, up to quadratic term in t/t_H, to

$$Z^{\text{GOE}}(t) = \mathrm{e}^{-t/\tau_d}\left(2 + \frac{2t}{t_H} + (N-2)\,\frac{t^2}{t_H^2} + ...\right), \tag{6.26}$$

where $N = t_H/\tau_d$ is the number of dissociation channels open.
Going back to the auto-correlation function by taking the inverse Fourier transform, we obtain for GOE

$$C^{\text{GOE}}(\Gamma) = 4\left(\frac{1}{N}\frac{1}{1+\Gamma^2} + \frac{1}{N^2}\frac{1-\Gamma^2}{(1+\Gamma^2)^2} + \frac{(N-2)}{N^3}\frac{1-3\Gamma^2}{(1+\Gamma^2)^3} + ...\right), \tag{6.27}$$

where $\Gamma = \omega\tau_d$. The first term, in accordance with Ref. [131], corresponds to the well known Ericson fluctuations. In the context of quantum chaos they have been checked numerically in Ref. [140] and experimentally in Ref. [144]. The second term is also in the results presented in Ref. [131], while the next order correction correspond to the first quantum corrections to $C(\Gamma)$. Eq. (6.27) is consistent with RMT calculations for indirect processes done in Ref. [138] and with its expansion in power of t/t_H conjectured in Ref. [145].

6.3 Ehrenfest time effects

We have seen in the previous chapter that Ehrenfest-time effects can be of importance in decay processes. Therefore we will study in this section τ_E-effects for the first quantum corrections to the statistics of photo-dissociation. We will follow our previous approach taking into account the different types of Ehrenfest times. The "opening" of the system w in this case corresponds to the number of dissociation channels times the de Broglie wavelength at energy E.

6.3.1 Ehrenfest time dependence of the leading quantum correction to the open trajectories contribution

We have shown before that we can write the OT contribution to the cross-section form factor as $\kappa\tilde{\rho}(t)$, with $\tilde{\rho}(t)$ defined as in the previous chapter. Its Ehrenfest

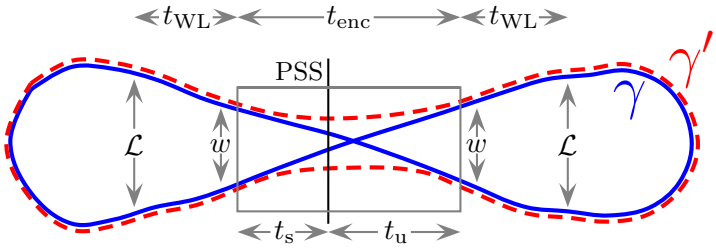

Figure 6.3: Sketch of a periodic orbit with a self-crossing for the semiclassical calculation with finite τ_E.

time dependence corresponds to Eq. (5.59) calculated at energy E:

$$Z^{1,2{\rm ll}+1{\rm ll}}(t) = e^{-t/\tau_d} e^{\frac{\tau_E^{\rm o}}{\tau_d}} \frac{(t-2\tau_E^e)^2}{\tau_d t_H} \theta(t-2\tau_E^e), \tag{6.28}$$

from which the correlation function can be obtained through the Fourier transform:

$$C_{\tau_E}^{1,2{\rm ll}+1{\rm ll}}(\omega) = 4\frac{\tau_d^2}{t_H^2} {\rm e}^{-\tau_E^{\rm c}/\tau_d} Re\left[\frac{(1-i\omega\tau_d)^3}{(1+(\omega\tau_d)^2)^3} {\rm e}^{-2i\omega\tau_E^e}\right]. \tag{6.29}$$

where $2\tau_E^e = \tau_E^{\rm c} + \tau_E^{\rm o}$. We notice that after time-integration, the auto-correlation function $C(\omega)$ shows an exponential suppression of quantum effects that depends on the Ehrenfest time of the closed system, similar to the exponential suppression of weak localization in transport in mesoscopic systems [35, 36, 37, 38, 39, 40].

6.3.2 Ehrenfest time dependence of the leading quantum correction to the periodic orbits contribution

A calculation of the Ehrenfest time dependence of the spectral form factor of closed systems was performed in Ref. [41]. We follow a similar approach, taking into account the opening of the system, and the two different Ehrenfest time scales. In this situation the stretches are required to be separated a distance $\mathcal{L}$ on the left and right hand side of the encounter. Therefore the minimal time for the orbits that have a self-encounter is $2t_{\rm enc} + 4t_{\rm WL}$. The first quantum correction to the spectral form factor is given by orbits sketched in Fig. 6.3 (denoted in the following by $(2)^1$). The corrected weight function is given by

$$w^{(2)^1}(u,s,t) = \frac{t(t-2t_{\rm enc}-4t_{\rm WL})}{2\Omega t_{\rm enc}} \theta(t-2t_{\rm enc}-4t_{\rm WL}) \tag{6.30}$$

The contribution to the auto-correlation function, after shifting the integral over time by $2t_{\rm enc}$, can be written as

$$C_{\tau_E}^{2,(2)^1}(\omega) = \frac{4}{t_H^3} Re \int_{4t_{\rm WL}}^{\infty} dt {\rm e}^{-(1+i\omega\tau_d)t/\tau_d} (t-4t_{\rm WL}) I^{(2)^1}(\omega,t), \tag{6.31}$$

with

$$I^{(2)^1}(\omega,t)=\frac{1}{\pi\hbar}\int_0^c du\int_0^c ds\mathrm{e}^{\frac{i}{\hbar}us}\frac{(t+2t_{\mathrm{enc}})^2}{t_{\mathrm{enc}}}\mathrm{e}^{-(1+2i\omega\tau_d)t_{\mathrm{enc}}/\tau_d}. \tag{6.32}$$

The integrals can be done as before (see appendix D). The final result is given by

$$C^{2,(2)^1}_{\tau_E}(\omega)=\frac{8\mathrm{e}^{(l_E^o-2l_E^c)}}{N^3}Re\left[\mathrm{e}^{-2i\Gamma l_E^c}\left(\frac{(1-2i\Gamma)}{(1+i\Gamma)^4}-\frac{4i\Gamma l_E^c}{(1+i\Gamma)^3}-\frac{2l_E^{c\,2}(1+2i\Gamma)}{(1+i\Gamma)^2}\right)\right], \tag{6.33}$$

where $\Gamma=\omega\tau_d$, $l_E^o=\tau_E^o/\tau_d$ and $l_E^c=\tau_E^c/\tau_d$. Taking the Fourier transform, the result for the spectral form factor of the open system is

$$Z^{2,(2)^1}_{\tau_E}(t)=\mathrm{e}^{-t/\tau_d}\mathrm{e}^{\tau_E^o/\tau_d}\left(-2\frac{t^2}{t_H^2}\left(1+\frac{\tau_E^c}{\tau_d}\right)+\frac{t^3}{\tau_d t_H^2}\right)\theta(t-2\tau_E^c), \tag{6.34}$$

when $\tau_d\to\infty$ and the system is closed, Eq. (6.34) is consistent with Ref. [41]. Similarly as for Eq. (6.28) a step function appears, requiring that only trajectories longer than $2\tau_E^c$ give some contribution, which is larger than $2\tau_E^e$ since the orbits have to close themselves. For those orbits the contribution is enhanced by $\mathrm{e}^{\tau_E^o/\tau_d}$, again showing the enhanced probability of surviving for periodic orbits with a self-encounter. As in Eq. (6.29), Eq. (6.33) shows that the quantum corrections in the cross-section auto-correlation function are exponentially suppressed due to the minimal time that self-encounters require. In the case of periodic orbits, the suppression is stronger (since $\tau_E^c>\tau_E^o$) because the stretches of the encounter must close themselves on both sides. Actually, if $w\ll\mathcal{L}$ such that $\tau_E^o\ll\tau_d$ but τ_E^c is comparable to τ_d, quantum effects coming from open trajectories could be visible, while those from periodic orbits can be neglected.

In this chapter we have implemented our previous semiclassical approach to the survival probability to a typical example of quantum decay processes, namely the indirect photo-dissociation of molecules. We have seen how the semiclassical analysis leads to two kind of contributions: one corresponding to trajectories leaving the system and the other one related to trajectories trapped inside the system. A semiclassical calculation with finite Ehrenfest time shows that quantum corrections in the cross-section auto-correlation function are exponentially suppressed, due to the minimal time for the existence of orbits with self-encounters that lead to quantum corrections.

Chapter 7

Conclusions and Outlook

7.1 Conclusions

In this thesis we have studied, on one hand, the effect of bifurcations on the spectral statistics of a Hamiltonian system. In this case study we worked out for the quartic oscillator how (pitchfork) bifurcations affect the density of states and thereby further measures of spectral correlations. This requires a detailed knowledge about the classical bifurcation scenario in that system. We have performed in Chapter 2 a comprehensive semiclassical calculation for the density of states invoking uniform approximations for the bifurcating orbits involved. All features of the coarse-grained quantum density of states are adequately, and to high precision (mean level spacing), semiclassically reproduced, which is not evident in such a system with mixed phase space dynamics. Our semiclassical evaluation of the spectral rigidity and spectral form factor close to the bifurcation (Chapter 3) shows strong deviations from the RMT behaviour, even though the phase space is predominantly chaotic and the bifurcation-affected phase space region appears negligible. This confirms that spectral statistics is rather susceptible to bifurcation effects. Moreover we could unveil the role of orbit pairs born at the bifurcation which prevail with near-degenerate actions for larger control parameter regimes and strongly affect the spectral statistics. Such orbit pairs are obviously classically correlated and require a treatment beyond the diagonal approximation.

This analysis moreover implies that in a comprehensive semiclassical approach to spectral correlations in mixed systems, which still remains as a challenge, off-diagonal contributions in the occurring multiple sums over periodic orbits should be considered, analogously to the purely hyperbolic case.

Based on the bifurcation theory developed in the context of photo-absorption spectra we have defined in Chapter 4 a bifurcation scenario for open orbits satis-

fying the stationary conditions for the transmission coefficients in the scattering approach to transport in mesoscopic systems. Bifurcations are defined as collapse of stationary points as some parameters are changed. This concept can be extended from periodic orbits, which are stationary points of the Poincaré map, to scattering orbits, which are stationary points of a generating function of type F_1. A special semiclassical treatment for the transmission coefficients has to be followed in order to regularize contributions coming from such bifurcation scenarios. We have given two typical examples for bifurcations of low codimension: the tangent and the pitchfork bifurcation. The appropriate normal forms used for the regularization are the same as the ones used in the density of states, therefore, as in the spectral statistics, the semiclassical weight of these trajectories in the transmission amplitudes is enhanced in comparison with isolated orbits and this enhancement is expressed in a different $\hbar$-scaling of the amplitudes. But, contrary to what would be expected from the effect of bifurcations in spectral statistics, the contribution of a single open-orbit bifurcation does not dominate the conductance of the systems. This results from the fact that the different $\hbar$ dependence of an open-orbit bifurcation appearing in a single transmission probability is not enough to counteract the sum over all other chaotic trajectories contributing to all the scattering channels.

On the other hand, we have studied in Chapter 5 the semiclassical approximation to the survival probability and another source of deviations from Random Matrix theory, namely the effect of finite Ehrenfest time scales. For open systems the Ehrenfest time can be of relevance if it is comparable to the typical time that the particles remain inside the system. We have numerically studied the decay of a localized wave function inside a chaotic billiard. The results left evidence that Ehrenfest time effects can be of consideration. They show up as a shift in the appearance of quantum corrections to the decay. These quantum corrections come from the standard "two-leg-loops" contributions together with the new diagrams, "one-leg-loops", that have to be taken into account in order to preserve normalization. The Ehrenfest time dependence of the decay probability shows two competing effects: on one hand, for short times trajectories cannot form a self encounter and therefore quantum corrections do not appear. On the other hand, if the time is long enough for the formation of such a self encounter, the probability of staying is enhanced, due to the closeness of the stretches of the encounter.

Finally, in Chapter 6, we have applied the semiclassical tools discussed in Chapter 5 to study the statistics of dissociation of molecules through absorption of light in indirect processes, in which the time scale of the dissociation is rather large and the complexity of the dynamics can show up in the statistics of the

photo-dissociation cross section. We have seen that the related form factor of the cross section, i.e., the Fourier transform of the cross section auto-correlation function, can be written as a sum of two contributions. The first one is related to open trajectories and corresponds the survival probability (multiplied by a factor of 2 in the case of time reversal symmetry). The second one is the spectral form factor related to the periodic orbits that are trapped inside the system. The results are consistent with Random Matrix Theory predictions. Moreover, within our semiclassical approach we have calculated the Ehrenfest time dependence of these contributions, showing again two competing effects in the leading quantum corrections to the cross section form factor: the need of a minimal time in order to have a self-encounter versus the enhanced probability of staying of trajectories with a self-encounter. This minimal time is larger for periodic orbits than for open trajectories, and therefore quantum corrections coming from periodic orbits with self-encounters should show up later than those of open trajectories. The effect of finite Ehrenfest time scales on the auto-correlation function is an exponential suppression of quantum corrections, as in the case of transport through mesoscopic systems. This suppression is stronger for quantum corrections coming from periodic orbits.

7.2 Open questions and outlook

There are several interesting open questions which we would like to discuss in some detail.

One of these is the study of the effect of bifurcations in spectral determinants. For a semiclassical calculation of individual quantum energy levels it is more convenient to use formulations in terms of spectral determinants instead of the density of states. Moreover, spectral determinants can be related with wave functions and with expectation values [146]. Spectral determinants are functions whose zeros are given by the eigenvalues E_m of a quantum Hamiltonian. They are entire functions of the energy, real valued for real energy, and can be expressed as a product over the energy level as

$$Z(E) = \prod_n A(E, E_n)(E - E_n), \tag{7.1}$$

where $A(E, E_n)$ are non-vanishing functions of E making the product convergent. A semiclassical expression for $Z(E)$ can be done in terms of pseudo-orbits, i.e, set of orbits, whose amplitudes, in the stationary phase approximation, correspond to the product of the semiclassical amplitudes entering the density of states. Therefore, it is expected that bifurcations could be important in quantities like the auto-correlation function of $Z(E)$.

Considering the topic of Ehrenfest time effects, which we have studied in the context of decay, it would be interesting to study the logarithmic $\hbar$-dependence of the quantum corrections. Typical numerical evaluations of Ehrenfest time effects are done in maps (or in systems that can be easily reduced to maps, like the kicked rotor), which are numerically much simpler than billiards, and in which it is possible to increase the size of the system by several orders of magnitude. Although they are not the most realistic systems, which is why we did not consider them, they allow one to study numerically the $\hbar$-dependence of the quantum corrections and the effects of different Ehrenfest time scales.

It is also an interesting outlook to develop a semiclassical approach to decay for times comparable with the Heisenberg time. Semiclassics in this regime has only been considered in Ref. [147], studying spectral statistics. The analysis in Ref. [147] starts from the consideration of correlations of the spectral determinant. A connection between scattering processes and spectral determinants was first proposed in Ref. [148], in the frame of the Fredholm theory, and the link between correlations of the scattering matrix and the decay has been discussed in Ref. [75] related to the quest of the continuity equation and the semiclassical approximation. A combination of these analyses can give a light on a semiclassical approximation to decay for long times.

The most fundamental open question is perhaps the rôle of periodic orbits in the semiclassical scattering description of transport. In Chapter 4, we have mentioned that according to Ref. [117] bifurcations of periodic orbits that are inside the system are dominant in the conductance moments in antidot lattices (even powers of the oscillatory part of the conductance). These bifurcations are of periodic orbits, and they enter into play in the semiclassical description of transport within the Kubo formalism. A semiclassical approximation to this formalism was performed in Refs. [149, 150], where it was shown that the longitudinal conductivity can be written as a smooth part (classical) and an oscillatory part, given in terms of periodic orbits as

$$\delta\bar{\sigma}_{xx} = \frac{2g_s e^2}{hV} \sum_j \mathrm{e}^{-T_j/2\tau_{\mathrm{el}}} C_j(v_x, v_x) A_j(E) \cos\left[\frac{S_j(E)}{\hbar} - \frac{\pi}{2}\sigma_j\right], \qquad (7.2)$$

in a similar way as for the oscillatory part of the density of states. Here $C_j(v_x, v_x) = \int_0^\infty dt \mathrm{e}^{-t/\tau_{\mathrm{el}}} \int_0^{t_{pj}} dt' v_x(t') v_x(t+t')$ is the auto-correlation function of the longitudinal velocities v_x along the primitive periodic orbit pj and τ_{el} is the elastic scattering length. For very long trajectories one can approximate the integral over the trajectory length by its phase space average, if the system is ergodic. The longitudinal conductivity can be approximated to $\delta\bar{\sigma}_{xx}(E) \approx \bar{\sigma}^c_{xx}(E)\delta g(E)$. It is clear in this approach that periodic orbit bifurcations can be dominant when

considering moments of the conductivity, $\langle(\delta\bar{\sigma}_{xx})^{2m}\rangle$, as they are for the spectral statistics. That the conductance and the longitudinal conductivity are equivalent in a two-probe sample, has been shown quantum-mechanically based on the continuity equation [151]. Semiclassically is not yet clear how periodic orbits participate in the scattering semiclassical description of transport. There should be a classical mechanism that relates trajectories escaping with the classical repeller (the set of solutions that never leave the system). A similar situation was recently discussed in Ref. [152] related to the correlations of the time delay, which can also be described in terms of the scattering matrix or in terms of the density of states, giving rise to two different semiclassical expressions. The connection between the two approaches was found by introducing the contribution of scattering trajectories that spend long times near trapped periodic orbits. This does not yet solve the problem of transport as pointed out in Ref. [152], since these correlations turn out to be zero in this case. Further research into this direction seems promising to understand the dynamical mechanisms behind linear response theory in transport through mesoscopic devices with chaotic and mixed dynamics.

Appendix A

Reduced density of states of the separable quartic oscillator

Let us consider the semiclassical density of states of the QO for the EES reduced representation. We can calculate the density corresponding to n_x and n_y being even $g_{\rm EE}(E)$, which contains the density of the two irreducible representations $g_{\rm EES}(E)$ and $g_{\rm EEA}(E)$. The difference between the two is given by the density $g_{\rm S}(E)$ when $n_x = n_y = 2n'$. The reducible densities can be calculated as

$$g_{\rm EES}(E) = \frac{g_{\rm EE}(E) + g_{\rm S}(E)}{2}, \tag{A.1}$$

and

$$g_{\rm EEA}(E) = \frac{g_{\rm EE}(E) - g_{\rm S}(E)}{2}. \tag{A.2}$$

The 1-dimension EBK spectrum is given by

$$E_{n_x} = \frac{1}{\tilde{a}}\left(n_x + \frac{1}{2}\right), \tag{A.3}$$

where $\tilde{a} = 4\left(\frac{2\mathbf{K}}{3\pi}\right)$.

Taking $n_x = 2n'_x$ we have that the one-dimensional density corresponding to even n_x is

$$\begin{aligned} g^{\rm sc}_{x,{\rm E}}(E) &= \sum_{n'_x=0}^{\infty} \delta(E - E_{2n'_x}) = \sum_{k_x=-\infty}^{\infty} \int_0^{\infty} \delta(E - E_{2n}) {\rm e}^{2\pi i k_x n} dn & \text{(A.4)} \\ &= \sum_{k_x=-\infty}^{\infty} \int \delta\left(\frac{(\tilde{a}E)^{3/4}}{2} - \frac{1}{4} - n\right) \left(\frac{3\tilde{a}^{3/4}}{8E^{1/4}}\right) {\rm e}^{2\pi i k_x n} dn & \text{(A.5)} \\ &= \frac{3}{8}\tilde{a}^{3/4} E^{-1/4} \sum_{k_x=-\infty}^{\infty} \exp\left(\pi i k_x (\tilde{a}E)^{3/4} - i\frac{\pi}{2}k_x\right). & \text{(A.6)} \end{aligned}$$

The two-dimensional density of states is found by convolution of the one-dimesional one. Thus

$$\begin{aligned} g^{\rm sc}_{\rm EE}(E) &= \int_0^E g_{x,\rm E}(E-E')g_{x,\rm E}(E')dE' \qquad (A.7)\\ &= \frac{9}{64}\tilde{a}^{3/2}\sum_{k_x,k_y=-\infty}^{\infty} \mathrm{e}^{-i\frac{\pi}{4}k_x - i\frac{\pi}{4}k_y}\int_0^E (E-E')^{-1/4}E'^{-1/4}\mathrm{e}^{i\Phi_E(E')}dE'. \end{aligned}$$

with $\Phi_E(E') = \pi\tilde{a}^{3/4}((E-E')^{3/4}k_x + E'^{3/4}k_y)$.

From $k_x = k_y = 0$ we have the smooth part of the density of states

$$\bar{g}^{\rm sc}_{\rm EE}(E) = \frac{\mathbf{K}}{2\pi\hbar}E^{1/2}. \qquad (A.8)$$

The integral can be evaluated by stationary phase approximation for $k_x \neq 0$, $k_y \neq 0$ as for the full density of states [80]. The stationary points are the same, namely $E^* = Ek_y^4/(k_x^4+k_y^4)$. Moreover there are end - point corrections due to the limits of integration (see [87]). The result is

$$\begin{aligned} \delta g^{(1)}_{\rm EE}(E) &= 2\left(\frac{\mathbf{K}}{\pi\hbar}\right)^{\frac{3}{2}}(4E)^{\frac{1}{8}}\sum_{k_x,k_y=1}^{\infty}\frac{k_xk_y}{(k_x^4+k_y^4)^{5/8}}\cos\left[\frac{1}{2\hbar}S_{k_xk_y}(E) - \frac{\pi}{2}(k_x+k_y) - \frac{\pi}{4}\right]\\ &+\left(\frac{2\mathbf{K}}{3\pi\hbar}\right)(4E)^{-\frac{1}{4}}\sum_{k_x,k_y=1}^{\infty}(-1)^{(k_x+k_y)}\times\\ &\times\left\{\frac{1}{2k_x-1}\left[\sin\left((2k_y-1)\frac{S_A}{2\hbar}\right) - \cos\left(k_y\frac{S_A}{\hbar}\right)\right]\right.\\ &\left.+\frac{1}{2k_y-1}\left[\sin\left((2k_x-1)\frac{S_A}{2\hbar}\right) - \cos\left(k_x\frac{S_A}{\hbar}\right)\right]\right\}. \qquad (A.9) \end{aligned}$$

We see that the end-point corrections can be neglected since they go very fast to zero as $E \to \infty$.

When $k_x = 0$ or $k_y = 0$ the evaluation is more cumbersome. This case together with the end-point corrections corresponds to the contribution of the librational orbits A. It can be written as

$$\delta g^{\rm A}_{\rm EE}(E) = \frac{8\mathbf{K}^2}{3\pi^2\hbar^2}\sqrt{E}\sum_{k=-\infty}^{\infty}\mathrm{e}^{i\pi k/2}\int_0^1\frac{du}{(1-u^{\frac{4}{3}})^{\frac{1}{4}}}\exp\left(ik\frac{S_A}{2\hbar}(1-u^{\frac{4}{3}})^{\frac{3}{4}}\right), \quad (A.10)$$

whose evaluation can be done asymptotically [88]. And the final result is the one shown in Eq. (2.21) (the second sum) multiplied by a factor of 2.

Finally we calculate the density $g^{\rm S}(E)$ by taking $n_x = n_y = 2n$, thus

$$\begin{aligned} g^{\rm sc}_{\rm S}(E) &= \sum_{n=0}^{\infty} \delta(E - E^{\rm EBK}_{2n,2n}) \\ &\quad \sum_{k=-\infty}^{\infty} \int_0^{\infty} \delta\left(\frac{(\tilde{a}E/2)^{3/4}}{2} - \frac{1}{4} - n\right) \left(\frac{3(\tilde{a}/2)^{3/4}}{8E^{1/4}}\right) {\rm e}^{2\pi i k_x n} dn \\ &= \frac{1}{2^{\frac{3}{4}}} \frac{2\mathbf{K}}{\pi\hbar} (4E)^{-\frac{1}{4}} \left(1 + \sum_{k=1}^{\infty} \cos\left(\frac{S_A}{2^{\frac{7}{4}}\hbar} k - \frac{\pi}{2} k\right)\right). \end{aligned} \tag{A.11}$$

The mean density for the reduced representations EES and EEA is slightly corrected by $\pm\bar{g}_{\rm S}(E)/2$ from the approximation $\bar{g}(E)/8$:

$$\bar{g}^{\rm sc}_{\rm EES}(E) = \frac{\mathbf{K}}{4\pi\hbar} E^{1/2} + \frac{1}{2^{\frac{7}{4}}} \frac{2\mathbf{K}}{\pi\hbar} (4E)^{-\frac{1}{4}}, \tag{A.12}$$

and

$$\begin{aligned} \delta g_{\rm EES}(E) &= \left(\frac{\mathbf{K}}{\pi\hbar}\right)^{\frac{3}{2}} (4E)^{\frac{1}{8}} \sum_{k_x,k_y=1}^{\infty} \frac{k_x k_y}{(k_x^4 + k_y^4)^{5/8}} \cos\left[\frac{1}{2\hbar} S_{k_x k_y}(E) - \frac{\pi}{2}(k_x + k_y) - \frac{\pi}{4}\right] \\ &+ \frac{1}{2^{\frac{3}{4}}} \frac{(\mathbf{K})^{\frac{3}{4}}}{(\pi\hbar)^{\frac{5}{4}}} (4E)^{-\frac{1}{16}} \sum_{k=1}^{\infty} \frac{1}{k^{\frac{3}{4}}} \cos\left[\frac{k}{2\hbar} S_A(E) - \frac{\pi}{2} k - \frac{3\pi}{8}\right] \\ &+ \left(\frac{2\mathbf{K}}{3\pi\hbar}\right) (4E)^{-\frac{1}{4}} \sum_{k_x,k_y=1}^{\infty} (-1)^{(k_x+k_y)} \frac{1}{2k_x - 1} \\ &\times \left[\sin\left((2k_y - 1)\frac{S_A}{2\hbar}\right) - \cos\left(k_y \frac{S_A}{\hbar}\right)\right] \\ &+ \frac{1}{2^{\frac{7}{4}}} \frac{2\mathbf{K}}{\pi\hbar} (4E)^{-\frac{1}{4}} \sum_{k=1}^{\infty} \cos\left(\frac{S_A}{2^{\frac{7}{4}}\hbar} k - \frac{\pi}{2} k\right) \end{aligned} \tag{A.13}$$

The dominant contributions come from the tori where $k_x \neq 0$, $k_y \neq 0$. In Eq. (2.21) we only note the most important contributions, though for the numerical comparison we have taken all the previous terms into account.

Appendix B

Ehrenfest time dependence of the decay probability

Recalling Eq. (5.56) we have that

$$\rho_{\tau_E}^{1,2\mathrm{ll}}(s) = \frac{2}{t_H}\int_0^\infty t^2\, \mathrm{e}^{-(1+s\tau_d)(t+2t_{\mathrm{WL}})/\tau_d} I^{2\mathrm{ll}}(s)dt, \tag{B.1}$$

where,

$$I^{2\mathrm{ll}}(s) = \frac{1}{\pi\hbar}\int_0^c du \int_0^c ds \frac{e^{\frac{i}{\hbar}us}}{t_{\mathrm{enc}}} \mathrm{e}^{t_{\mathrm{enc}}/\tau_d}\mathrm{e}^{-2(1+s\tau_d)t_{\mathrm{enc}}/\tau_d}. \tag{B.2}$$

Making the change of variables $x = us/c^2$ and $\sigma = c/u$ we obtain

$$I^{2\mathrm{ll}}(s) = \frac{r\lambda}{\pi}\int_0^1 dx \cos(rx) x^{\frac{1}{\lambda\tau_d}(1+2s\tau_d)}, \tag{B.3}$$

where $r = c^2/\hbar$ and the integral over σ has already been performed. We make the change of variables $y = rx$ then

$$I^{2\mathrm{ll}}(s) = \frac{\lambda}{\pi} r^{-\frac{1}{\lambda\tau_d}(1+2s\tau_d)} \int_0^r dy \cos(y) y^{\frac{1}{\lambda\tau_d}(1+2s\tau_d)}. \tag{B.4}$$

We perform the integral by partial integration, neglecting highly oscillating terms as in Eq. (5.42):

$$I^{2\mathrm{ll}}(s) = \frac{\lambda}{\pi} r^{-\frac{1}{\lambda\tau_d}(1+2s\tau_d)} \int_0^\infty dy \cos(y) y^{\frac{1}{\lambda\tau_d}(1+2s\tau_d)} = -\frac{(1+2s\tau_d)}{2\tau_d} e^{-(1+2s\tau_d)\tau_E^o/\tau_d}, \tag{B.5}$$

where we have taken $\tau_E^{\mathrm{o}} = \lambda^{-1}\ln(c^2/\hbar)$ and $\hbar \to 0$ keeping τ_E^o/τ_d finite. Going back to the decay we have that

$$\rho_{\tau_E}^{1,2\mathrm{ll}}(s) = -2\frac{\tau_d^2}{t_H}\mathrm{e}^{-\frac{\tau_E^c}{\tau_d}} \frac{(1+2s\tau_d)}{(1+s\tau_d)^3}\mathrm{e}^{-2s\tau_E^e}. \tag{B.6}$$

The inverse Laplace transform leads us to

$$\rho^{2\mathrm{ll}}(t) = e^{-t/\tau_d} e^{\frac{\tau_E^o}{\tau_d}} \left(\frac{(t-2\tau_E^e)^2}{2\tau_d t_H} - \frac{2(t-2\tau_E^e)}{t_H} \right) \theta(t-2\tau_E^e), \tag{B.7}$$

where $\theta(t-2\tau_E^e)$ is the step function. Clearly from the definitions of τ_E^{o} and t_{WL} we have that $\tau_E^{\mathrm{o}} + 2t_{\mathrm{WL}} = \tau_E^{\mathrm{c}}$ and $2\tau_E^e = \tau_E^{\mathrm{c}} + \tau_E^{\mathrm{o}}$.

For the 1ll we have Eq. (5.58):

$$\rho_{\tau_E}^{1,1\mathrm{ll}}(s) = \frac{8}{t_H} \int_0^\infty t\, \mathrm{e}^{-(1+s\tau_d)(t+2t_{WL})/\tau_d} I^{1\mathrm{ll}}(s) dt, \tag{B.8}$$

with

$$I^{1\mathrm{ll}}(s) = \frac{1}{\pi\hbar} \int_0^c du \int_0^c ds \int_0^{\lambda^{-1}\ln(c/|s|)} dt' \frac{e^{\frac{i}{\hbar}us}}{t_{\mathrm{enc}}} \mathrm{e}^{-(1+2s\tau_d)t_{\mathrm{enc}}/\tau_d}, \tag{B.9}$$

where $t_{\mathrm{enc}} = t' + \lambda^{-1}\ln(c/|u|)$. We make the change of variables $x = us/c^2$ and $\sigma = c/u$ and $t'' = t' + \lambda^{-1}\ln(c/|u|)$, obtaining

$$I^{1\mathrm{ll}}(s) = -\frac{\lambda r \tau_d}{\pi(1+2s\tau_d)} \int_0^1 dx \cos(rx) x^{\frac{1}{\lambda\tau_d}(1+2s\tau_d)}. \tag{B.10}$$

The integral is the same as before, then

$$\rho_{\tau_E}^{1,1\mathrm{ll}}(s) = 2\frac{\tau_d^2}{t_H} \mathrm{e}^{-\frac{\tau_E^c}{\tau_d}} \frac{2}{(1+s\tau_d)^2} \mathrm{e}^{-2s\tau_E^e}. \tag{B.11}$$

Summing up the two contribution we obtain

$$\rho_{\tau_E}^{1,2\mathrm{ll}+1\mathrm{ll}}(s) = 4\frac{\tau_d^2}{t_H^2} \mathrm{e}^{-\frac{\tau_E^c}{\tau_d}} \left[\frac{(1-s\tau_d)^3}{(1+s\tau_d))^3} \mathrm{e}^{-2s\tau_E^e} \right]. \tag{B.12}$$

The total quantum correction coming from 1ll and 2lls is then

$$\rho^{1\mathrm{ll}}(t) = e^{-t/\tau_d} e^{\frac{\tau_E^o}{\tau_d}} \frac{2(t-2\tau_E^e)}{t_H} \theta(t-2\tau_E^e). \tag{B.13}$$

Appendix C

Variance of the decay for a Gaussian initial state

Recalling Eq. (5.64),

$$\begin{aligned}\langle \mathrm{var}\rho(t)\rangle^{\mathrm{d}}_{\Delta t} &= \Big\langle \frac{1}{(2\pi\hbar)^4}\int_A \prod_{i=1}^{4} d\mathbf{q}_i \sum_{\substack{\gamma_1(\mathbf{q}_1\to\mathbf{q}_3,t)\\ \gamma_2(\mathbf{q}_2\to\mathbf{q}_3,t)}} |D_{\gamma_1}|^2|D_{\gamma_2}|^2 \mathrm{e}^{\frac{i}{\hbar}(\mathbf{p}_{\gamma_1,f}-\mathbf{p}_{\gamma_2,f})\cdot\mathbf{q}_4} \\ &\quad \times\rho^*_W\left(\mathbf{q}_1,\mathbf{p}_{\gamma_1,o}\right)\rho_W\left(\mathbf{q}_2,\mathbf{p}_{\gamma_2,o}\right)\Big\rangle_{\Delta t}, \end{aligned} \tag{C.1}$$

We apply the sum rule as in Chapter 6, but in the time domain

$$\sum_{\gamma:(\mathbf{r}\to\mathbf{r}',t)} |D_\gamma|^2(...) = \int d\mathbf{p}\int d\mathbf{p}'\delta(\mathbf{r}(t)-\mathbf{r}')\delta(\mathbf{p}(t)-\mathbf{p}')(...) \tag{C.2}$$

$p(\mathbf{r},\mathbf{p},\mathbf{r}',\mathbf{p}',t) = \delta(\mathbf{r}(t)-\mathbf{r}')\delta(\mathbf{p}(t)-\mathbf{p}')$ is the classical probability of going from a point $(\mathbf{r},\mathbf{p})$ in phase space to a point $(\mathbf{r}',\mathbf{p}')$ in a time t, with the evolution given by H. We can replace this, for large time, for its phase space averages, in the case of an ergodic system:

$$\bar{p} = \frac{\delta(H(\mathbf{r},\mathbf{p})-H(\mathbf{r}',\mathbf{p}'))}{\Omega(H(\mathbf{r},\mathbf{p}))}. \tag{C.3}$$

For a billiard this yields

$$\begin{aligned}\langle \mathrm{var}\rho(t)\rangle^{\mathrm{d}}_{\Delta t} &= \frac{1}{(2\pi\hbar)^4(\pi A)^2}\int\prod_{i=1}^{4} d\mathbf{q}_i d\mathbf{p}_i \rho_W\left(\mathbf{q}_1,\mathbf{p}_1\right)\rho_W\left(\mathbf{q}_2,\mathbf{p}_2\right) \\ &\quad \times \mathrm{e}^{\frac{i}{\hbar}(\mathbf{p}_3-\mathbf{p}_4)\cdot\mathbf{q}_4}\mathrm{e}^{-t/\tau_d(p_1)}\mathrm{e}^{-t/\tau_d(p_2)}\delta(\mathbf{p}_1^2-\mathbf{p}_3^2)\delta(\mathbf{p}_2^2-\mathbf{p}_4^2). \end{aligned} \tag{C.4}$$

The integral over $\mathbf{q}_3$ gives a factor A since the integrand does not depend on this variable. The integral over $\mathbf{q}_4$ selects $\mathbf{p}_3$ near $\mathbf{p}_4$. Extending the limits of

integration to R^2 this selection becomes a sharp delta function. Thus,

$$\begin{aligned}\langle \mathrm{var}\rho(t)\rangle^{\mathrm{d}}_{\Delta t} &= \frac{1}{(2\pi\hbar)^2\pi^2 A}\int d\mathbf{q}_1 d\mathbf{q}_2 \prod_{i=1}^{4} d\mathbf{p}_i \rho_W(\mathbf{q}_1,\mathbf{p}_1)\,\rho_W(\mathbf{q}_2,\mathbf{p}_2)\\ &\quad\times\delta(\mathbf{p}_3-\mathbf{p}_4)\mathrm{e}^{-t/\tau_d(p_1)}\mathrm{e}^{-t/\tau_d(p_2)}\delta(\mathbf{p}_1^2-\mathbf{p}_3^2)\delta(\mathbf{p}_2^2-\mathbf{p}_4^2).\\ &= \frac{1}{(2\pi\hbar)^2\pi^2 A}\int d\mathbf{q}_1 d\mathbf{q}_2 \prod_{i=1}^{3} d\mathbf{p}_i\,\rho_W(\mathbf{q}_1,\mathbf{p}_1)\,\rho_W(\mathbf{q}_2,\mathbf{p}_2)\\ &\quad\times\mathrm{e}^{-t/\tau_d(p_1)}\mathrm{e}^{-t/\tau_d(p_2)}\delta(\mathbf{p}_1^2-\mathbf{p}_2^2)\delta(\mathbf{p}_2^2-\mathbf{p}_3^2).\end{aligned}$$

In the last equality we used the identity $\delta(f_1-f_2)\delta(f_2-f_3)=\delta(f_1-f_3)\delta(f_2-f_3)$. Now we can performed the integral over $\mathbf{p}_3$, thus

$$\int d\mathbf{p}_3\delta(\mathbf{p}_3^2-\mathbf{p}_2^2)=\int_0^{2\pi}d\theta\int_0^{\infty}p_3dp_3\delta(p_3^2-p_2^2)=\pi\int_0^{\infty}du\delta(p_2^2-u)=\pi \quad \text{(C.5)}$$

Then

$$\begin{aligned}\langle \mathrm{var}\rho(t)\rangle^{\mathrm{d}}_{\Delta t} &= \frac{1}{(2\pi\hbar)^2\pi A}\int \prod_{i=1}^{2} d\mathbf{q}_i d\mathbf{p}_i\,\rho_W(\mathbf{q}_1,\mathbf{p}_1)\,\rho_W(\mathbf{q}_2,\mathbf{p}_2)\\ &\quad\times\mathrm{e}^{-t/\tau_d(p_1)}\mathrm{e}^{-t/\tau_d(p_2)}\delta(\mathbf{p}_1^2-\mathbf{p}_2^2).\end{aligned}$$

Let us now use the Fourier representation of the remaining delta function:

$$\langle \mathrm{var}\rho(t)\rangle^{\mathrm{d}}_{\Delta t}=\frac{1}{(2\pi\hbar)^2 2\pi^2 A}\int_{-\infty}^{\infty}dk\left|\int d\mathbf{q}d\mathbf{p}\,\rho_W(\mathbf{q},\mathbf{p})\,\mathrm{e}^{-t/\tau_d(p)}\mathrm{e}^{ik\mathbf{p}^2}\right|^2. \quad \text{(C.6)}$$

Substituting Eq. (5.36) in Eq. (C.6) and integrating over the coordinates we obtain

$$\langle \mathrm{var}\rho(t)\rangle^{\mathrm{d}}_{\Delta t}=\frac{2\sigma^4}{(\pi\hbar)^2 A}\int_{-\infty}^{\infty}dk\left|\int d\mathbf{p}\exp\left(-\frac{\sigma^2}{\hbar^2}\left[(\mathbf{p}-\mathbf{p}_o)^2\right]+ik\mathbf{p}^2\right)\mathrm{e}^{-t/\tau_d(p)}\right|^2 \quad \text{(C.7)}$$

For $p_o\sigma\gg\hbar$ we can neglect the p dependence of the function $\mathrm{e}^{-t/\tau_d(p)}$ since the Gaussian factor strongly selects $\mathbf{p}\approx\mathbf{p}_o$. The remaining Gaussian integral over p gives

$$\int d\mathbf{p}\exp\left(-\frac{\sigma^2}{\hbar^2}\left[(\mathbf{p}-\mathbf{p}_0)^2\right]+ik\mathbf{p}^2\right)=\frac{\pi\hbar^2}{\sigma^2}\frac{\exp(ikp_0^2/(1-ik\hbar^2/\sigma^2))}{1-ik\hbar^2/\sigma^2} \quad \text{(C.8)}$$

Then

$$\langle \mathrm{var}\rho(t)\rangle^{\mathrm{d}}_{\Delta t}=\frac{2\hbar^2\mathrm{e}^{-2t/\tau_d^o}}{A}\int dk\frac{1}{1+k^2\hbar^4/\sigma^4}\exp\left(\frac{-2k^2\hbar^2p_0^2/\sigma^2}{1+k^2\hbar^4/\sigma^4}\right) \quad \text{(C.9)}$$

Defining $a=\hbar/(\sigma p_0)$ and making the change of variables $u=k\hbar^2/(a\sigma^2)$ we have

$$\langle \mathrm{var}\rho(t)\rangle^{\mathrm{d}}_{\Delta t}=\frac{2a\sigma^2\mathrm{e}^{-2t/\tau_d^o}}{A}\int du\frac{1}{1+a^2u^2}\exp\left(\frac{-2u^2}{1+a^2u^2}\right). \quad \text{(C.10)}$$

a is a small parameter and in the semiclassical limit it goes to zero, so we take the limit $a \to 0$ in the integral and approximate the integral over u as $\int du \mathrm{e}^{-2u^2}$, yielding

$$\langle \mathrm{var}\rho(t) \rangle^{\mathrm{d}}_{\Delta t} = \frac{2a\sigma^2 \mathrm{e}^{-2t/\tau_d^o}}{A} \sqrt{\frac{\pi}{2}} = \frac{2\hbar\sigma}{Ap_0} \sqrt{\frac{\pi}{2}}. \tag{C.11}$$

Appendix D

Ehrenfest time dependence of the spectral form factor for open systems

Recalling Eq. (6.31):

$$C^{2,(2)^1}_{\tau_E}(\omega) = \frac{4}{t_H^3} Re \int_{4t_{\rm WL}}^{\infty} dt \mathrm{e}^{-(1+i\omega\tau_d)t/\tau_d}(t-4t_{\rm WL}) I^{(2)^1}(\omega,t), \tag{D.1}$$

with

$$I^{(2)^1}(\omega,t) = \frac{1}{\pi\hbar}\int_0^c du \int_0^c ds \mathrm{e}^{\frac{i}{\hbar}us}\frac{(t+2t_{\rm enc})^2}{t_{\rm enc}}\mathrm{e}^{-(1+2i\omega\tau_d)t_{\rm enc}/\tau_d}. \tag{D.2}$$

This can be written as

$$I^{(2)^1}(\omega,t) = \frac{1}{\pi\hbar}\left(t^2 - 4t\frac{d}{d\tau_d^{-1}} + 4\frac{d^2}{d(\tau_d^{-1})^2}\right)\int_0^c du\int_0^c ds \mathrm{e}^{\frac{i}{\hbar}us}\frac{\mathrm{e}^{-(1+2i\omega\tau_d)t_{\rm enc}/\tau_d}}{t_{\rm enc}}. \tag{D.3}$$

Proceeding with the integrals over (u,s) as in the Appendix B we obtain

$$\begin{aligned} I^{(2)^1}(\omega,t) &= -\frac{1}{2}\left(t^2 - 4t\frac{d}{d\tau_d^{-1}} + 4\frac{d^2}{d(\tau_d^{-1})^2}\right)\left((\tau_d^{-1}+2i\omega)e^{-(\tau_d^{-1}+2i\omega)\tau_E^o}\right) \\ &= e^{-\frac{\tau_E^o}{\tau_d}(1+2i\omega\tau_d)}\left[-(1+2i\omega\tau_d)\frac{(t+2\tau_E^o)^2}{2\tau_d} + 2(t+2\tau_E^o)\right]. \end{aligned} \tag{D.4}$$

Substituting in the (D.1) and shifting the integral by $4t_{\rm WL}$

$$C^{2,(2)^1}_{\tau_E}(\omega) = \frac{4\mathrm{e}^{\frac{\tau_E^o}{\tau_d}}}{t_H^3} Re\int_0^{\infty} dt \mathrm{e}^{-(1+i\omega\tau_d)\frac{(t+2\tau_E^c)}{\tau_d}} t\left[-(1+2i\omega\tau_d)\frac{(t+2\tau_E^c)^2}{2\tau_d} + 2(t+2\tau_E^c)\right],$$

yielding

$$C^{2,(2)^1}_{\tau_E}(\omega) = \frac{8\mathrm{e}^{(l^o_E - 2l^c_E)}}{N^3} Re\left[\mathrm{e}^{-2i\Gamma l^c_E}\left(\frac{(1-2i\Gamma)}{(1+i\Gamma)^4} - \frac{4i\Gamma l^c_E}{(1+i\Gamma)^3} - \frac{2{l^c_E}^2(1+2i\Gamma)}{(1+i\Gamma)^2}\right)\right],$$

where $\Gamma = \omega\tau_d$, $l^o_E = \tau^o_E/\tau_d$ and $l^c_E = \tau^c_E/\tau_d$. The Fourier transform leads to

$$Z^{2,(2)^1}_{\tau_E}(t) = \mathrm{e}^{-t/\tau_d}\mathrm{e}^{\tau^o_E/\tau_d}\left(-2\frac{t^2}{t^2_H}\left(1+\frac{\tau^c_E}{\tau_d}\right) + \frac{t^3}{\tau_d t^2_H}\right)\theta(t-2\tau^c_E). \tag{D.5}$$

Bibliography

[1] V. I. Arnold, *Mathematical methods of classical mechanics*. Springer, New Aork, 1978.

[2] The action-angle variables do not always exist globally in integrable systems; see, e.g., D. A. Sadovskii and B. Zhilinskii, Phys. Lett. A **256**, 235 (1999), or H. Dullin, A. Giacobbe and R. Cushman, Physica D **190** 15, (2004).

[3] E. Madelung, Z. Phys. **40**, 322 (1926).

[4] J. B. Keller and S. I. Rubinow, Ann. Phys. **9**, 24 (1960).

[5] G. Wentzel, Z. Phys. **38**, 518 (1926). H. Kramers, Z. Phys. **39**, 828 (1926). L. Brillouin, Compt. Rend **183**, 24 (1926).

[6] P. Gaspard, *Chaos, Scattering and Statistical Mechanics*. Cambridge University Press, Cambridge, 1998.

[7] H. J. Stöckmann, *Quantum Chaos: An Introduction* (Cambridge University Press, Cambridge, England, 1999).F. Haake,*Quantum Signatures of Chaos*, 2nd ed. (Springer, Berlin, 2001).

[8] M. V. Berry, Proc. R. Soc. A **413**, 183-198, (1987).

[9] E. P. Wigner, Proc. 4th Can. Math. Congr., Toronto, 174 (1959).

[10] F. Dyson and M. Mehta, J. Math. Phys. **4**, 701 (1963). M. Mehta *Random Matrices and the Statistical Theory of Energy Levels* (Academic Press, 1990).

[11] O. Bohigas, M. J. Giannoni, and C. Schmit, Phys. Rev. Lett. **52**, 1 (1984).

[12] R. P. Feynman, Rev. Mod. Phys. **20**,367 (1948).

[13] M.C. Gutzwiller: *Chaos in Classical and Quantum Mechanics* (Springer, New York, 1990).

[14] M.V. Berry and M. Tabor, Pro. Soc. Lond. A **356**, 375 (1977).

[15] G. Casati and B. V. Chirikov, Phys. Rev. Lett. **54**, 1350 (1985).

[16] M. Robnik and G. Veble, J. Phys. A **31**, 4669 (1998).

[17] E. Bogomolny, Nonlinearity **13**, 947 (2000).

[18] J. Hannay and A. M. Ozorio de Almeida, J. Phys. A **17**, 3429 (1984).

[19] M.V. Berry, Pro. Soc. Lond. A **400**, 229 (1985).

[20] N. Argaman, F. M. Dittes, E. Doron, J. P. Keating, A. Yu. Kitaev, M. Sieber, and U. Smilansky, Phys. Rev. Lett. **71**, 4326 (1993).

[21] M. Sieber and K. Richter, Phys. Scr. T **90**, 128 (2001); M. Sieber, J. Phys. A **35**, L616 (2002).

[22] M.C. Gutzwiller, J. Math. Phys. **12**, 343 (1971).

[23] M. Brack and R. Bhaduri: *Semiclassical Physics* (Westview Press, Boulder, 2003).

[24] V. M. Strutinsky, Nukleonika (Poland) **20**, 679 (1975); V. M. Strutinsky and A. G. Magner, Sov. J. Part. Nucl. **7**, 138 (1976) [Elem. Part. & Nucl. (Atomizdat, Moscow) **7**, 356 (1976)].

[25] M. Berry and M. Tabor, Pro. Soc. Lond. A **349**, 101 (1976); J. Phys. A **10**, 371 (1977).

[26] S. C. Creagh and R. G. Littlejohn, Phys. Rev. A **44**, 836 (1991); J. Phys. A **25**, 1643 (1992).

[27] O. Bohigas. In *Chaos and Quantum Physics* (Les Houches, Session LII), 87, 1989.

[28] G. Berkolaiko, H. Schanz, and R. S. Whitney, Phys. Rev. Lett. **88**, 104101 (2002).

[29] M. Turek and K. Richter, J. Phys. A: Math. Gen. **36**, L455 (2003); D. Spehner, J. Phys. A: Math. Gen. **36**, 7269 (2003); S. Müller, Eur. Phys. Jour. B **34**, 305 (2003);

[30] M. Turek, D. Spehner, S. Müller, and K. Richter Phys. Rev. E **71**, 016210 (2005).

[31] S. Heusler, S. Müller, P. Braun and F. Haake, J. Phys. A **37** L31-L37 (2004). S. Müller, S. Heusler, P. Braun, F. Haake, and A. Altland, Phys. Rev. Lett. **93**, 014103 (2004); S. Müller, S. Heusler, P. Braun, F. Haake and A. Altland, Phys. Rev. E **72**, 046207 (2005).

[32] H. Poincaré, *Les Méthodes Nouvelles de la Mécanique Céleste*, Paris: Gauthier-Villars, 1982.

[33] H. Schomerus, P. Jacquod, J. Phys. A **38**, 10663 (2005).

[34] B. V. Chirikov, F M. Izrailev, and D. L. Shepelyanskii, Sov. Sci. Rev. C **2**, 209 (1981).

[35] I. L. Aleiner and A. I. Larkin, Phys. Rev. B **54**, 14423 (1996).

[36] O. Yevtushenko, G. Lütjering, D. Weiss and K. Richter, Phys. Rev. Lett. **84**, 542 (2000).

[37] I. Adagideli, Phys. Rev. B **68**, 233308 (2003).

[38] S. Rahav and P. W. Brouwer, Phys. Rev. Lett. **96**, 196804 (2006).

[39] P. Brouwer and S. Rahav, Phys. Rev. B **74**, 075322 (2006).

[40] Ph. Jacquod and R. Whitney, Phys. Rev. B **73**, 195115 (2006).

[41] P. Brouwer, S. Rahav and C. Tian, Phys. Rev. E **74**, 066208 (2006).

[42] O. Brodier, P. Schlagheck, and D. Ullmo, Phys. Rev. Lett. **87**, 064101 (2001); Ann. Phys. (Leipzig) **300**, 88 (2002); C. Eltschka and P. Schlagheck, Phys. Rev. Lett. **94**, 014101 (2005).

[43] M. Berry and M. Robnik, J. Phys. A **17**, 2413 (1984).

[44] T. Seligman and J. Verbaarschot, J. Phys. A **18**, 2227 (1985).

[45] T. Poston and I. Stewart, *Catastrophe Theory and its Applications*, Pitman, Boston, 1978. P. T. Saunders, *An Introduction to Catastrophe Theory*, Cambrigde University Press, Cambrigde, 1980. D. P. L. Castriagiano and S. A. Hayes, *Catastrophe Theory*, Addison-Wesley, Reading, 1993.

[46] K. R. Mayer, Trans. Am. Math. Soc. **149**, 95 (1970).

[47] A. M. Ozorio de Almeida and J. H. Hannay, J. Phys. A **20**, 5873 (1987).

[48] M. Sieber, J. Phys. A **29**, 4715 (1996); H. Schomerus and M. Sieber, J. Phys. A **30**, 4537 (1997); M. Sieber and H. Schomerus, J. Phys. A **31**, 165 (1998).

[49] M.V. Berry, J. P. Keating, and S. Prado, J. Phys. A **31**, L245 (1998).

[50] In Ref.[1] it is noted that the transformations necessary to arrive at the normal forms can not be proven generally to be canonical. An example for transcritical bifurcations can be found in M. Brack and A. Tanaka, Phys. Rev. E **77**, 046205 (2008).

[51] M. V. Berry, J. P. Keating, and H. Schomerus, Pro. Soc. Lond. A **456**, 1659 (2000).

[52] R. .L. Weaver. J. Acoust. Soc. Am. **85**, 1005 (1989).

[53] H. J. Stöckmann, and J. Stein Phys. Rev. Lett. **64**, 2215 (1990).

[54] U. Kuhl, H.-J. Stöckmann, and R. Weaver, J. Phys. A **38**, 10433 (2005). Y. V. Fyodorov, D. V. Savin, and H.-J. Sommers, J. Phys. A **38**, 10731 (2005). H.-J. Stöckmann, *Quantum Chaos– An Introduction*, (University Press, Cambridge, 1999).

[55] C. Marcus, A. Rimberg, R. Hopkings and A. Gossard, Phys. Rev. Lett. **69**, 506 (1992).

[56] A. M. Chang, H. U. Baranger, L. N. Pfeiffer and K. W. West, Phys. Rev. Lett. **73**, 2111 (1994).

[57] R. Akis, D. K. Ferry, and J. P. Bird, Phys. Rev. Lett. **79**, 123 (1997).

[58] R. Kumar, A. Vengurlekar, A. Venu Gopal, T. Mélin, F. Laruelle and B. Etienne, Phys. Rev. Lett. **81**, 2578 (1998).

[59] G. Bacher, R. Weigand, J. Seufert, V. Kulakovskii, N. Gippius, A. Forchel, K. Leonardi and D. Hommel, Phys. Rev. Lett. **83**, 4417 (1999).

[60] R. A. Méndez-Sánchez, U. Kuhl, M. Barth, C. H. Lewenkopf, and H.-J. Stöckmann, Phys. Rev. Lett.**91**, 174102 (2003). U. Kuhl, M. Martínez-Mares, R. A. Méndez-Sánchez, and H.-J. Stöckmann, Phys. Rev. Lett. **94**, 144101 (2005). S. Hemmady, X. Zheng, E. Ott, T. M. Antonsen, and S. M. Anlage, Phys. Rev. Lett. **94**, 014102 (2005). J. Barthélemy, O. Legrand, and F. Mortessagne, Europhys. Lett. **70**, 162 (2005).

[61] O. I. Lobkis, I. S. Rozhkov, and R. L. Weaver, Phys. Rev. Lett. **91**, 194101 (2003).

[62] M. Raizen, C. Salomon and Q. Niu, Phys. Today **50**, 30 (1997).

[63] S. Wilkinson et al, Nature **287**, 575 (1997).

[64] N. Friedman, A. Kaplan, D. Carasso and N. Davidson, Phys. Rev. Lett. **86**, 1518 (2001).

[65] A. Kaplan, N. Friedman, M. Andersen and N. Davidson, Phys. Rev. Lett. **87**, 274101 (2001).

[66] W. Fang, A. Yamilov and H. Cao, Phys. Rev. A **72**, 023815 (2005); J. U. Nčkel and D. A. Stone, Nature (London) **385**, 45 (1997); T. Harayama, P. Davis and K. S. Ikeda, Phys. Rev. Lett. **90**, 063901 (2003); J. Wiersig and M. Hentschel, Phys. Rev. A **73**, 031802(R) (2006); Phys. Rev. Lett. **100**, 033901 (2008).

[67] T. Guhr, A. Müller-Groeling, and H. A. Weidenmüller, Phys. Rep. **299**, 189 (1998).

[68] Y. Fyodorov and H. J. Sommers, J. Math. Phys. **38**, 1918 (1997).

[69] C. Manderfeld and H. Schomerus, Phys. Rev. E **63**, 066208 (2001).

[70] J. Tworzydlo, A. Tajic and C. W. J. Beenakker, Phys. Rev. B **69**, 165318 (2004).

[71] H. Schomerus and J. Tworzydlo, Phys. Rev. Lett. **93**, 154102 (2004).

[72] M. Gutiérrez, M. Brack, K. Richter and A. Sugita, J. Phys. A **40**, 1525 (2007).

[73] D. Waltner, M. Gutiérrez, A. Goussev and K. Richter, Phys. Rev. Lett. **101**, 174101 (2008).

[74] M. Gutiérrez, D. Waltner, J. Kuipers and K. Richter, arXiv:0811.1884 (submitted to Phys. Rev. E).

[75] J. Kuipers, D. Waltner, M. Gutiérrez and K. Richter, arXiv:0811.2164 (submitted to Nonlinearity).

[76] B. Gutkin, D. Waltner, M. Gutiérrez, J. Kuipers and K. Richter (to be published).

[77] O. Bohigas, S. Tomsovic, and D. Ullmo, Phys. Rep. **223**, 43 (1993).

[78] B. Eckhardt, G. Hose, and B. Pollack, Phys. Rev. A **39**, 3776 (1989).

[79] M. Brack, M. Mehta, and K. Tanaka, J. Phys. A **34**, 8199 (2001).

[80] M. Brack, S. Fedotkin, A. Magner, and M. Mehta, J. Phys. A **36**, 1095 (2003).

[81] A. B. Eriksson and P. Dahlqvist, Phys. Rev. E **47**, 1002 (1993).

[82] I. Gradshteyn, I. Ryzhik, *Tables of Integrals, Series and Products*, 5th edition (New York: Academic) ch 8.1 (1994).

[83] H. Yoshida, Celest. Mech. **32**, 73 (1984).

[84] For a review of group theory and its relation with Quantum Mechanics see A. W. Joshi. *Elements of Group Theory for Physicist* (New Age International Limited, Publishers, India, 1997).

[85] R. A. Pullen and A. R. Edmonds, J. Phys. A **14**, L477 (1981).

[86] B. Lauritzen, N. D. Whelan, Ann. Phys. **244** 112, (1995).

[87] see, e.g., R. Wong: *Asymptotic Approximation of Integrals* (Academic Press, San Diego, 1989).

[88] We are grateful to K. Jänich for his assistance in evaluating the boundary term in Eq. (2.19).

[89] The parameter a appearing in the corresponding normal form, in the notation of [48], was obtained analytically in [80].

[90] J. Robbins, Phys. Rev. A **40**, 2128 (1989).

[91] B. Lauritzen, Phys. Rev. A **43**, 603 (1991).

[92] S. C. Creagh, J. Phys. A **26**, 95 (1993).

[93] J. Robbins, private communication (2006).

[94] A. Sugita, Ann. Phys. (N. Y.) **288**, 277 (2001).

[95] S. C. Creagh, J. M. Robbins, and R. G. Littlejohn, Phys. Rev. A **42**, 1907 (1990).

[96] The numerical determination of the periodic orbits and their stabilities was done with the program developed by Ch. Amann in Ch. Amann and M. Brack, J. Phys. A **35**, 6009 (2002).

[97] C. W. J. Beenakker and H. van Houten, *Semiconductor Heterostructures and Nanostructures*, Solid States Physics **44**, 1 (1991).

[98] S. Datta, *Electronic Transport in Mesoscopic Systems* (Cambridge University Press, Cambridge, 1995).

[99] *Mesoscopic Quantum Physics*, ed. by E. Akkermans, G. Montambaux, J. L. Pichard and J. Zinn-Justin (Elsevier, New York, 1995).

[100] *Mesoscopic Electronic Transport*, ed. by L. L. Sohn, L. P. Kouwenhoven and G. Schön, NATO ASI Series E **345** (Kluwer, Dordrecht, 1997).

[101] K. Richter, *Semiclassical Theory of Mesoscopic System*, Springer, Germany, 1999.

[102] R. Jalabert, lectures given in the CXLIII Course "New Directions in Quantum Chaos" on the International School of Physics "Enrico Fermi"; Varenna, Italy, July 1999.

[103] S. Chakravarty and A. Schmid, Phys. Rep. **140**, 193 (1996). P. A. Lee and T. V. Ramakrishnan, Rev. Mod. Phys. **27**, 287 (1985).

[104] D. Weiss, K. Richter, A. Menschig, R. Bergmann, H. Schweizer, K. von Klitzming, and G. Weimann, Phys. Rev. Lett. **70**, 4118 (1993).

[105] R. Landauer, Phil. Mag. **21**, 863 (1970).

[106] R. A. Jalabert, H. U. Baranger and A. D. Stone, Phys. Rev. Lett. **65**, 2442 (1990). H. U. Baranger, R. A. Jalabert and A. D. Stone, Chaos **3**, 665 (1993).

[107] T. Bartsch, J. Main and G. Wunner, Phys. Rev. A **67**, 063410 (2003).

[108] M. L. Du and J. B. Delos, Phys. Rev. A **38**, 1896 (1988).

[109] E. B. Bogomolny, Zh. Eksp.Teor. Fiz. **96**, 487 (1989).

[110] H. Goldstein, *Classical Mechanics*, Addison-Wesley, 1965.

[111] M. Golubitsky and D. G. Schäffer. *Singularities and groups in bifurcation theory* (Springer- Verlag, New York, 1985).

[112] T. Bartsch, J. Main and G. Wunner, Phys. Rev. A **67**, 063411 (2003).

[113] M. Abramowitz and I. A. Stegun, (Eds.). *Handbook of Mathematical Functions with Formulas, Graphs, and Mathematical Tables*, 9th printing. New York: Dover, 1972.

[114] M. Sieber, J. Phys. A **32**, 7679 (1999).

[115] K. Richter and M. Sieber, Phys. Rev. Lett. 89, 206801 (2002).

[116] S. Heusler, S. Müller, P. Braun and F. Haake, Phys. Rev. Lett. **96**, 066804 (2006). S. Müller, S. Heusler, P. Braun and F. Haake, New J. Phys. **9**, 12 (2007).

[117] J. P. Keating, S. D. Prado, and M. Sieber, Phys. Rev. B **72**, 245334 (2005).

[118] M. Wilkinson, J. of Phys. A20, 2415 (1987).

[119] A. Goussev and K. Richter, Phys. Rev. E **75** 015201(R) (2007).

[120] H. De Raedt, Comp. Phys. Rep. **7**, 1-72 (1987).H. De Raedt, Annu. Rev. Comput. Phys. **4**, 107 (1996).

[121] T. Baumert, M. Grosser, R. Thalweiser and G. Gerber, Phys. Rev. Lett. **67**, 3753 (1991).

[122] A. Bäcker. *Classical and Quantum chaos in Billiards.* PhD thesis, Universität Ulm, 1998.

[123] A. Krámli, N. Simányi and D. Szász, Commun. Math. Phys. **125**, 439 (1989).

[124] K. Frahm, Phys. Rev. E **56**, R6237 (1997).

[125] D. Savin and V. Sokolov, Phys. Rev. E **56**, R4911 (1997); D. Savin and J. Sommers, Phys. Rev. E **68**, 036211 (2003).

[126] G. Casati, G. Maspero and D. Shepelyansky, Phys. Rev. E **56**, R6233 (1997); G. Casati, G. Maspero and D. Shepelyansky, Phys. Rev. Lett. **82**, 524 (1997); G. Casati, I. Guarneri and G. Maspero, Phys. Rev. Lett. **84**, 63 (1999).

[127] M. Puhlmann, H. Schanz, T. Kottos and T. Geisel, Europhys. Lett. **69**, 313 (2005).

[128] F. Cucchietti, H. Pastawski and R. Jalabert, Phys. Rev. B **70**, 035311 (2004).

[129] A. Goussev, D. Waltner, K. Richter, and R. A. Jalabert, New J. Phys. **10**, 093010 (2008).

[130] R. Whitney and Ph. Jacquod, Phys. Rev. Lett. **96**, 206804 (2006).

[131] O. Agam, Phys. Rev. E **61**, 1285 (2000).

[132] S. Reid and H. Reisler, J. Chem. Phys. **101**, 5683 (1994).

[133] A. Dobbyn, J. Stumpf, M. Keller, W. Hase and R. Schinke, J. Chem. Phys. **102**, 7070 (1995).

[134] U. Peskin, U. Miller and H. Reisler, J. Chem. Phys. **102**, 8874 (1995).

[135] B. Grémaud and D. Delande, Europhys. Lett. **40**, 363 (1997).

[136] R. Schinke, *Photodissociation Dynamics*. (Cambridge University Press, Cambridge, England, 1993).

[137] Y. Fyodorov and Y. Alhassid, Phys. Rev. A **58** R3375 (1998).

[138] Y. Alhassid and Y. Fyodorov, J. Chem. Phys. **102**, 9577 (1998).

[139] C. E. Porter, *Statistical Theory of Spectra: fluctuations* (Academic Press, New York, 1965).

[140] J. Main and G. Wunner, J. Phys. B **27**, 1994 (1994). V. V. Flambaum, A. A. Gribakina and F. Gribakin, Phys. Rev. A **54**, 2066 (1996).

[141] B. Eckhardt, S. Fishman and I. Varga, Phys. Rev. E **62**, 7867 (2000).

[142] N. Argaman, Phys. Rev. Lett. **75**, 2750 (1995); and Phys. Rev. B **53**, 7035 (1996).

[143] J. Kuipers and M. Sieber, Nonlinearity **20**, 909 (2007).

[144] G. Stania and H. Walther, Phys. Rev. Lett. **95**, 194101 (2005).

[145] T. Gorin, J. Phys. A **38**, 10805 (2005).

[146] see M. Sieber, Nonlinearity **20**, 2721 (2007) and references therein.

[147] S. Heusler, S. Müller,A. Altland,P. Braun and F. Haake, Phys. Rev. Lett. **98**, 044103 (2007).

[148] B. Georgeot and R. Prange, Phys. Rev. Lett. **74**, 4110 (1995).

[149] K. Richter, Europhys. Lett. **29** , 7 (1995).

[150] G. Hackenbroich and F. von Oppen, Europhys. Lett. **29**, 151 (1995). G. Hackenbroich and F. von Oppen, Z. Physik. B **97**, 157 (1995).

[151] M. Hastings, A. Douglas Stone and H. Baranger, Phys. Rev. B **50**, 8230 (1994). H. Baranger and A. Douglas Stone, Phys. Rev. B **40**, 8169 - 8193 (1989).

[152] J. Kuipers and M. Sieber, Phys. Rev. E **77**, 046219 (2008).

Acknowledgments

I am very thankful to my two supervisors during this time, Klaus Richter and Matthias Brack, for their invaluable guidance and encouragement during these years. It was an honor and a great luck to have worked with two exceptional people as they are. I would like to thank the University of Regensburg and the Graduiertenkolleg for the financial support and the opportunity of working at this nice place.

Concerning the first part of the thesis, I would like to thank Matthias Brack for his close supervision, his interest, experience and motivation in the topic of bifurcations and trace formulae, to Prof. Jänich for the nice discussions in the common seminar of mathematical tools in physics and to A. Sugita for providing me the code to diagonalize the quartic oscillator.

A part of the work presented here was done in cooperation with Daniel Waltner, Klaus Richter, Arseni Goussev and recently Jack Kuipers. I am grateful to Daniel Waltner for the interesting discussions, his fruitful ideas and almost two years of collaboration. A very special thanks goes to Arseni Goussev, first for providing me the program to calculate the propagation of wave packets, and also for the nice and motivating discussions we had. I am truly thankful to Klaus Richter for his interest, his supervision and for sharing his very broad and rich experience.

I want to thank Juan Diego Urbina, Matthias Brack, Peter Schlagheck and Marcus Bonanca for proof reading some parts of this thesis and commenting on it.

I would like to thank some colleagues at Regensburg with whom I had the pleasure of discussing several topics of semiclassics: Marcus Bonanca, Cyril Petitjean, Peter Schlagheck, Inanc Adagideli, Tobias Kramer; and for fruitful discussions during their visits in Regensburg or in workshops to Martin Sieber, Jon Keating, Denis Ullmo, Piet Brouwer, Rodolfo Jalabert, Dima Savin, Gregor Tanner, Achim Richter, Arnd Bäcker, and in general to the quantum chaos community.

Thanks to my office-mates during these three years: Oleg Zaitsev, Andreas Koch and Jérôme Roccia, for the nice time and discussions.

I am very grateful to Angela Reisser, Monika Maschek and to the secretary of the Graduiertenkolleg, Ulla Turba, for their always kind help.

I am very thankful to Christian Reichl, Martin Utz and Andreas Helzel for their invaluable friendship. A very special thanks goes to Juan Diego Urbina for the exciting discussions that we had, his constant support and motivation, the time, the trust and the humor. I would like to thank my good old mates that are always there: Miguel Gualdrón, Lucía Rivera, Karen Rodríguez and Arturo Argüelles. To all the people with whom I have shared time, thoughts, music, books, holidays, etc, during these years I would like to thank. A very special thanks go to Thomas Dittrich, for his support and friendship.

Finally I thank my family for their support and love, especially to Tere (Gutiérrez), for her care, her friendship and her trust.